

# Master's thesis

---

## Depositional environment and hydrocarbon potential of Oligo-/Miocene rocks in the Vrancea Nappe (Eastern Carpathians, Romania)

by

Juliane Hentschke



Supervisor: Professor Reinhard F. Sachsenhofer, Chair in Petroleum Geology,  
Department of Applied Geosciences and Geophysics, University of Leoben

February 2015

Ich versichere an Eides statt, die vorliegende Arbeit selbständig und nur mit Hilfe der angegebenen Quellen verfasst zu haben.

.....

## **Acknowledgements**

I am heartily thankful to my supervisor, Professor Sachsenhofer, whose encouragement, guidance and professional competence helped me writing this thesis. His support and patience from the initial to the final stage enabled me to develop an understanding of the subject.

I am particularly grateful for the assistance and mentoring given by Csaba Krezsek and his colleagues from Petrom during my field work in Romania. Moreover, I want to thank him for arranging the TOC/RockEval measurements of my samples.

Moreover, I want to thank Mr. Pene who organised the field trip to Romania.

Stjepan Coric provided me with very valuable results of his investigation regarding nannoplankton.

I would like to offer my special thanks to Achim Bechtel and Reinhard Gratzner, who gave me guidance and support in handling the organic geochemical data and interpreting them.

Advice given by Susanne Strobl and Doris Groß has been a great help in creating thin polished sections and the following evaluation of the maceral content of those.

Furthermore, I would like to offer my special thanks to Alessandra Meixner for the XRF measurements and accompanying explanations.

Finally, I wish to acknowledge the help provided by Frieder Jacobi. He went along with me during almost my whole study and gave me valuable advice and compassion.

## Zusammenfassung

Im Zuge der Isolierung der Paratethys an der Eozän/Oligozän-Grenze wurden organisch reiche Sedimente abgelagert, die in vielen Teilen der Paratethys, inklusive des Karpatenbogens, wichtige Kohlenwasserstoffmuttergesteine bilden.

Die oligozänen/miozänen Ablagerungen der Ostkarpaten wurden bezüglich Sedimentologie und Stratigraphie bereits beschrieben; dabei wurden auch RockEval Daten mitgeteilt. Allerdings ist eine detaillierte Untersuchung des organischen Materials ausständig.

Ziele dieser Studie sind (1) die Bestimmung der wichtigsten Faktoren, die die Ablagerung des organischen Material gesteuert haben, (2) die Erfassung der vertikalen Änderungen des Kohlenwasserstoffpotentials, (3) die Unterscheidung des gebildeten Öls aus verschiedenen Einheiten innerhalb des Profils aufgrund der Biomarker-Variabilität, und (4) einen möglichen Zusammenhang zwischen Intensität der Gammastrahlung und erhöhtem Anteil an organischem Material zu evaluieren.

Um diese Ziele zu erreichen, wurden mehr als 150 Proben der Menilite Formation entlang des Tazlau Flusses entnommen. Entlang des Profils lassen sich innerhalb der Menilite Formation vom Liegenden zum Hangenden folgende Einheiten unterscheiden: Lower Menilite Member (LMM), Bituminous Marl Member (BMM), Lower Dysodilic Shale Member (LDSM), Kliwa Sandstone Member (KSM), Upper Dysodilic Shale Member (UDSM).

Unter der Menilite Formation liegt die Bisericani Formation, welche im submarinen Hangbereich abgelagert wurde. Ein Übergang zu anoxischem Milieu ermöglichte die Ablagerung der LMM mit hohen TOC Gehalten und Kerogentyp II. Die Auswertung von kalkigem Nannoplankton ergab, dass die überlagernde BMM in die Nannoplankton Zonen NP21-22 einzustufen ist. Der organische Anteil wird durch autochthone marine Organismen und bakterielle Biomasse gebildet. Moderate TOC Gehalte sind auf die Verdünnung durch karbonatisches Material zurückzuführen. Die Salinität variierte zwischen reduziert und leicht erhöht. Die Redoxbedingungen variierten von anoxisch zu (dys)oxisch. Die LDSM besteht aus bituminösen Tonstein- und Sandstein-Ablagerungen eines tiefmarinen Fächerbereiches. Das anoxische Milieu förderte die Akkumulation von Biomasse (Kerogentyp II). Trotz hoher Wasserstoffindex(HI)-Werte bilden Landpflanzen einen großen Teil der Biomasse. Ein Abfall des HIs im oberen Teil der LDSM ist durch erhöhten Landpflanzeneintrag und gesteigerten Sauerstoffgehalt zu erklären. Der Salzgehalt variierte stark. Die Rinnensedimente der KSM trennen die LDSM von der UDSM. Der tiefere Teil der UDSM wurde in einem tiefmarinen Fächer abgelagert, der obere Teil in der Beckenebene. MTTC Werte nehmen nach oben zu. Sie stellen einen Trend von leicht erhöhtem zu geringem Salzgehalt dar. Sauerstoffarme, aber nicht stark anoxische Bedingungen werden durch die Pr/Ph Verhältnisse indiziert. Aryl-Isoprenoide deuten eine durch Salinitätsschwankungen gesteuerte zeitweilige Anoxie der photischen Zone an. Organische und anorganische Redoxanzeiger lassen einen leichten Anstieg des Sauerstoffgehalts innerhalb der UDSM vermuten. Die Biomasse der UDSM ist eine Mischung aus autochthonem organischen Material und Landpflanzen und wurde als Kerogentyp II identifiziert. An der Grenze zwischen Gura Soimului Formation und UDSM trat eine starke Veränderung der Sauerstoffbedingungen auf. Die GSF ist im Tazlau Profil durch mehrere Mega-Olistolithe gekennzeichnet.

## Abstract

The isolation of the Paratethys at the Eocene/Oligocene boundary favored the formation of organic-rich sediments that have been deposited within the restricted basin. These sediments act as hydrocarbon source rocks in many parts of the Paratethys area including the Carpathian Foredeep.

Oligo/Miocene rocks in the Eastern Carpathians have been studied previously using sedimentological techniques and some RockEval data. However a detailed study of the organic matter is still missing. For this reason, the present study aims (1) to determine the main factors controlling the deposition of organic matter, (2) to detect vertical variations in the source rock potential, (3) to test the possibility to distinguish oil generated from different units within Oligo/Miocene succession, and (4) to test, whether the source richness can be related to the gamma ray (GR) response in boreholes.

To achieve the goals, more than 150 samples have been taken along the Tazlau river. The profile includes Eocene Bisericani Formation, Oligo-/Miocene Menilite Formation and lower Miocene Gura Soimului Formation. The Menilite Formation is composed from base to top by Lower Menilite Member (LMM), Bituminous Marl Member (BMM), Lower Dysodilic Shale Member (LDSM), Kliwa Sandstone Member (KSM), and Upper Dysodilic Shale Member (UDSM).

The Bisericani Formation includes deposits of a slope apron system. A major change towards anoxic conditions caused deposition of the LMM with high TOC contents and a kerogen type II. Calcareous nannoplankton dates the overlying BMM into nannoplankton zones NP21-22. The organic matter mainly derived from autochthonous marine organisms including bacterial biomass. TOC contents are moderate because of dilution by carbonate minerals. Salinity and redox conditions varied from reduced to slightly enhanced and from strictly anoxic to dysoxic, respectively. The LDSM contains black shale and sandstone beds deposited in a deep marine depositional lobe. Anoxic environments caused accumulation of abundant organic matter with kerogen type II. Despite of high HI values, landplants form a significant part of the organic matter. A decrease in HI in the uppermost part of the LDSM is due to increasing contributions of landplants and increased oxygen contents. Salinity varied significantly. The channel fill sediments of the KSM separate LDSM and UDSM. The lower part of the UDSM accumulated in a lobe, whereas its upper part represents a basin plain setting. MTTC ratios increase upwards and reflect a trend from slightly enhanced to slightly decreased normal marine salinities. Whereas oxygen-depleted, but not strictly anoxic conditions, are indicated by Pr/Ph ratios, the presence of aryl-isoprenoids suggests temporary photic zone anoxia controlled by salinity variations. Organic and inorganic redox proxies suggest a subtly upward increase in the availability of oxygen within the UDSM. The organic matter is a mixture of autochthonous organic matter and landplants and is classified as kerogen type II. A major change towards oxic conditions occurred at the boundary between the UDSM and the Gura Soimului Formation. The GSF in the Tazlau profile is characterized by thick mega-olistolithes.

## Contents

---

<b>1</b>	<b>Introduction and Objectives .....</b>	<b>10</b>
<b>2</b>	<b>Geological Setting .....</b>	<b>12</b>
<b>3</b>	<b>Samples and Methods.....</b>	<b>16</b>
3.1	Study section and sampling procedure .....	16
3.2	Field measurements.....	17
3.3	Sample preparation.....	17
3.4	RockEval pyrolysis .....	17
3.5	Leco .....	20
3.6	Biomarkers .....	20
3.7	Inorganic geochemistry and proxies .....	26
3.8	Organic Petrology (VR, Maceral analysis).....	29
3.9	Pyrolysis-GC.....	29
3.10	Nannoplankton.....	29
<b>4</b>	<b>Results.....</b>	<b>30</b>
4.1	Lithology .....	30
4.2	Calcareous Nannoplankton (Stjepan Coric).....	35
4.3	Spectral gamma radiation .....	36
4.4	Bulk geochemical parameters .....	40
4.5	Biomarker .....	47
4.6	Organic Petrology.....	60
4.7	Pyrolysis-GC.....	62
4.8	Inorganic Geochemistry .....	64
<b>5</b>	<b>Discussion.....</b>	<b>72</b>
5.1	Reliability of spectral gamma measurements.....	72
5.2	Relation between TOC and gamma-ray response.....	73
5.3	Maturity.....	75
5.4	Depositional Environment.....	75
5.5	Hydrocarbon Potential .....	85
5.6	Parameters for the distinction of oil generated from different members.....	88
<b>6</b>	<b>Conclusions.....</b>	<b>89</b>
<b>7</b>	<b>References.....</b>	<b>92</b>
<b>8</b>	<b>Appendix .....</b>	<b>98</b>

## Figures

---

Figure 1: Paleogeographic position of the Paratethys during early Oligocene time (Sachsenhofer et al. 2009).....	10
Figure 2: Location of Tazlau in the Eastern Carpathians .....	11
Figure 3: Tectonic units of the Carpathians and Dinarides (simplified after Schmid et al. 2006).....	12
Figure 4: Paleogeographic position during Cretaceous to Miocene convergence between Africa and Eurasia (after Amadori et al, 2012) .....	13
Figure 5: Geological map and cross section of the Eastern Carpathian Chain (Amadori et al. 2012).....	14
Figure 6: Sampling points according to the different field campaigns .....	16
Figure 7: Calculation of TOC using RockEval 6 (after Behar, 2001).....	18
Figure 8: Procedure for biomarker analysis .....	21
Figure 9: Geochemical process involved in the formation of pyrite (Berner 1984) and Fe-S-OC ternary diagram showing key constant ratio lines of pyrite formation (Berner 1984).....	27
Figure 10: Generalized patterns of sedimentary Mo-TOC covariation associated with deepwater renewal in silled anoxic basins (Algeo & Lyons 2006) .....	28
Figure 11: Overview of studied profile. The color code represents different lithologies. The boundary between the lower and upper part of the section (see Figure 14) is also shown.....	30
Figure 12: Overview of studied profile with strike and dip. Colored boxes show sample number .....	30
Figure 13: Bituminous Marl Mbr.: Marl with thin sandstone lenses (sample 3) .....	31
Figure 14: Lithological Profile of the Tazlau section. Note the different scale! .....	32
Figure 15: Lower Dysodilic Shale Mbr.: Alternation of Kliwa-type sandstone and black shale. A) samples 41A/B, B) sample 42 .....	33
Figure 16: Lower Dysodilic Shale Mbr. A) Alternation of Kliwa-type sandstone and black shale (sample II-41), B) Slump (sample II-48), C) Black Shales (sample II-60) .....	34
Figure 17: Gura Soimului Fm. A) Greyish shale (sample II-77), B) mega breccia, C) greyish shale (sample 92), D) sandstone layers in the uppermost part of the GSF.....	35
Figure 18: Plots of dose radiation versus .....	37
Figure 19: Plot of dose radiation versus total inorganic carbon (TIC) for the Bituminous Marl Mbr. ....	38
Figure 20: Depth trends of dose radiation, and radioactive elements .....	39
Figure 21: Vertical variation of bulk geochemical parameters (total organic carbon [TOC], CaCO <sub>3</sub> , sulfur [S], TOC/S) .....	41
Figure 22: Vertical variation of hydrogen index (HI) and oxygen index (OI) .....	42
Figure 23: TOC/S cross plot for samples from the A) Bisericani Fm. and the Bituminous Marl Mbr., B) Lower Dysodilic Shale Mbr., C) Upper Dysodilic Shale Mbr. and D) Gura Soimului Fm. ....	43
Figure 24: Plots of hydrogen index versus oxygen index and Tmax, S2 versus TOC for different stratigraphic units. Hydrogen index, Tmax, S2 and TOC data from samples from Bisericani Formation (grey symbol) and the Lower Menilite Member are taken from Amadori et al. (2012). ....	46
Figure 25: GC MS of the aliphatic hydrocarbon fractions of sample 30 (Lower Dysodilic Shale Mbr.) and sample 93 (Gura Soimului Fm.) .....	47
Figure 26: GC MS of the aromatic hydrocarbon fractions of sample 30 (Lower Dysodilic Shale Mbr.) and sample 93 (Gura Soimului Fm.) .....	48
Figure 27: Variation of a) relative proportions of middle- and long-chain <i>n</i> -alkanes. b) CPI and Pr/Ph ratio and c) MTTC ratio and C19 Aryl Isoprenoids versus depth .....	50
Figure 28: Cross plot of short and long chain <i>n</i> -Alkanes.....	51

Figure 29: Pristane/Phytane-CPI .....	51
Figure 30: Pristane/ <i>n</i> -C <sub>17</sub> versus Phytane/ <i>n</i> -C <sub>18</sub> ratio (Peters, 1999) .....	52
Figure 31: Pr/Phy versus MTTC ratio; for legend see Figure 30 .....	53
Figure 32: Depth profiles: a) C <sub>27</sub> , C <sub>28</sub> and C <sub>29</sub> Steranes/sum Steranes; b) hopanes and steranes; c) steroids/hopanoids and S/(S+R) hopanes; d) 4-Methylsteranes and Benzohopanes.....	55
Figure 33: Distribution of steranes. Modified, (Huang & Meinschein 1979) .....	56
Figure 34: Pristane/Phytane (Pr/Ph) ratio versus Gammacerane Index .....	56
Figure 35: Depth profiles. a) arboranes and diterpenoids; b) cadalenes; c) C <sub>25</sub> thiophenes .....	58
Figure 36: Dibenzothiophene/Phenanthrene versus Pristane/Phytane (Hughes et al. 1995) .....	59
Figure 37: Contribution of various macerals. GSF=Gura Soimului Fm., UDSM=Upper Dysodilic Shale Mbr., LDSM=Lower Dysodilic Shale Mbr., BMM=Bituminous Marl Mbr. ....	61
Figure 38: Diterpenoids versus Vitrinite.....	61
Figure 39: Characterisation of petroleum type organofacies based on carbon chain length distribution. (Horsfield 1989).....	62
Figure 40: Screening data from pyrolysis gas chromatography: sulfur discriminator (Eglinton et al. 1990) .....	63
Figure 41: Characterisation of petroleum type organofacies based on phenol content.....	63
Figure 42: Element concentrations (%) versus depth .....	67
Figure 43: Plot of major element oxides (Al <sub>2</sub> O <sub>3</sub> *5 – SiO <sub>2</sub> – CaO*2). For comparison, average shale (AS), K-feldspar, and kaolinite are plotted as well (after Wedepohl, 1971). ....	68
Figure 44: Plots of A) CaO, B) Sr and C) MnO versus total inorganic carbon (TIC).....	69
Figure 45: Plots of A) TiO <sub>2</sub> and B) Zr versus Al <sub>2</sub> O <sub>3</sub> (carbonate free). See Figure 44 for color-code.....	70
Figure 46: Gamma ray Potassium versus XRF Potassium.....	72
Figure 47: Plot of Dose Rate versus TOC for different stratigraphic units .....	74
Figure 48: Paleogeographic interpretation of the Late Eocene-Oligocene depositional system within the Bistrita half-window (modified from Miclaus et al., 2009; 2010). The sketch suggests that the study area is located west of a forebulge in an area with active faulting.....	75
Figure 49: Depth profiles of Mo/TOC (after Algeo & Lyons 2006) and V/(V+Ni) ratios (after Hatch & Leventhal 1992) and their paleoenvironmental interpretation.....	78
Figure 50: Fe-S-TOC ternary diagram .....	79
Figure 51: Pr/Ph versus Cadalene.....	81
Figure 52: Steroid/Hopanoid ratio versus C <sub>25</sub> HBI Thiophenes .....	82
Figure 53: Cross plot of C <sub>19</sub> aryl-isoprenoids versus MTTC ratio for samples from the Upper Dysodilic Shale Member .....	83
Figure 54: Genetic Potential versus TOC for different stratigraphic units .....	86
Figure 55: Cartoons showing depositional systems of the Tazlau area during Eocene to early Miocene time (slightly modified after Miclaus et al., 2009). The position of the Tazlau section is indicated by an arrow. Explanations of the depositional environment and hydrocarbon potential are added .....	90



## Tables

---

Table 1: Stratigraphy of the Vrancea Nappe and characteristics of the main lithofacies (according to references listed in table).....	15
Table 2: Biomarkers for the characterization of the depositional environment, organic matter source and thermal maturity (Peters et al., 2005).....	22
Table 3: Comparison of dose rate, uranium, thorium and potassium concentrations in different stratigraphic units.....	37
Table 4: Total organic carbon (TOC), CaCO <sub>3</sub> , sulphur (S), TOC/S and hydrogen index (HI) for different stratigraphic units.....	40
Table 5: Bulk parameter for the Bisericani Fm. and the Lower Menilite Mbr. from Amadori et al. (2012) .....	43
Table 6: Concentrations and concentration ratios of <i>n</i> -alkanes and isoprenoids as well as derived source- and facies-related parameters. ....	49
Table 7: Overview of steranes (Ster) and hopanes (Hop) .....	54
Table 8: Arboranes. cadalenes. diterpenoids and C <sub>25</sub> thiophenes.....	57
Table 9: Maceral percentages. The values are calculated on whole rock (light blue) and mineral matter free basis .....	60
Table 10: Concentrations (in %) of elements and element oxides determined with a handheld XRF instrument (missing values are below the detection limit) .....	64
Table 11: Concentrations (in %) of elements and element oxides determined with a handheld XRF instrument (missing values are below the detection limit) .....	65
Table 12: Concentrations (in ppm and %) of elements and element oxides of samples 98. II-67, II-79 using XRF technique and traditional pellets.....	66
Table 13: Potassium measured by xrf and gamma ray tool.....	72
Table 14: Generative potential of source rocks (Peters & Cassa 1994).....	85
Table 15: Calculation of the Source Potential Index (SPI) for the Tazlau section .....	86
Table 16: Average values and standard deviation of biomarker ratios for different members (sandy samples without hydrocarbon potential are neglected).....	88

# 1 Introduction and Objectives

Oligocene to Lower Miocene rocks in the Paratethys region are of special interest as they are the main hydrocarbon source rock in this area. In the eastern Paratethys the Oligocene to Lower Miocene sediments are termed Maykop or Ruslar Formation (Sachsenhofer et al. 2009), whereas in the Carpathians and the Molasse Basin (Northern Alpine Foreland Basin) these sediments are known as Menilite Formation (Köster, Kotarba, et al. 1998; Köster, Rospondek, et al. 1998) and Schöneck Formation (Schulz et al. 2002), respectively (Figure 1).

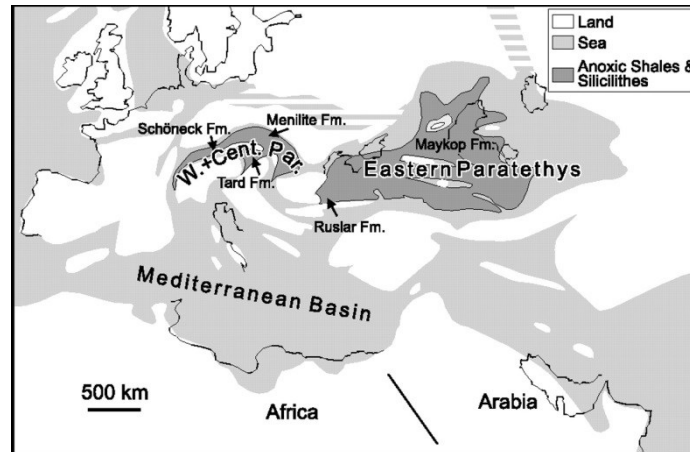


Figure 1: Paleogeographic position of the Paratethys during early Oligocene time (Sachsenhofer et al. 2009)

Apart from their economic significance, Oligo-/Miocene rocks provide a detailed archive for changes in the depositional environment, which are reflected i.a. by varying TOC content and type of organic matter. Thus, changes of depositional environment have also a major impact on the hydrocarbon potential of specific areas and the characteristics of generated oils.

The aim of this study is to characterize the depositional environment, maturity and hydrocarbon potential of the Oligo-/Miocene section in the Vrancea Nappe in the Eastern Carpathians of Romania. To reach the goal, about 150 samples have been taken in an outcrop section located south of Piatra Neamț near Tazlau (Figure 2). The samples have been analyzed using bulk geochemical methods, biomarker analysis, organic petrology and inorganic geochemical techniques.

Near Tazlau steeply dipping rocks of the Oligo-/Miocene section are exposed along the Tazlau River. The Tazlau profile is a key section for the understanding of the evolution of the Eastern Carpathians during Oligocene and Miocene times and has been described recently by different authors including Amadori et al. (2012), Guerrero et al. (2012) and Miclaus & Schieber (2014).



Figure 2: Location of Tazlau in the Eastern Carpathians

## 2 Geological Setting

The Romanian Carpathians belong to the Alpine orogenic belt (Figure 3). The arc-shaped belt of the Carpathians was formed during the Cenozoic emplacement of continental blocks, identified as ALCAPA (Alps-Carpathians-Pannonia) (Csontos 1995), Tisza and Dacia (Sandulescu 1980; Sandulescu & Micu 1989) (Figure 3). These blocks consist of basement units covered by different Triassic and Jurassic sediments (Csontos 2004).

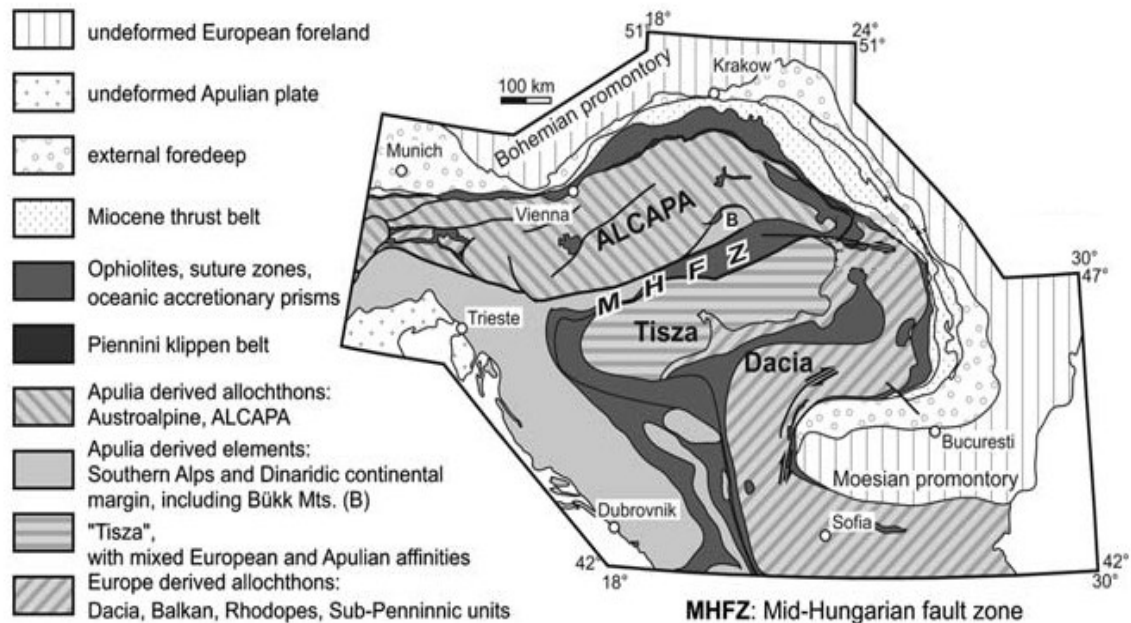


Figure 3: Tectonic units of the Carpathians and Dinarides (simplified after Schmid et al. 2006)

In Cretaceous time the crustal blocks, separated by branches of the Tethys Ocean (e.g., Vardar, Severin oceans), were located between the African and European plates (including Moesian platform) (Radulescu & Sandulescu 1973; Csontos 2004) (Figure 4).

Convergence between the African and Eurasian plates took place during Cretaceous to Miocene time. Subduction was caused by the northward movement of the Apulia-Adria block. The closure of the oceanic domains started in Albian time (Sandulescu 1980; Csontos 2004) with an eastward direction. During the Cenomanian, the convergence rate between the Dacia block (or "Rhodopian" allochthon, (Burchfiel 1980; Schmid et al. 2008; Tischler et al. 2008)) and the Moesian plate decreased. The ongoing subduction caused collision between the Apulia-Adria and Rhodopian blocks during Coniacian time. The Apulia-Adria block rotated counterclockwise while the Rhodopians rotated clockwise as it moved around the Moesian plate (Burchfiel 1980).

The closure ended after the Late Miocene with continental collision between the (north)eastward moving ALCAPA, Tisza and Dacia blocks and the European foreland (c. 11 Ma, (Matenco & Bertotti 2000; Tischler et al. 2008)). Balla (1987) described this as a soft collision, Ratschbacher et al. (1991a,b) mentioned that the collision was triggered by a combination of lateral extrusion and the retreat (roll-back) of a subducting eastern European oceanic lithospheric slab. The emplacement of these blocks was accompanied by large-scale strike-slip movements, extension, shortening and rotations (Ratschbacher et al. 1993; Csontos 2004).

The Severin Ocean (Figure 4) located between the Dacia block and the Moldavidian Basin was separated from the latter by a structural high, known as Peri-Moldavian Cordillera (Bancila 1958 in Amadori et al. 2012), which provided clastic material to the internal and external basin. From Early Cretaceous to Early

Miocene time, the Moldavidian Basin was a foreland basin in which the sedimentary axis migrated from the internal to the external part (Grasu et al. 1999; Amadori et al. 2012). Beginning in Middle Miocene time, a new collision and clockwise rotation with southward convergence direction occurred (Amadori et al. 2012).

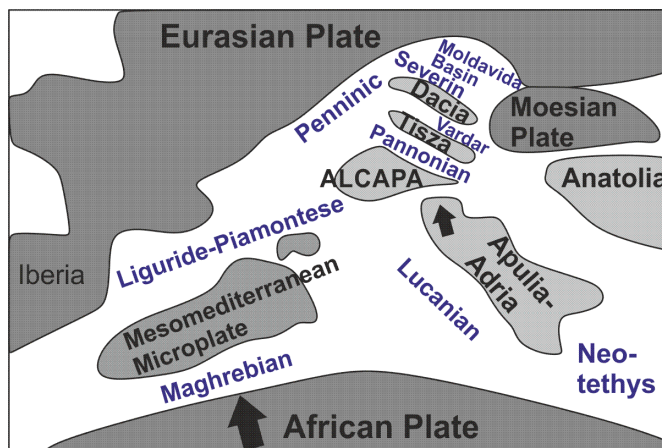


Figure 4: Paleogeographic position during Cretaceous to Miocene convergence between Africa and Eurasia (after Amadori et al, 2012)

The collision formed the Carpathian foreland fold-and-thrust-belt (Sandulescu & Micu 1989; Matenco & Bertotti 2000). Within the Eastern Carpathians (Figure 5), the Tisza block forms the Inner Dacides, the Vardar-Mures Ocean became the Transylvanides/Pienides Unit, and Dacia became the Middle Dacides (Csontos 2004; Schmid et al. 2008). The Severin Ocean and the Peri-Moldavian Cordillera form the Outer Dacides (Amadori et al. 2012). The former Moldavidian Basin forms the Moldavidian Units of the Outer Carpathians (Sandulescu 1990; Golonka et al. 2006; Amadori et al. 2012), which are subdivided from W to E (from internal to external) into five tectonic units (Figure 5):

- Telejean or Convolute Flysch,
- Audia-Macla,
- Tarcau,
- Vrancea or Marginal Fold and
- Pericarpathian nappes.

Thus, the Vrancea Nappe, exposed in the Gura Humorului (GHO), Bistrita (BHW) and Oituz half-windows (OHW) (Matenco & Bertotti 2000) (Figure 5), represents a central part of the Moldavidian Basin, whereas the tectonically more external Pericarpathian Nappe represents its marginal (platform) area (Amadori et al. 2012). Syn-tectonic Cretaceous to Miocene deposits of the Moldavidian Basin contain heterogenic, mainly fine-grained, siliciclastic and carbonatic deposits (sandy marls, limestones, calcarenites, arenites, minor polygenic conglomerates) including pelagic black shales, bituminous marls, and siliceous deposits (Amadori et al. 2012). Coarse-grained siliciclastic deposits supplied from different source areas occur in the upper part of the section (Amadori et al. 2012).

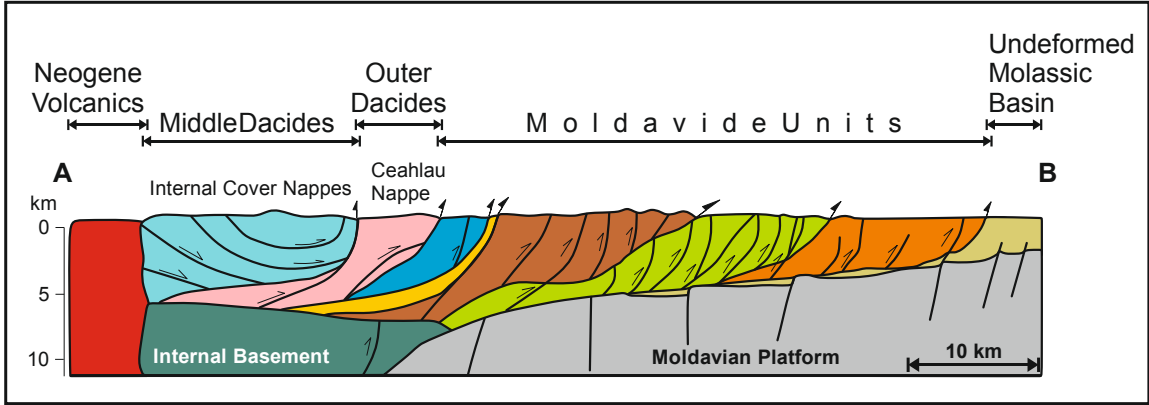
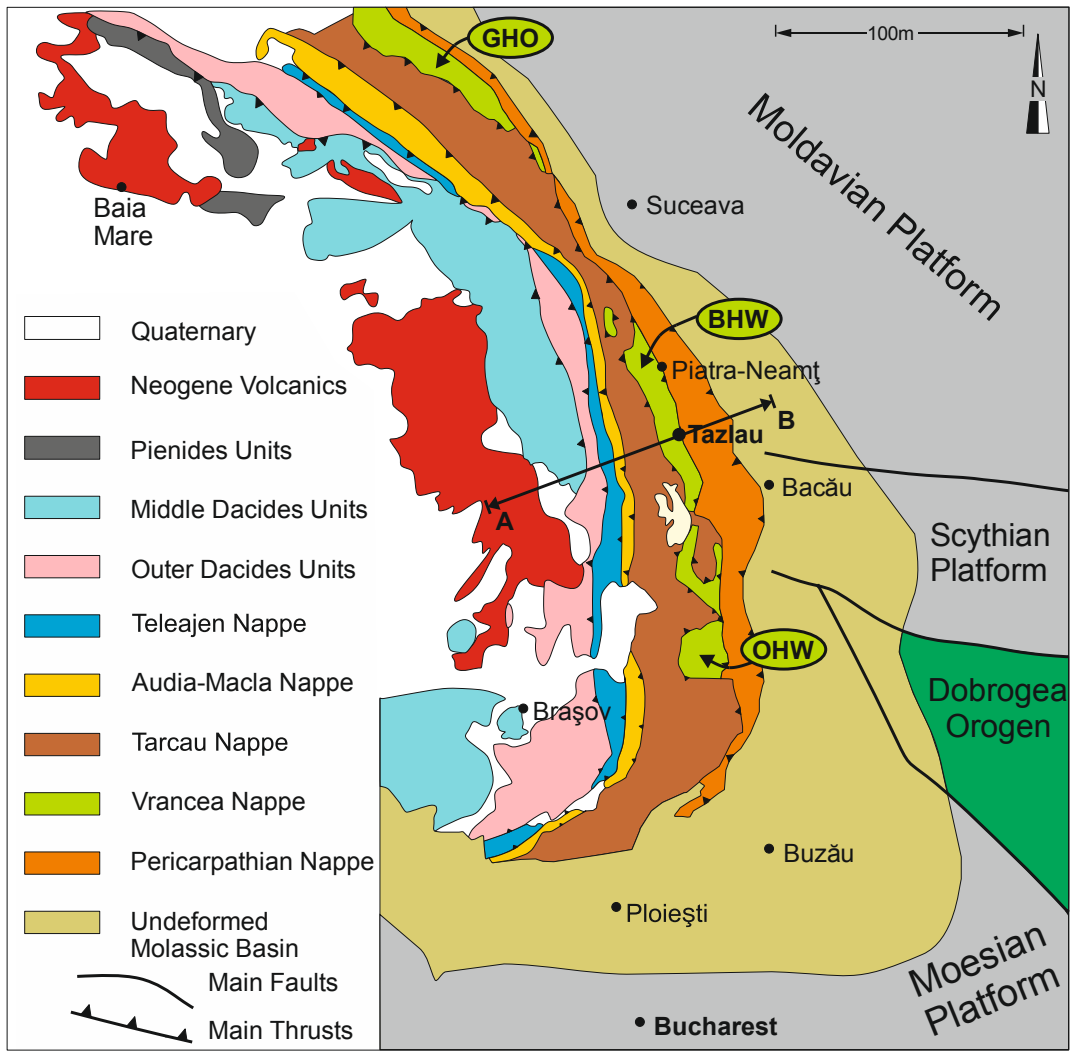


Figure 5: Geological map and cross section of the Eastern Carpathian Chain (Amadori et al. 2012)

Traditionally, the Eocene to Lower Miocene succession in the Vrancea Nappe is subdivided from base to top into: Bisericani Beds, Lower Menilites, Bituminous Marls, Lower Dysodilic Shales, Kliwa Sandstones, Upper Dysodilic Shales and Menilites, and Gura Soimului Beds (Melinte-Dobrinescu & Brustur 2008; Miclaus et al. 2009). Recently, the traditional subdivision has been modified by Amadori et al. (2012; Table 1).

For this thesis, the traditional classification is adopted. However, the organic-rich Oligo-/Miocene sediments are combined into the Menilite Formation, a term, which is used in the Polish and Ukrainian Carpathians (Köster, Rospondek, et al. 1998; Köster, Kotarba, et al. 1998; Kotarba et al. 2007). The Menilite Formation overlies the Bisericani Formation and is separated from the base to the top into:

Lower Menilite Mbr., Bituminous Marl Mbr., Lower Dysodilic Shale Mbr., Kliwa Sandstone Mbr. and Upper Dysodilic Shale Mbr. The Menilite Fm. is overlain by the Gura Soimului Fm. The lithology of the rocks is summarized in Table 1. The exact age of the succession is still a matter of discussion. For example, the generally accepted age of the Bituminous Marl Mbr. is Rupelian (nannoplankton zone 23; e.g. Miclaus & Schieber, 2014), whereas Amadori et al. (2012) postulate a Chattian age. In contrast, the early Burdigalian age (NN2-NN3) of the Gura Soimului Formation is well established (Tabara & Popescu 2012).

**Table 1: Stratigraphy of the Vrancea Nappe and characteristics of the main lithofacies (according to references listed in table)**

Lithology	Amadori et al., 2012 Guerrera et al., 2012		Miclaus et al., 2009		This thesis	
	Unit	Stage	Unit	Stage	Unit	Stage
chaotic polygenic breccias with metamorphic and sedimentary clasts and turbiditic greyish shales	GSF	Burdigalian	GS	Burdigalian	GSF	Burdigalian
laminated black shales, thin siltites, quartzarenites, subarkoses, thin bentonitic clay beds	Dysodilic Shale Mbr	Aquitainian	UDS	Aquitainian	UDSM	Aquitainian
black sandy-silt shales, quartzarenite beds of Kliwa type		Chattian	Kliwa Sdst	Chatt	Kliwa Sdst Mbr	
greenish shales, disorganized polygenic conglomerates with green schist, sandstones	LDS			LDSM	Menilite Fm	
laminated bituminous marls, chert beds and lenses, thin quartzarenites, (marls with metamorphic clasts up to 30 cm in diameter)	BMM			BM		BMM
silicified shales, black chert beds, black shales, quartzarenites, brownish marls, black chert (frequent fish fragments)	LMM		LM	LMM		
creamy marls, greyish marly clays, thin limestone beds, marls, micaceous greenish-grey mudstones, sideritic limestones in lens, thin siltites, limestones	BF	Rupelian	BF	Eocene	BF	Eocene

BF: Bisericani Formation, LMM: Lower Menilites Member, BMM: Bituminous Marl Member, LDSM: Lower Dysodilic Shale Member, UDSM: Upper Dysodilic Shale Member, GSF: Gura Soimului Formation

### 3 Samples and Methods

The following chapter describes the sample location, the sampling procedure and the applied analytical techniques. A table showing the performed analyses for each sample is added in the Appendix.

#### 3.1 Study section and sampling procedure

The Tazlau section is located in the Bistrita half-window of the Vrancea nappe (Sandulescu 1990). It is exposed in the riverbed of the Tazlau River south of the village of the same name and is about 700 m long (coordinates: 46°43'14.80' N, 26°27'5.00''E to 46°43'17.60''N, 26°27'43.00''E).

A first sampling and logging campaign took place between 9<sup>th</sup> and 11<sup>th</sup> of July 2012 (sample number 1 to 98). To complete the profile, a second campaign (number II-1 to II 85; Figure 6) has been performed (7<sup>th</sup> - 13<sup>th</sup> August 2012). Unfortunately, the section was not exposed continuously. Especially in the lower part of the succession the Eocene and Oligocene rocks were covered by river deposits. In well exposed shaly units, samples have been taken every 2 m. In marl and sandstone units, samples have been taken every 5 m. Each sample has a volume of around 250 cm<sup>3</sup>. After sampling, the sample site was photographed (see photo documentation in the Appendix) and the samples were packed and labelled.

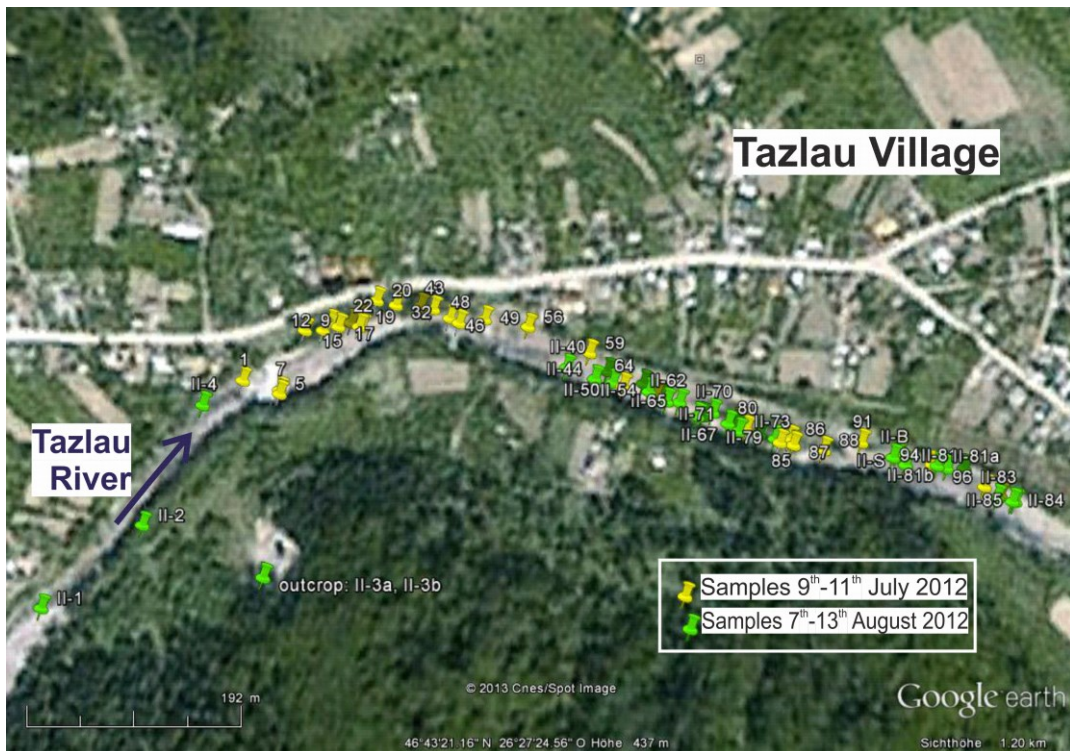


Figure 6: Sampling points according to the different field campaigns



## 3.2 Field measurements

A handheld gamma-ray tool (Gamma Surveyor II by GF Instruments), provided by Petrom, was used for spectral measurements with determination of concentrations of K, U, Th (% , ppm, ppm) and of natural gamma dose rate (nGy/h).

During the field work, the gamma radiation was measured at each sampling site. However, usage of the gamma-ray tool was impossible at sites within the course of the river covered by water. The measurement time was one minute. Resulting values are shown in the Appendix. In addition, strike and dip of several layers were determined.

## 3.3 Sample preparation

Sample preparation was made at Montanuniversitaet Leoben. Samples have been washed to clean them from possible contaminations, like biomass or anthropogenic materials. After drying, a representative part of the samples was crushed using a jaw crusher, then with a mortar and finally a powder has been created using a swing mill. The powder was used for various analytical methods (see below). A part of the crushed material has been handed over to Stjepan Coric to analyse calcareous nannoplankton.

Polished blocks, used for maceral analysis and vitrinite reflectance measurements, were prepared from uncrushed parts of the samples.

## 3.4 RockEval pyrolysis

RockEval pyrolysis was performed by Petrom (Geological Laboratory OMV Petrom S.A., E&P-Development Business Unit-ICPT; Campina). A Rock-Eval 6 instrument of Vinci Technologies has been used. The description of the instrument follows (Behar 2001).

**The Rock-Eval 6 apparatus** enables programmed heating of rock samples in an inert atmosphere. For determination of Rock-Eval parameters plus TOC, the apparatus is equipped with an oven for combustion of the rock residue after pyrolysis and an infra-red cell ensuring the continuous monitoring of CO and CO<sub>2</sub> released during both pyrolysis and combustion. The typical sample amount ranges from 50 to 70 mg. The pyrolysis furnace is able to reach a final temperature of 800 °C using micro-ovens for combustion.

After heating the samples, the flame ionization detector (FID) observes released hydrocarbons at 300 °C, the so-called thermo-vaporized free hydrocarbons (S1) and the pyrolysis products from cracking of organic matter (S2) between 300 and 650 °C (Behar 2001).

An average value of 83 wt. % for the carbon content of the S1 and S2 hydrocarbons independent of the organic matter type is assumed to calculate the corresponding absolute organic carbon content of released hydrocarbons (Espitalie et al. 1985).

The total CO signal monitored during pyrolysis is divided into two surfaces (Figure 7). The first one (S3CO) integrates the CO released up to the temperature where a minimum of CO production is observed (between 450 and 600 °C). If the minimum is not detected, the integration limit is fixed at 550°C as default parameter. This surface corresponds to the release of functions linked to organic matter and this signal will be integrated into the calculation of TOC.

The upper limit defined for the previous surface is the start for the second surface ( $S3'CO$ ). The end of the measurement is the final point for this surface. This surface belongs to the reactivity of  $CO_2$  released during the thermal decomposition of carbonates on the organic matter. According to the Boudouard reactions, producing two  $CO$  molecules, one with a carbon of organic origin integrated into the calculation of TOC, and one with a carbon of mineral origin.

During the oxidation stage, one  $CO$  signal ( $S4CO$ ) is integrated from beginning to end of the measurement. All the carbon contained in this  $CO$  is of organic origin.

Coincidental, the  $CO_2$  yield during the pyrolysis stage is split into  $S3$  and  $S3'$ .  $S3$  corresponds to  $CO_2$  released at the same time as the  $S1$  peak added to that obtained between  $300^\circ$  and  $400^\circ C$  with an organic origin.  $S3'$  represents the  $CO_2$  recorded between  $400^\circ C$  and the end of the measurement, with a mineral origin.

During the oxidation stage (Figure 7), the  $CO_2$  production curve exhibits a minimum between  $550^\circ$  and  $720^\circ C$ , when the rock contains carbonates. The  $S4CO_2$  represents the amount of  $CO_2$  generated between  $300^\circ C$  and the temperature of the defined minimum.  $S5$  corresponds to the counterpart up to the end of the measurement (mineral origin of carbon). The upper temperature of  $650^\circ C$  for pyrolysis of source rocks was chosen in order to obtain a complete  $S2$  signal while a minimum of carbonates will decompose during this step.

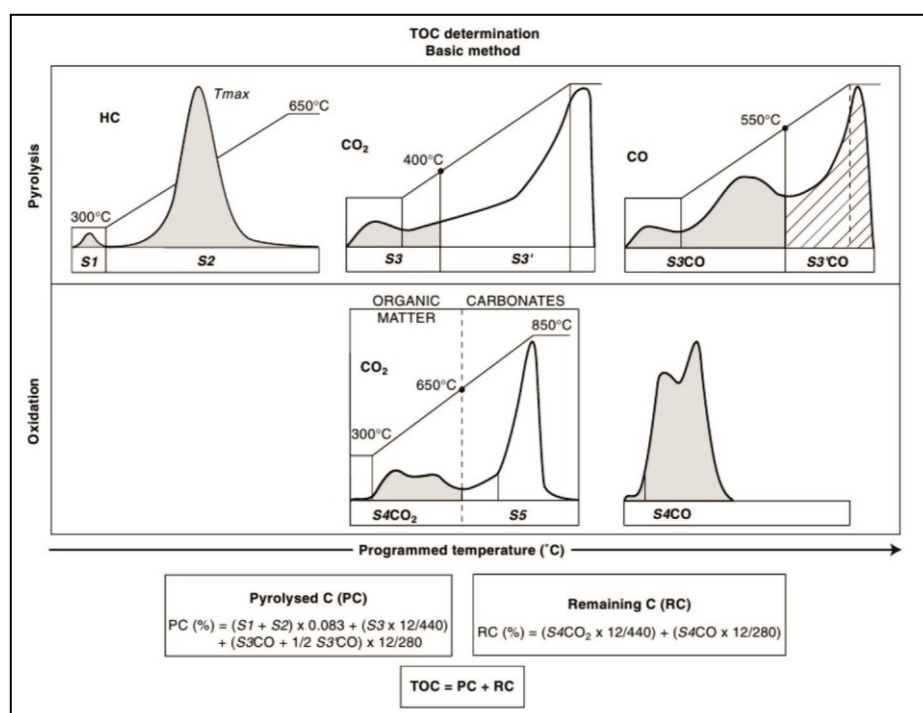


Figure 7: Calculation of TOC using RockEval 6 (after Behar, 2001)

In the present thesis the following parameters have been used (Espitalie et al. 1977):

**S1:** free hydrocarbons (HC) in sediment [mg HC/g rock sample]

**S2:** amount of HC formed from kerogen during pyrolysis [mg HC/g rock sample]

**S3:** amount of  $CO_2$  formed from kerogen during pyrolysis [mg  $CO_2$ /g rock sample]

**PI:** Production Index  $PI = \frac{S_1}{(S_1+S_2)}$

**HI:** Hydrogen Index      $HI = \frac{S_2}{TOC} * 100$  [mg HC/g TOC]

**OI:** Oxygen Index      $OI = \frac{S_3}{TOC} * 100$  [mg CO<sub>2</sub>/g TOC]

**T<sub>max</sub>:**                    Temperature, where the maximum amount of S<sub>2</sub> HC is formed [°C]

The HI and the OI are used to define different kerogen types. The description of the kerogen types follows (Tissot & Welte 1984; Peters & Cassa 1994).

- **Type I kerogen** has a high HI (> 600 mg HC/g TOC), a high initial H/C atomic ratio, and a low initial O/C atomic ratio. It is dominated by liptinite macerals. Vitrinite and inertinite occur in minor amounts. It is typical for lipid-rich algal or for severely biodegraded organic matter. Alkanes dominate the pyrolysis products. Although the sulfur content is low, sulfur-rich type I kerogen (IS) can occur. This type is typical for lacustrine environments.
- **Type II kerogen** occurs in many marine petroleum source rocks and oil shales. It has a high HI value (250-600 mg HC/g TOC) and moderately high H/C and low O/C ratios. Liptinite macerals dominate this type of kerogen but minor amounts of vitrinite and inertinite can occur. Sulfur is more abundant in this type than in other kerogen types and occurs in cyclic systems and in sulfide-compounds. High sulfur content is called IIS and generates petroleum at lower stages of maturity. It is usually related to marine sediments where an autochthonous organic matter, derived from a mixture of phytoplankton, zooplankton and microorganisms (bacteria), has been deposited in a reducing environment.
- **Type III kerogen** has a HI value between 50 and 250 mg HC/g TOC and low initial H/C but high initial O/C atomic ratio. This type contains remains of terrigenous plants and, therefore, it is dominated by vitrinite. Condensed and oxygenated functional groups are characteristic. Degradation by microorganisms is limited due to high sedimentation rates and rapid burial. If it is buried deep enough, it might be a good source rock for gas. But it is less convenient for oil generation.
- **Type IV kerogen** has a HI smaller than 50 mg HC/g TOC, low H/C ratio and a low to high O/C atomic ratio. Dominated by inertinite macerals, it can be derived from reworked or oxidized other kerogen types.

### 3.5 Leco

A Leco CS-300 analyzer at Montanuniversitaet Leoben was used to determine total carbon (TC) and total sulfur (S) contents. 70 to 80 mg powdered samples were pretreated with alcohol.

Dried samples were burnt at 1500 °C using an induction oven under oxygen atmosphere. Within this process, carbon reacts to CO<sub>2</sub>, which is determined by an infrared-detector. The CO<sub>2</sub> concentration gives information relating to the carbon content.

The total inorganic carbon (TIC) and the TOC/S ratio were calculated using the TC results.

$$\text{TIC}=\text{TC}-\text{TOC}$$

Assuming calcite to be the only carbonate mineral present, the calcite equivalent percentage can be calculated:  $\text{TIC} * 8.33$  (8.33 = molecular weight of CaCO<sub>2</sub>/molecular weight of C) (Bernard et al. 2004).

### 3.6 Biomarkers

The analysis of the biomarkers (see also Figure 8) was performed in the Fritz-Ebner-GC/MS-laboratory at the Chair of Petroleum Geology (Montanuniversitaet Leoben).

First, the powdered and weighted samples were put into an automatically extractor (Dionex ASE<sup>®</sup> 200 accelerated solvent extractor). There they were stowed with dichloromethane for one hour at 75 °C and 50 bars. Afterwards, the obtained extract was evaporated at 35 °C using a Zymark Turbo-Vap 500, closed cell concentrator. After drying overnight, the samples were weighted. The dried extract was combined with a mixture of hexane and dichloromethane (80:1 according to volume), centrifuged twice and finally decanted. Thereafter the heavy, insoluble fraction (asphaltene) and the soluble fraction (maltene) were dried and weighted. After solving the maltenes with hexane, they were put into a Köhnen-Willsch medium pressure liquid chromatography construction where they were separated into NSO components, aliphatic and aromatic hydrocarbons. Then, the extracts had to evaporate and dry. Subsequently, the aliphatic and aromatic fractions were weighted, solved with dichloromethane and charged with a standard (n-tetracosane and 1,1'-binaphthyl). The final analysis was made with a gas chromatograph, equipped with a 30 m DB-1fused silica capillary column (i.d. 0.25 mm), and coupled with a mass spectrometer (Finnigan MAT GCQ ion trap ms). The final oven temperature was 300 °C, the carrier gas was helium and the temperature of the injector was 275 °C. The mass spectrometer was operated in the electron impact mode over a scan range from 50 m/z to 650 m/z (0.7 s total scan time).

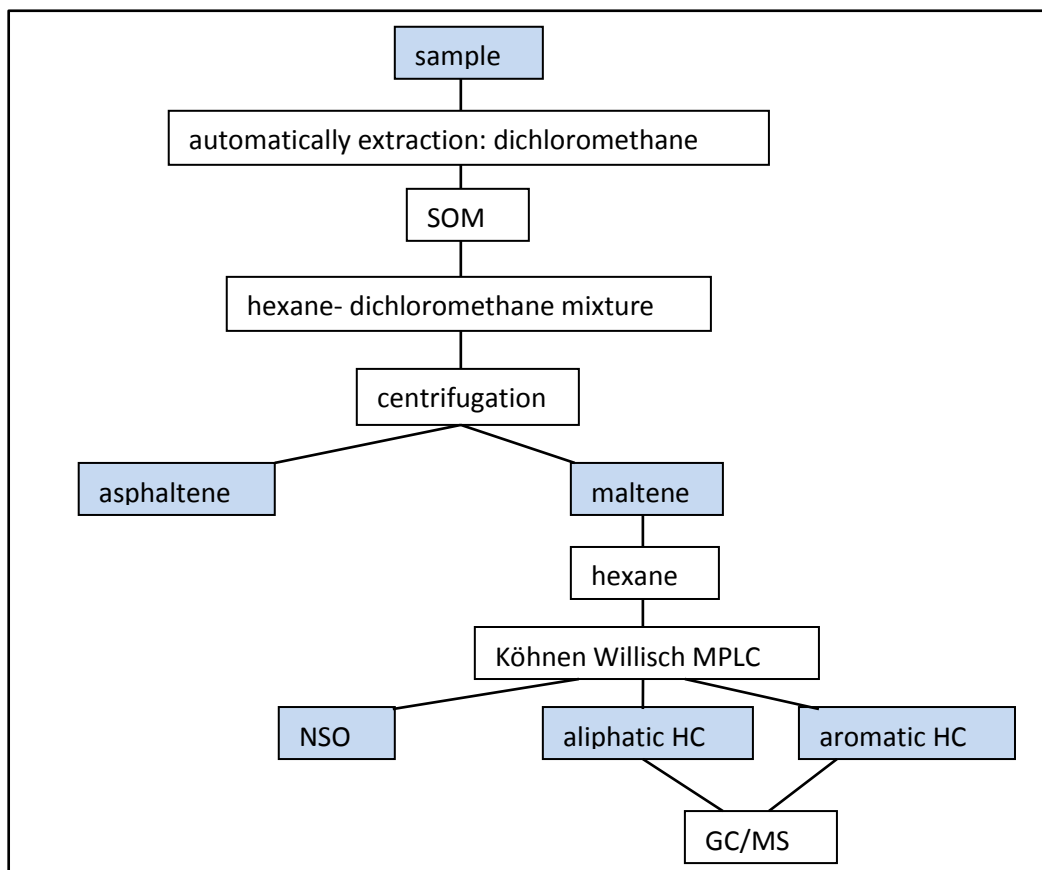


Figure 8: Procedure for biomarker analysis

For the data manipulation the Thermo Scientific™ Xcalibur software was used. The identification of the various components was made based on the retention time in the total ion current chromatogram and the mass spectra. Relative and absolute concentrations of aliphatic and aromatic components were calculated using integration and comparison of the various peaks. In addition, the usage of standards that were added to the extracts in a known concentration is necessary to calculate the concentrations. The concentrations were normalized to the TOC content, too.

Biomarkers are organic compounds that retained structural information present in their biological precursors. They are derived from lipids (fatty acids, alcohols, alkenones etc.) synthesized by phyto- and zooplankton, bacteria and plants. Their analysis provides information on the origin of organic matter in source rocks, the environmental conditions during deposition and diagenesis as well as the degree of biodegradation (Peters et al. 2005). Table 2 summarizes various biomarkers and their significance for the reconstruction of depositional environments, organic matter source and thermal maturity. A more detailed discussion is given in the following sections.

Table 2: Biomarkers for the characterization of the depositional environment, organic matter source and thermal maturity (Peters et al., 2005)

<b>Biomarker</b>	<b>Indicator</b>
Aryl-Isoprenoids	photic zone anoxia
<i>n</i> -alkanes: long chain middle chain short chain	higher plants macrophytes, algae or bank vegetation algae or microorganisms
Bicadinanes	angiosperms of the family Dipterocarpaceae
Botryococcane	<i>Botryococcus braunii</i> (race B-red) lacustrine algae
Cadalenes	higher plants
CPI	higher land plants (diagenesis)
C <sub>25</sub> HBI thiophenes	diatoms
β-Carotane	lacustrine depositional environment
Diasterane/Sterane	source rock mineralogy
Diterpanes (beyerane, phyllocladane, kaurane, pimarane, labdane)	gymnosperms (e.g. conifers of the family Podocarpaceae)
DBT/Phenanthrene	Availability of H <sub>2</sub> S
Hopanes	prokaryotes
Methylsterane	dinoflagellates or bacteria
Monoaromatic steroid aromatization TA/(MA+TA)	highly specific for immature to mature range
MTTC ratio	salinity
Oleanane	angiosperms
Pristane/phytane ratio	>3: oxic <1: anoxic
Steranes	eukaryotes
Sterane carbon number	depositional environment
Sterane/hopanes	high ratio: marine algal-dominated low ratio: prokaryote-dominated
Sterane isomerization 20S/(20S+20R)	highly specific for immature to mature range
Terpanes Ts/(Ts+Tm)	some interference from depositional environment; immature to mature or postmature range

\*) greyish marked biomarkers were used in present study

### 3.6.1 Chain Length Distribution

Long-chain n-alkanes (n-C27-31) with a marked odd- over even carbon number predominance are derived from epicuticular waxes synthesized by higher plants (Eglinton & Hamilton 1967). Short-chain n-alkanes (n-C15-19) are characteristic for the contribution of algae and microorganisms (Sabel et al. 2005), whereas intermediate homologues (n-C21-25) are formed by macrophytes, algae or bank vegetation (Ficken et al. 2000)

### 3.6.2 Carbon Preference Index (CPI)

The ratio of of n-alkanes with odd carbon numbers to those with even carbon numbers in the n-C24 to n-C34 range is reflected by the carbon preference index (CPI) (Bray & Evans 1961). The CPI is calculated as follows:

$$\text{CPI} = 0.5 * \left( \frac{C_{25} + C_{27} + C_{29} + C_{31} + C_{33}}{C_{24} + C_{26} + C_{28} + C_{30} + C_{32}} + \frac{C_{25} + C_{27} + C_{29} + C_{31} + C_{33}}{C_{26} + C_{28} + C_{30} + C_{32} + C_{34}} \right)$$

Immature material of higher land plants is dominated by odd-numbered n-alkanes (CPI >3). With proceeding diagenesis the odd over even predominance decreases leading to CPI=1.0. However, the contribution of organic matter from microorganisms and/or microbial activity may lead to decreasing CPI values.

### 3.6.3 Pristane/Phytane ratio

The source of the C<sub>19</sub> (pristane) and C<sub>20</sub> (phytane) isoprenoid hydrocarbons is the phytol side chain of chlorophyll (Didyk et al. 1978). Reducing or anoxic conditions in sediments promote cleavage of the phytol side chain to yield phytol, which undergoes reduction to dihydrophytol and then to phytane. Oxidic conditions promote the competing conversation of phytol to pristane (by oxidation of phytol to phytenic acid. decarboxylation to pristane, reduction to pristane) (Didyk et al. 1978). Phytane can be generated by phytanyl lipids which are formed by methanolic or halophilic bacteria (Sabel et al. 2005). Pristane might be formed from tocopherol (Goossens et al. 1984) as well.

Assuming chlorophyll as a source of pristane and phytane the Pr/Phy ratio can be used as a redox indicator (Didyk et al. 1978). Pr/Ph ratios <1 indicate anaerobic conditions during early diagenesis. In an oxic, dysaerobic milieu the Pr/Phy ratio is >1. However,

### 3.6.4 Arylisoprenoids

Arylisoprenoids are formed during early diagenesis by the diaromatic carotenoid isorenieratene (Hartgers et al. 1994). This accessory pigment is formed by the brown strain of the “green sulfur bacteria” Chlorobiacea (Sabel 2006). Chlorobiacea are anaerobic and photoautotrophic bacteria. Therefore they need light for the photosynthesis and H<sub>2</sub>S as a proton donor. Consequently, these bacteria live in the photic zone in anoxic environments and are an indicator for „photic zone anoxia“ (Hollander et al. 1993; Hartgers et al. 1994).

Unfortunately, 2,3,6-trimethyl substituted aryl isoprenoids can be generated also from other carotenoid precursors, such as β-carotane, so they are not specific markers of *Chlorobiaceae*. However, these bacteria are anomalously enriched in <sup>13</sup>C, and their pigments are isotopically heavy. In order to act as markers for photic zone anoxia, the isorenieratene derivatives must display heavy isotopic values (e.g. -10 to -20‰, around 15‰ heavier than algal lipids; (Koopmans et al. 1996)).

### 3.6.5 MTTC ratio

The origin of methylated 2-methyl-2-(trimethyltridecyl)chromans (MTTCs) is still under discussion (Hollander et al. 1993). Regardless of their potential biological precursor methylated MTTCs have been used for palaeosalinity reconstruction (Hollander et al. 1993). The MTTC ratio is defined as the concentration ratio of trimethyl MTTC relative to the sum of methylated MTTCs (Sinninghe Damsté et al. 1987).

### 3.6.6 Steranes, Hopanes

Steranes are derived from the sterols of cell membranes of eukaryotes, mainly algae and higher plants (Mackenzie et al. 1982). The conversion of sterols to steranes occurs without loss or gain of carbon atoms. Hence, the sterane carbon number distribution of a source rock or crude oil will reflect the carbon number distributions of the sterols of the organisms active in the depositional environment of the source rock, provided that there have been no significant losses of steranes with a particular carbon number during the maturation of the source rock. Based on the consistency of sterane carbon number distributions in large data sets of oils and extracts for a given source rock unit, it can be reasonably assumed that throughout maturation in the oil window no major changes in carbon number distribution occur (Sabel 2006).

Methylsteranes are specific for marine and non-marine dinoflagellates or bacteria. A freshwater setting contains more 4-Methylsteranes than a saline setting (Peters et al. 2005).

Hopanes found in the aliphatic fraction are pentacyclic triterpenoids derived from cell membranes of prokaryotes (heterotrophic bacteria and also phototrophic cyanobacteria) (Ourisson et al. 1979). The availability of benzohopanes is an indicator for evaporite or carbonate depositional environments. They are formed by cyclization of extended hopanoid side chains (Sabel 2006).

### 3.6.7 Gammacerane Index

The Gammacerane index (GI) is calculated as follows:

$$= \frac{\text{Gammacerane} * 100}{(\text{Gammacerane} + \text{C}_{30} 17\alpha(\text{H})21\beta(\text{H}) \text{Hopane})}$$

Gammacerane is a C<sub>30</sub> pentacyclic triterpane in which each ring contains six carbon atoms. Hypersaline, restricted marine and lacustrine environments often develop anoxic conditions if saline deep water is covered by water of lower density. Sedimentary rocks that were deposited under these conditions often contain high relative concentrations of gammacerane, which is a biomarker generally associated with water column stratification (Sinninghe Damsté et al. 1995).

Water column stratification is often accompanied by reduced oxygen content in bottom waters, which results in low Pr / Ph ratios.



### 3.6.8 Arboranes, Cadalenes, Diterpenoids, C<sub>25</sub> Thiophenes

The biological origin of arborane-type triterpenoids has been controversially discussed (Hauke et al. 1992). Derivates of arborane are formed during early diagenesis. They are derived from isoarborinol or arborinone (Sabel 2006). Isoarborinol was found in families of higher land plants (Sabel 2006). But it is also possible that fossil isoarborinol is formed by unknown aerobic bacteria or algae (Hauke et al. 1992).

Cadalene (4-isopropyl-1,6-dimethylnaphthalene) is a polycyclic aromatic hydrocarbon with the chemical formula C<sub>15</sub>H<sub>18</sub> and a cadinane skeleton. It is derived from generic sesquiterpenes and ubiquitous in essential oils of many higher plants. Cadalene, together with retene and simonellite, is a biomarker of higher plants. Abietatetraene, simonellite, tetrahydroretene and retene have been quantified. These compounds are aromatic diterpenoids of the abietane-type. They are found in fossil gymnosperms of the families Pinaceae, Taxodiaceae and Cupressaceae (Sabel 2006). A taxonomic classification of various conifers is not possible based on the relative abundances of diterpenoids.

The C<sub>25</sub> highly-branched isoprenoid (HBI) alkenes have been identified in recent diatoms from the genera *Haslea* and *Rhizosolenia* (Sabel et al. 2005). Based on the structure and the position of double bonds, the compounds readily incorporate inorganic sulfur during diagenesis leading to the formation of HBI thiophenes. They are considered to be omnipresent in recent coastal sediments and are common in lake sediments (Peters et al. 2005). As diatoms evolved during the Jurassic, HBIs (highly branched isoprenoids) can be used as an age-related marker. The compounds are applicable to chemostratigraphic studies and may provide facies markers for source rocks deposited in upwelling zones when seasonal diatom blooms occur (Peters et al. 2005). Abundant nutrients linked with coastal upwelling result in increased biological productivity. An oxygen minimum zone promotes preservation and a widespread occurrence of source facies dominated by diatom input (Peters et al. 2005).

### 3.6.9 DBT/Phenanthrene

Both phenanthrene (Phen) and dibenzothiophene (DBT) are not inherited from the biomass but are products of early diagenesis. Thus, the DBT/Phen ratio is predominantly controlled by the environment. While the detailed synthetic pathway for the formation of DBT is under discussion, its origin must be attributed to the interaction of hydrogen sulfide or polysulfides with an organic substrate. This fact implies that the DBT/Phen ratio reflects the availability of reduced sulfur for interaction with organic matter in the depositional/diagenetic environment (Bechtel et al. 2012). Sufficiently high SO<sub>4</sub><sup>-</sup> ion concentrations (such as found in seawater), the presence of sulphate-reducing bacteria, and sufficiently low concentrations of reactive iron are additional prerequisites for high DBT/Phen ratios. The DBT/Phen ratio is also a good discriminator of siliciclastic versus non-siliciclastic source rock lithologies (Hughes et al. 1995).

A low DBT/Phen and a Pr/Ph ratio <1 indicate reducing depositional conditions where low sulphate ion concentrations precluded the formation of significant amounts of reactive sulfur. Those values occur in lacustrine settings or in fresh to brackish environments in which sulphate reduction is replaced by fermentation (Hughes et al. 1995).

Samples with a DBT/Phen ratio <1 and Pr/Ph ratio between 1 and 3 contain a slight to moderate excess of pristane over phytane and represent marine or lacustrine siliciclastic source rocks (Hughes et al. 1995).

### 3.7 Inorganic geochemistry and proxies

The element composition of about powdered 50 samples has been determined using a handheld XRF instrument Nitron XL3t at the Department of General and Analytical Chemistry (Montanuniversitaet Leoben). In a first step, the reliability of these data has been cross-checked against traditional XRF pellets. Three samples were chosen and two pellets were made of each sample. For this, the pellet was formed using 1 g of powdered and burned sample and 8 g of di-lithium-tetra borate. After melting this mixture with the Fusion Machine Type VAA2 and cooling of the pellet, the pellet was put into the x-ray spectrometer PANalytical Axios. The final interpretation was made using GeoWSU calibration.

The significance of selected element concentrations for the reconstruction of depositional environments are discussed in the following sections.

#### 3.7.1 TOC, S, Fe

TOC (RockEval), sulfur (Leco) and Fe concentrations (XRF) can be used to make statements on redox conditions during sediment accumulation.

The TOC/S ratio is determined by the oxygenation level of bottom water, whereby oxic marine deposits are typically characterized by a TOC/S ratio of 2.8 (Hofmann et al. 2000). Lower TOC/S ratios and sulfur contents independent from the TOC content are often found in anoxic/euxinic environments. High TOC/S ratios may indicate environments with reduced salinity, where sulphate is totally consumed via sulphate reduction at sediment depths of only a few centimeters, leaving behind little pyrite and much organic matter (Berner 1984).

Dean & Arthur (1989) introduced a triangle plot to show relative concentrations of TOC, S and Fe independent of dilution effects caused by biogenic silica or  $\text{CaCO}_3$  (Figure 9). The pyrite line indicates an S/Fe ratio of 1.15 (54 % S and 46 % Fe) and the TOC/S line represents a ratio of 2.8 (Dean & Arthur 1989). An S/Fe ratio above 1.15 is possible if samples contain some other form of sulfur in addition to pyrite, like gypsum, organic-sulfur or barite. The alignment along the normal marine line is an indicator for an oxic depositional environment without iron limitation (Berner 1984; Dean & Arthur 1989).

Pyrite is formed in anoxic marine sediments by the reaction of dissolved hydrogen sulfide, produced by microbial sulphate reduction, with detrital iron-bearing minerals (Berner 1970; Berner 1984; Raiswell & Canfield 1998) (Figure 9). Although there are a variety of transformation pathways, the extent of pyrite formation is thought to be limited either by the microbial production of sulfide or by the availability of reactive iron minerals (Raiswell & Canfield 1998).

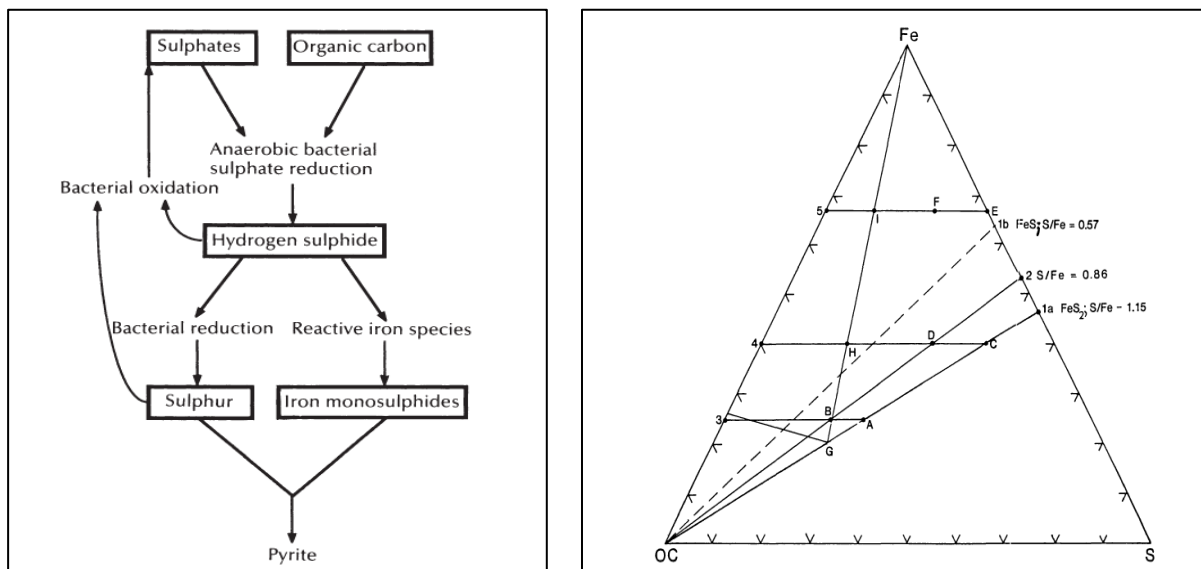


Figure 9: Geochemical process involved in the formation of pyrite (Berner 1984) and Fe-S-OC ternary diagram showing key constant ratio lines of pyrite formation (Berner 1984)

Moreover, differences in the metabolizability of organic matter by sulphate-reducing bacteria may cause variations in TOC/S ratios (Dean & Arthur 1989). Under *anoxic* bottom water conditions relatively fresh planktonically-derived organic material becomes available for bacterial sulphate reduction. Therefore, organic accumulation and bacterial sulphate reduction is high causing  $H_2S$  to build up in the bottom water and in the underlying sediments (Sweeney 1980). Within *euxinic* conditions pyrite can form in the water column, although there are only low amounts of organic matter. **Berner (1984)** figured out, that it is common, that under these conditions a higher proportion of less reactive iron minerals were converted to pyrite.

### 3.7.2 Molybdenum

Mo is enriched in reducing sediments relative to crustal values (Crusius et al. 1996; Tribovillard et al. 2004). Therefore, Mo concentrations preserve information of local redox conditions at the time of sediment formation (Dean & Arthur 1989; Tribovillard et al. 2004). Mo reflects euxinic conditions at the sediment-water interface or in the water column (Tribovillard et al. 2004; Bunte 2009). Sedimentary Mo accumulation is associated with the change from oxic to anoxic-sulfidic conditions on the seafloor (Algeo & Lyons 2006) (Figure 10).

In deep water exchange limited basins, aqueous Mo concentrations can seriously decimate through removal to the sediment without adequate resupply (Algeo & Lyons 2006). Reduced availability of aqueous Mo may leave a signature in the trace metal chemistry of organic-rich sediments, in which most Mo is of hydrogenous origin (Algeo & Lyons 2006).

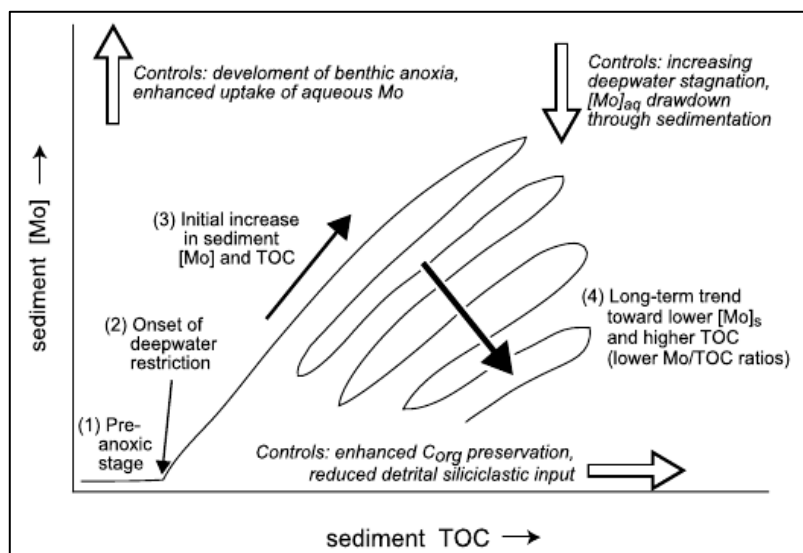


Figure 10: Generalized patterns of sedimentary Mo-TOC covariation associated with deepwater renewal in silled anoxic basins (Algeo & Lyons 2006)

Classifications of anoxic paleoenvironments using Mo/TOC relationships were applied by (Algeo & Lyons 2006). Sedimentary Mo/TOC ratios are useful to distinguish degrees of restriction of the subchemocline water mass in anoxic marine environments, with values of  $>35$ ,  $15\text{--}35$ , and  $<15(\times 10^{-4})$  associated with weak, moderate, and strong restriction (Algeo & Lyons 2006).

(Emerson & Huested 1991) showed that the concentrations of Mo and V in the water column are usually lower in anoxic basins than in oxic seawater due to their admission into highly anoxic sediments. They postulate that concentrations of Mo and V are controlled by their flux to sediments and water renewal from outside the basins and not by changes in the water column anoxia. This statement is supported by the absence of a systematic relationship between the deep-water Mo or V concentrations and  $\text{H}_2\text{S}$  content.

### 3.7.3 Vanadium and Nickel

V burial under anoxic conditions is known to be linked to OM (Emerson & Huested 1991; Morford & Emerson 1999). Similar to Mo, V is unreactive in oxic seawater. Therefore, both elements are concentrated in sediments overlain by anoxic waters (Brumsack & Gieskes 1983; Brumsack 1986). Under oxic conditions, vanadium should occur as V(V). V(IV) forms vanadium ions ( $\text{VO}^{2+}$ ) in a moderate reducing environment. By surface adsorption or by formation of organometallic ligands, the vanadium ions can be transferred to the sediment (Emerson & Huested 1991; Morford & Emerson 1999). Further reduction causes V to be reduced to V(III) by  $\text{H}_2\text{S}$ , which is released by bacterial sulphate reduction. V(III) can be taken up by geophyrins or be precipitated as the solid oxide  $\text{V}_2\text{O}_3$  or hydroxide  $\text{V}(\text{OH})_3$  phase (Bunte 2009). V can accumulate under a denitrifying environment.

(Lewan 1984) demonstrated that  $\text{V}/(\text{V}+\text{Ni})$  for OM that accumulated under euxinic conditions should be greater than 0.5. (Hatch & Leventhal 1992) compared  $\text{V}/(\text{V}+\text{Ni})$  ratios to other geochemical redox indicators, including degree of pyritization, and suggested ratios greater than 0.84 for euxinic conditions, 0.54–0.82 for anoxic waters, and 0.46–0.60 for dysoxic conditions.

### 3.8 Organic Petrology (VR, Maceral analysis)

For microscopically analysis polished blocks of selected core samples (chosen according to TOC contents) were prepared. A LEICA microscope was used to determine vol. % of maceral groups and pyrite. At least 400 points have been determined using incident and blue light excitation and point counting transects. Vitrinite reflectance was determined using the same instrument and following established procedures (Stach 1982). Results are presented as mean random reflectance values (Rr).

### 3.9 Pyrolysis-GC

Pyrolysis gas chromatography (Py-GC) analyses were done by GFZ Potsdam (GeoS4 GmbH) using the Quantum MSSV-2 Thermal Analysis System©. Thermally extracted (300°C, 10 min.) whole rock samples were heated in a flow of helium, and products released over the temperature range 300 to 600°C (40 K/min) were focused using a cryogenic trap, and then analyzed using a 50 m x 0.32 mm BP-1 capillary column equipped with a flame ionization detector. The GC oven temperature was programmed from 40°C to 320°C at 8°C/min. Boiling ranges ( $C_1$ ,  $C_{2-5}$ ,  $C_{6-14}$ ,  $C_{15+}$ ) and individual compounds (*n*-alkenes, *n*-alkanes, alkylaromatic hydrocarbons and alkylthiophenes) were quantified by external standardization using *n*-butane. Response factors for all compounds were assumed the same, except for methane whose response factor was 1.1.

### 3.10 Nannoplankton

Calcareous nannoplankton was studied on 80 samples by Stjepan Coric (Austrian Geological Survey, Vienna). Semi-quantitative investigations were performed on smear slides, which were prepared using standard techniques. Before preparation small amounts of sediment were treated by ultrasound in distilled water for a few seconds. Smear slides were analyzed with a light microscope less than 1000x (Leica DMLP microscope) magnification (crossed and parallel nicols).

## 4 Results

### 4.1 Lithology

The Tazlau profile has been recently logged by Amadori et al. (2012) and Guerrera et al. (2012). Some layers near the base of the profile (Globigerina Marls Mbr. of the Bisericani Fm., Lower Menilites Mbr.) could not be observed during the field work in July/August 2012. Therefore, the results of Amadori et al. (2012) and Guerrera et al. (2012) were considered in the present study.

For an overview, the profile, 700 m thick, is divided into a lower and an upper part in Figure 11 and Figure 14.

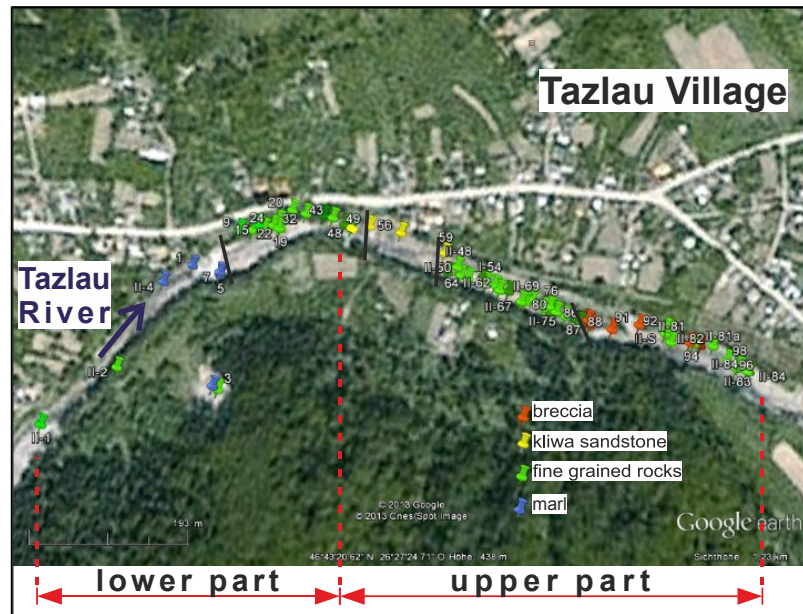


Figure 11: Overview of studied profile. The color code represents different lithologies. The boundary between the lower and upper part of the section (see Figure 14) is also shown

Compass measurements show a relative uniform north-south-strike. Higher dip angles (80°) are recognizable in greyish shales of the Gura Soimului Fm.



Figure 12: Overview of studied profile with strike and dip. Colored boxes show sample number

The studied section is described in the following from the base to the top:

#### 4.1.1 Bisericani Formation (BF)

The section starts with poorly exposed mudstones with low carbonate contents ( $\sim 8\%$  calcite<sub>equiv.</sub>). These rocks are attributed to the Bisericani Formation (Amadori et al. 2012).

#### 4.1.2 Menilite Formation

##### 4.1.2.1 Lower Menilite Member (LMM)

Siliceous shales and black shales of the LMM, about 4 m thick, have been described by Amadori et al. (2012), but have not been exposed during the field campaign in 2012.

##### 4.1.2.2 Bituminous Marl Member (BMM)

The carbonate-rich BMM (Figure 13) is about 70 m thick and has a bright brown/grey color. The color of the weathering crust is white. The BMM contains discontinuous darker (bituminous) layers (mm range) and chert beds. Layers with quartzarenites occur frequently forming lenses and small channels (5 cm in height) and often exhibit load- and flame structures. Rare vertical and horizontal bioturbation features are recognizable and often concentrated in distinct layers. The sedimentary structures show parallel and low angle cross-bedding and interlayers of sandstones with wave ripple cross-lamination. Slumping structures are common.

In agreement with lithology, the carbonate content is relative high ( $\sim 31.6\%$ , see chapter 4.4 Bulk geochemical parameters).



Figure 13: Bituminous Marl Mbr.: Marl with thin sandstone lenses (sample 3)

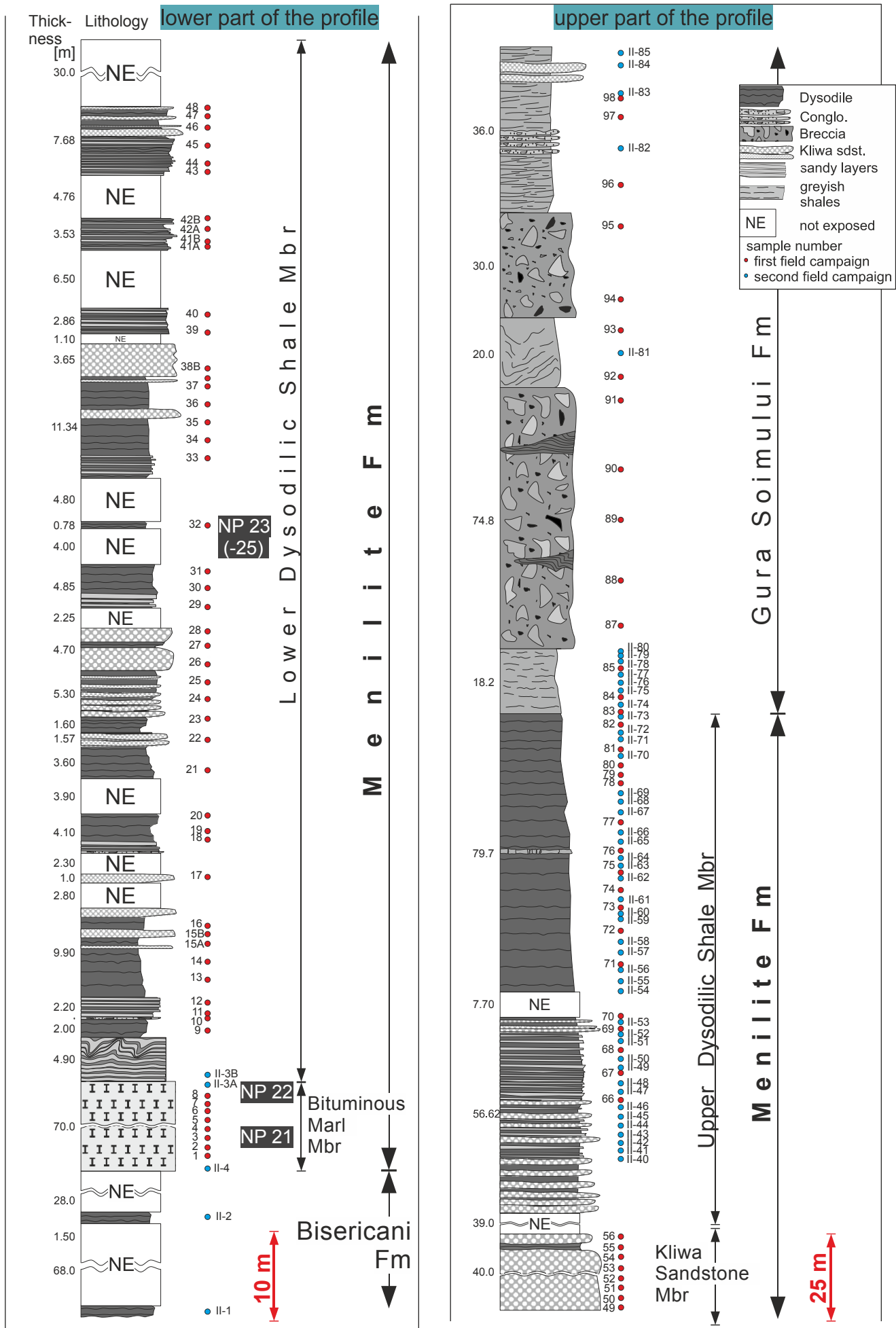


Figure 14: Lithological Profile of the Tazlau section. Note the different scale!



#### 4.1.2.3 Lower Dysodilic Shale Member (LDSM)

The contact between the marls of the BMM and the largely carbonate free LDSM is not exposed. The LDSM, 100 m thick, comprises silty-sandy black shale (dysodiles) with some intercalated thin-bedded Kliwa-type sandstone layers (Figure 15). Matrix-supported polygenic conglomerates with green clasts (sample 10) occur in the lower part of this member.

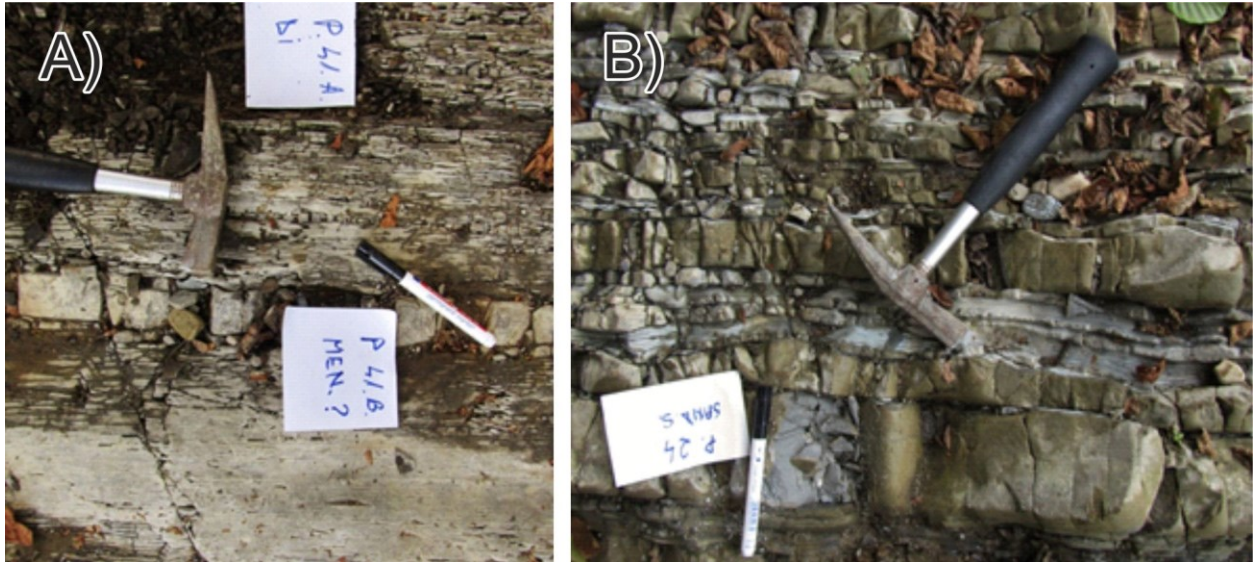


Figure 15: Lower Dysodilic Shale Mbr.: Alternation of Kliwa-type sandstone and black shale. A) samples 41A/B, B) sample 42

#### 4.1.2.4 Kliwa Sandstone Member (KSM)

The KSM separates the LDSM from the Upper Dysodilic Shale Mbr. (UDSM). It is 40 m thick and is composed of sandstone beds with a thickness of 1 to 2 m.

#### 4.1.2.5 Upper Dysodilic Shale Member (UDSM)

The UDSM is about 130 m thick. It consists of largely carbonate-free black shale and layers with quartzarenites (similar to those described within the LDSM) and subarkoses.

The lower part of the UDSM (samples 40 - 66) is characterized by an alternation of dysodilic shales with Kliwa-type sandstone layers, up to 50 cm thick (Figure 16). This interval is overlain by a succession with less sandstone beds, which are typically only 1 to 2 cm thick (samples 66-70). Slumping structures are present in this interval (Figure 16). This section will be called “heterogeneous part of the UDSM” in the following.

The upper part of the UDSM, about 80 m thick, is formed by dysodilic shale (Figure 16) with very rare sandstone (1 - 2 cm thick) layers (“homogeneous part of the UDSM”).

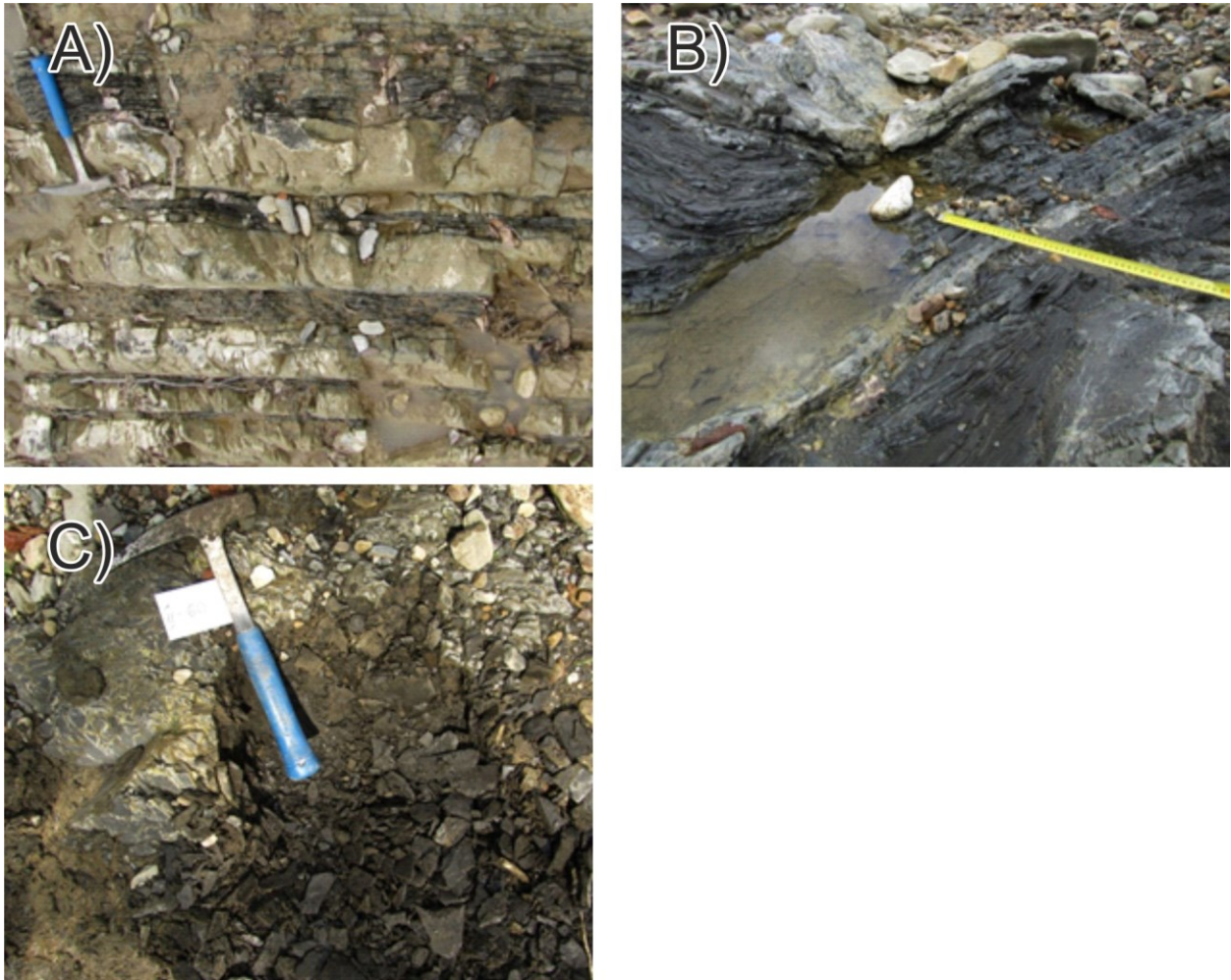


Figure 16: Lower Dysodilic Shale Mbr. A) Alternation of Kliwa-type sandstone and black shale (sample II-41), B) Slump (sample II-48), C) Black Shales (sample II-60)

#### 4.1.3 Gura Soimului Formation (GSF)

The boundary between the UDSM and the Gura Soimului Formation (GSF) is characterized by a change in the orientation of strike and dip and by a transition from (dark) gray to grayish-greenish mudstones. The latter prevail in the lower 20 m of the GSF (Figure 17A).

The mudstone interval is overlain by a mega breccia, interpreted as an olisthostrome. This polygenic conglomerate contains metamorphic and sedimentary clasts, up to 100 cm in diameter (Figure 17B). Metamorphic clasts include green phyllites, schists and quartzites supplied from a metamorphic basement, sedimentary components are represented by bright limestones, menilites, dysodilic shale, and Kliwa sandstones. The breccias are interbedded with greenish sandstones and slumped black shales.

Hard greyish shales occur between breccia layers. Some of these shales have sulfur impregnation and therefore, show a yellowish-greenish color (Figure 17C). The calcium carbonate content is generally very low. Thick shale layers (>10 m) often show slumping structures. Thin shale layers are often discontinuous.

The uppermost 35 m of the GSF include slumped beds of shales with sandstone interlayers (Figure 17D) as well as a conglomerate layer. The GSF is the youngest unit in the Bistita half-window of the Vrancea Nappe. The Vrancea Nappe is in tectonic contact with the “salted breccia and gypsum formation” of the Pericarpethian Nappe (Amadori et al. 2012).

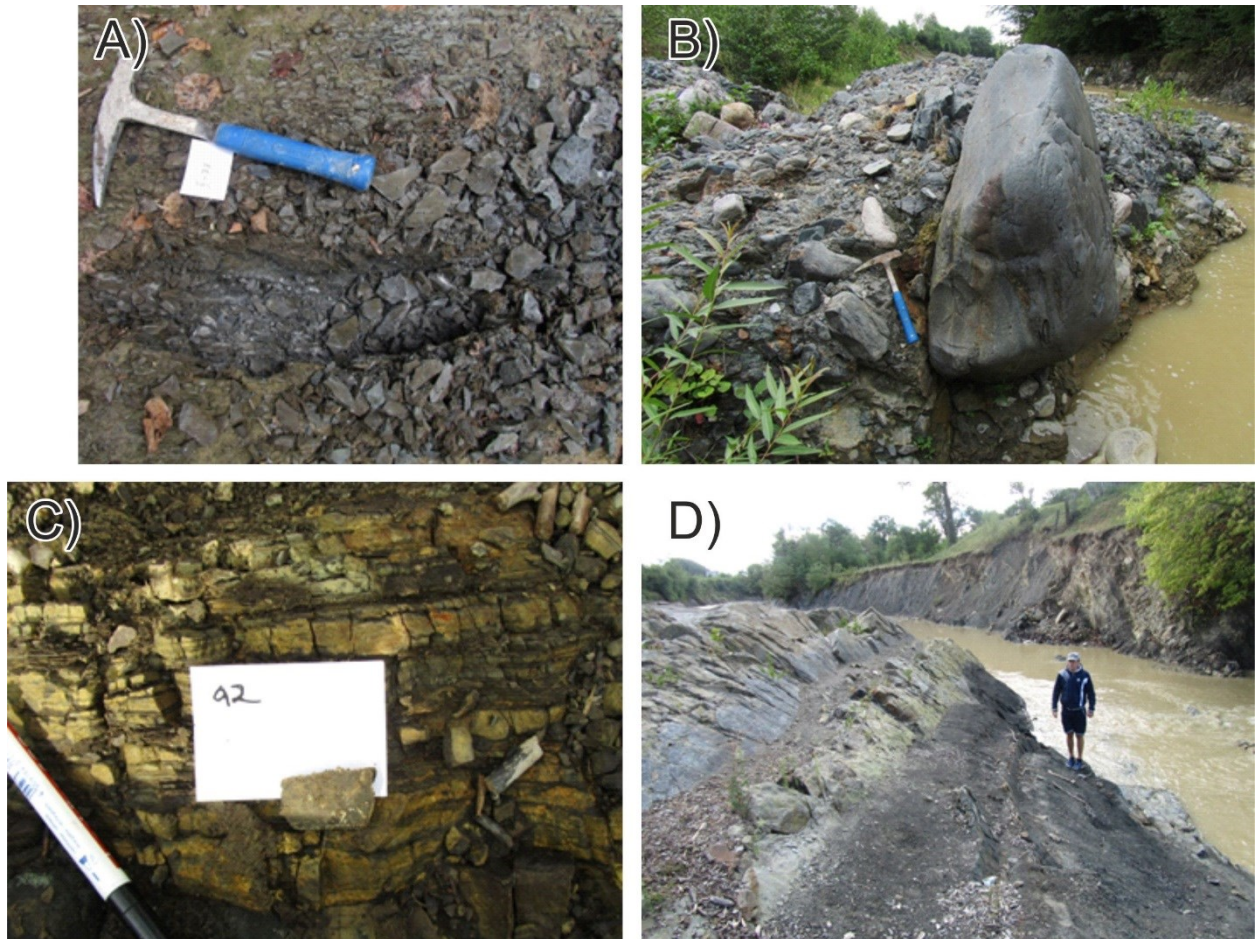


Figure 17: Gura Soimului Fm. A) Greyish shale (sample II-77), B) mega breccia, C) greyish shale (sample 92), D) sandstone layers in the uppermost part of the GSF

## 4.2 Calcareous Nannoplankton (Stjepan Coric)

Samples 1 to 8 from the **Bituminous Marl Mbr.** contain calcareous nannoplankton. Sample 5 contains *Ericsonia formosa* and *Reticulofenestra* but no *Ericsonia subdisticha*, so it might represent the upper nannoplankton zone NP21 zone (lower Rupelian). A lot of autochthonous nannoplankton with *Isolithus recurvus* and *Reticulofenestra umbilica* was found in sample 8. Consequently this sample represents the Rupelian NP 22 zone.

Samples 6 to 19, 22 to 26, 33 to 42B from the **Lower Dysodilic Shale Mbr.** are sterile in terms of calcareous nannoplankton (41B contains calcite crystals), but contain plant remains. Sample 10A, which underlies a conglomerate layer, contains redeposited material from the lower Eocene.

Diatoms are found in sample 20 and calcite crystals in samples 21 and 27. Sample 30 contains a low amount of nannoplankton, without *Reticulofenestra umbilica* but with more *Cyclicargolithus floridanus*. This might indicate NP 23, but could also represent NP 23-25. However markers for NP 24/25 are missing.

Samples 43-45A are sterile and contain plant remains. Sample 46A includes a few *Coccolithus pelagicus*. 46B contains diatoms (similar to diatoms from the Lower Badenian in Croatia, where they represent the beginning of a transgression).

The rest of the samples is sterile, only number 60 from the *Upper Dysodilic Shale Mbr.* contains a few *Reticulofenestra* sp.

### 4.3 Spectral gamma radiation

A spectral outcrop gamma log has been recorded using data from 142 sites, including almost all sample sites. Although radiation in sandstone beds has been determined as well, mudstone beds are overrepresented.

The used tool provides information on total dose radiation (DR) and the concentrations of uranium, potassium and thorium. Although the reliability of element concentrations (esp. potassium) is considered low all data are presented in this section.

Correlations between DR and element concentrations (Figure 18) suggest that DR is strongly correlated with uranium ( $R^2= 0.98$ ) and thorium ( $R^2=0.82$ ), but weakly with potassium ( $R^2=0.26$ ; Figure 20). However, because element concentrations are considered unreliable, the significance of these correlations must not be overestimated.

DR and element concentrations for all samples are summarized in the Appendix. The value ranges and average values for the Bisericani and Gura Soimului formations and each member of the Menilite Formation are shown in Table 3.

#### 4.3.1 Bisericani Formation (BF)

The values of this formation are statistically not meaningful (only two measuring points). In general, the values of DR, U, Th and K are similar for both sites (see Table 3).

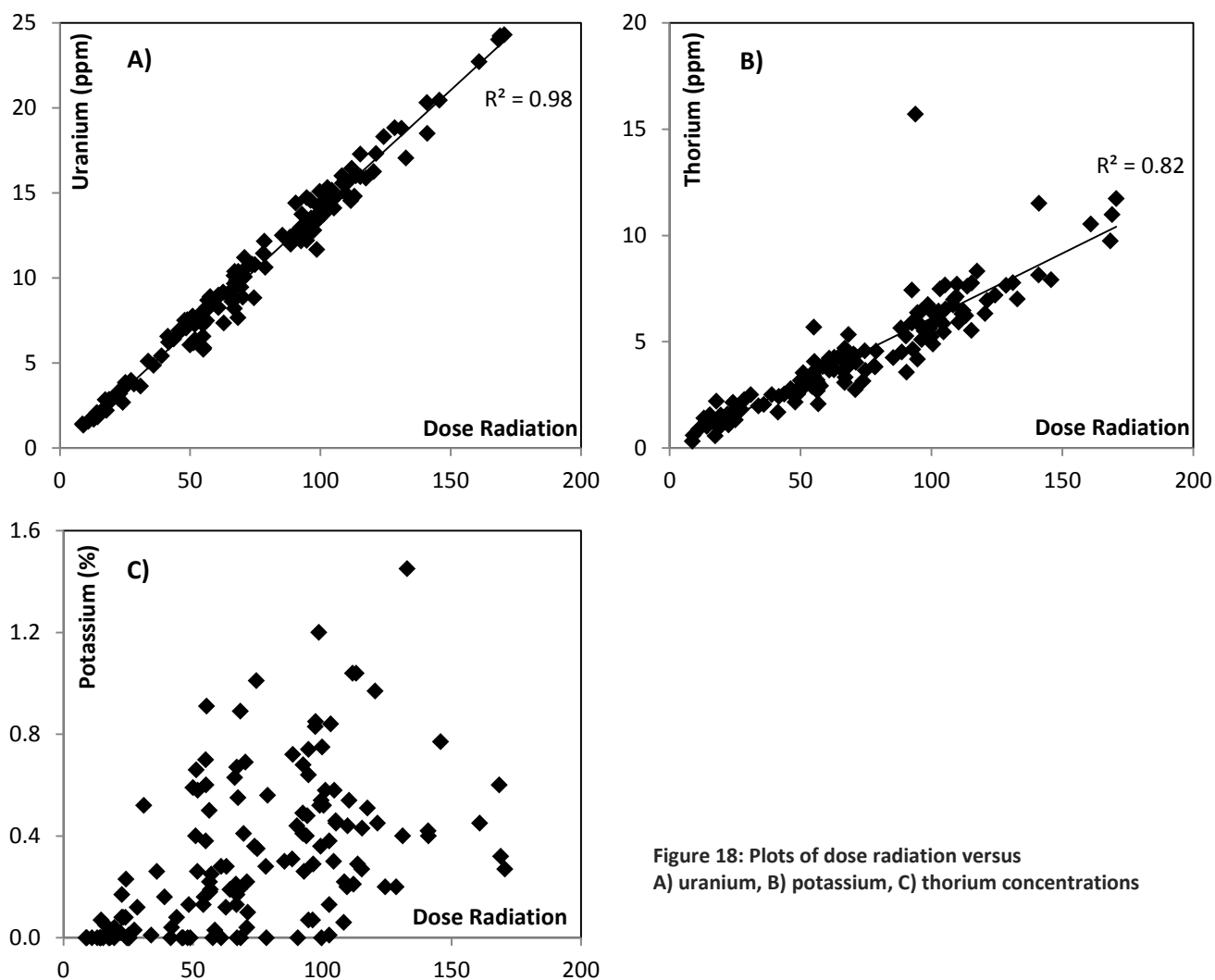


Figure 18: Plots of dose radiation versus  
A) uranium, B) potassium, C) thorium concentrations

Table 3: Comparison of dose rate, uranium, thorium and potassium concentrations in different stratigraphic units

Formation/ Member	Samples	Dose Radiation [nGy/h]	Uranium [ppm]	Thorium [ppm]	Potassium [%]
<b>Gura Soimului Fm.</b>	28	min-max 41.4-168.4 average 86.6	6.4-24.0 12.3	1.7-9.7 4.6	0-1.4 0.4
<b>Upp. Dysodilic Shale Mbr.</b>	50	min-max 8.7-170.7 average 93.5	1.4-24.3 13.32	0.3-11.7 5.7	0-0.8 0.3
<b>Kliwa Sdst. Mbr.</b>	8	min-max 9.1-23.0 (67.1*) average 15.9 (22.3*)	1.3-3.3 (8.2*) 2.2 (3.0*)	0.6-1.6 (4.7*) 1.1 (1.6*)	0-0.08 (0.67*) 0.03 (0.11*)
<b>Low. Dysodilic Shale Mbr.</b>	45	min-max 14.4-109.8 average 61.0	1.8-15.1 8.2	1.1-15.7 4.0	0-1.2 0.4
<b>Bituminous Marl Mbr.</b>	10	min-max 13.1-31.1 average 22.7	1.7-3.8 3.0	0.9-2.5 1.7	0-0.5 0.1
<b>Bisericani Fm.</b>	2	min-max 49.0-68.5 average 58.8	7.5-10.4 8.9	2.5-3.9 3.2	0 0

\*) Values of interbedded shale layer

## 4.3.2 Menilite Formation

### 4.3.2.1 Bituminous Marl Member (BMM)

Low concentrations of radioactive elements and, consequently, low dose radiation (DR) values are characteristic for the carbonate-rich rocks of the BMM. Values of DR, U and Th show a small range between minimum and maximum values. In contrast, potassium concentrations show stronger variations. Figure 19 shows a negative correlation ( $R^2 = 0.61$ ) between DR and total inorganic carbon (TIC) content, implying that DR is largely controlled by the carbonate content.

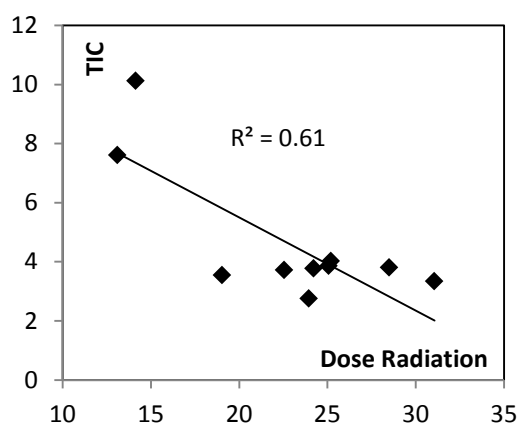


Figure 19: Plot of dose radiation versus total inorganic carbon (TIC) for the Bituminous Marl Mbr.

### 4.3.2.2 Lower Dysodilic Shale Member (LDSM)

The concentration of radioactive elements in the LDSM is controlled mainly by its shale content. Consequently, DR is higher in the LDSM than in the BMM (Table 3, Figure 20). Strongly varying values reflect the alternation between shale-rich and sand-rich layers.

### 4.3.2.3 Kliwa Sandstone Member (KSM)

Kliwa sandstones yield low values (which are connected to one curve in Figure 20). Concentrations of radioactive elements and DR of an interbedded shale layer are significantly higher (see Table 3, values written in brackets).

### 4.3.2.4 Upper Dysodilic Shale Member (UDSM)

Relative low and strongly varying values of DR, U and Th are measured in the sand-rich lower part of the UDSM. Higher values are observed in the shale-rich, more homogeneous upper part of the UDSM and reach maxima near the top of the UDSM (Figure 20).

## 4.3.3 Gura Soimului Formation (GSF)

Values in the greyish shales near the base of the GSF decrease upwards (Figure 20). The fluctuation seems to decrease as well, but this might be an effect caused by the larger distance between sampling points. Nevertheless, the values of DR, U and Th decrease while the concentration of potassium slightly increases (0.42 %). At the same time, however, it should be noted that measured values of the matrix might be influenced by the components as well (due to the partly low content of the matrix material).

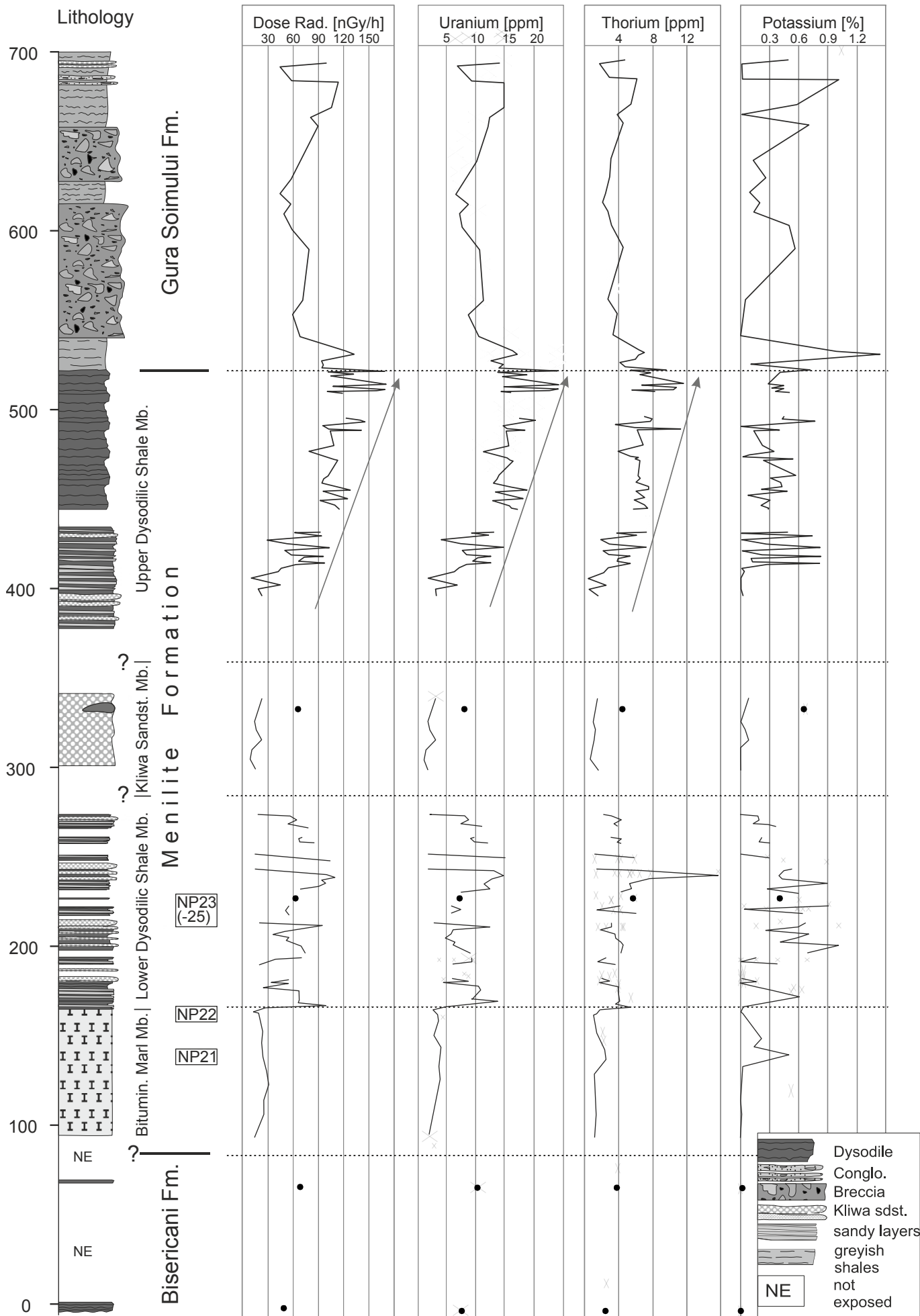


Figure 20: Depth trends of dose radiation, and radioactive elements

## 4.4 Bulk geochemical parameters

Analytical results are summarized in the Appendix. Average values together minimum and maximum values for each unit are listed in Table 4. The vertical variation of bulk parameters (TOC, CaCO<sub>3</sub>, S, TOC/S, HI, OI) is shown in Figure 21 and Figure 22. TOC is plotted versus sulphur contents for each unit in Figure 23. Crossplots of HI versus OI, HI versus T<sub>max</sub>, and S<sub>2</sub> versus TOC are shown in Figure 24.

Rock Eval parameter T<sub>max</sub> varies between 412 to 437°C. The average value (423°C) indicates that the organic matter is immature. There is no increase of T<sub>max</sub> with depth recognizable.

Table 4: Total organic carbon (TOC), CaCO<sub>3</sub>, sulphur (S), TOC/S and hydrogen index (HI) for different stratigraphic units

Formation/ Member	Samples	TOC [%]	CaCO <sub>3</sub> [%]	S [%]	TOC/S	HI [mgHC/ g TOC]	
<b>Gura Soimului Fm.</b>	21	min-max	0-1.59	0-7.25	0.02-2.88	0-8.26	0-331
		average	0.38	2.33	0.53	1.55	102
<b>Upper Dysodilic Shale Mbr.</b>	44						
homogeneous part (II-54-II-73)		min-max	0.63-13.39	0-14.83	1.65-7.18	0.18-3.37	86-460
		average	3.04	1.5	3.71	0.82	343
heterogeneous part (II-40-70)		min-max	0.51-3.87	0-0.92	0.35-3.38	0.93-1.45	252-403
		average	1.78	0.25	1.49	1.23	351
<b>Kliwa Sdst Mbr.</b>	1		0.73	0	0.42	1.75	386
<b>Lower Dysodilic Shale Mbr.</b>	45	min-max	0.06-13.22	0-10.5	0.10-2.75	0.21-6.22	50-695
		average	2.62	1.17	1.43	1.71	391
<b>Bituminous Marl Mbr.</b>	10	min-max	1.12-2.25	22.89-84.34	0.27-1.18	1.78-5.18	378-642
		average	1.72	38.76	0.48	3.95	530
<b>Bisericani Fm.</b>	2	min-max	0.62-0.74	6.16-10.16	0.83-1.01	1.78-1.82	170-251
		average	0.68	8.25	0.92	1.80	211



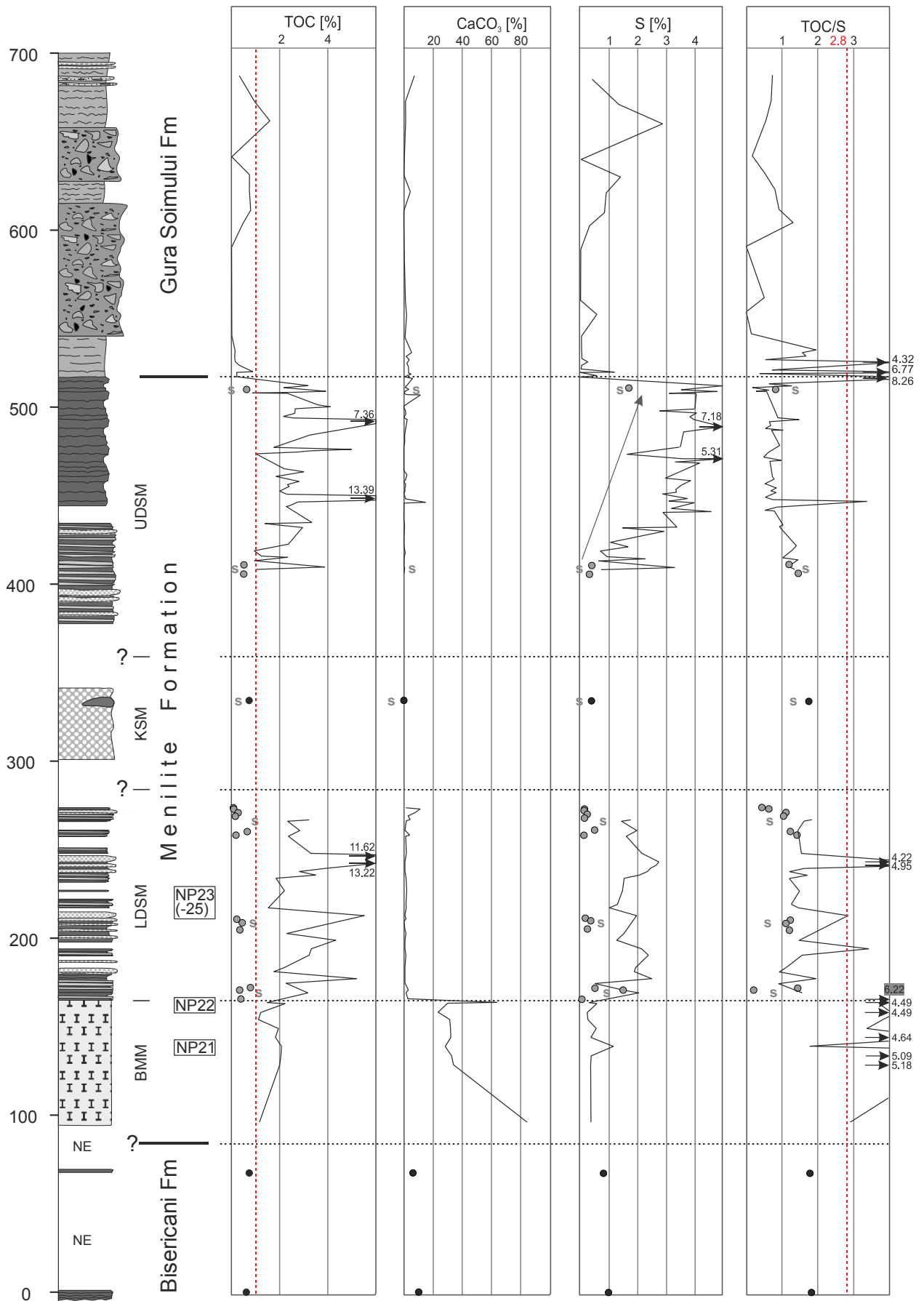


Figure 21: Vertical variation of bulk geochemical parameters (total organic carbon [TOC], CaCO<sub>3</sub>, sulfur [S], TOC/S)

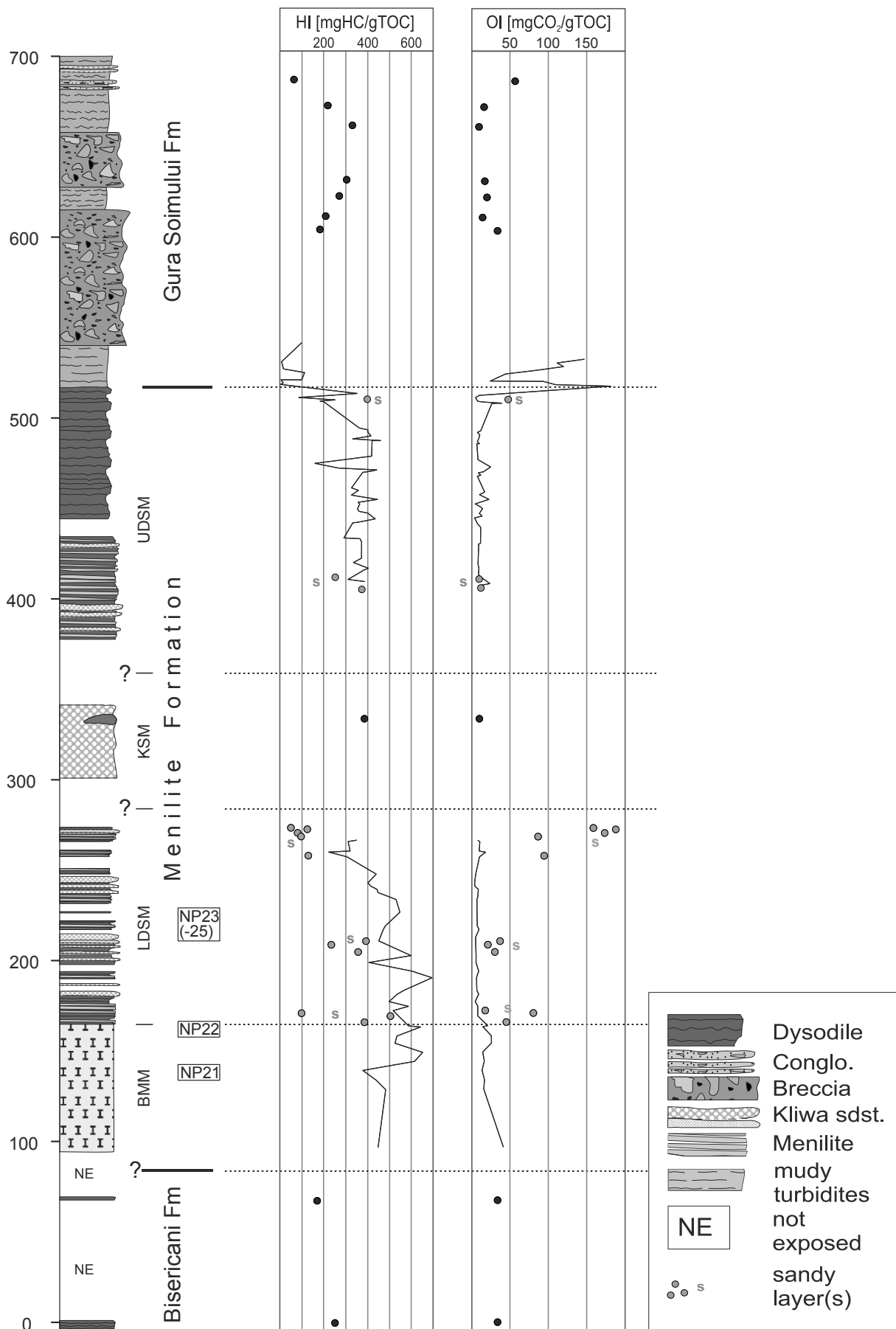


Figure 22: Vertical variation of hydrogen index (HI) and oxygen index (OI)

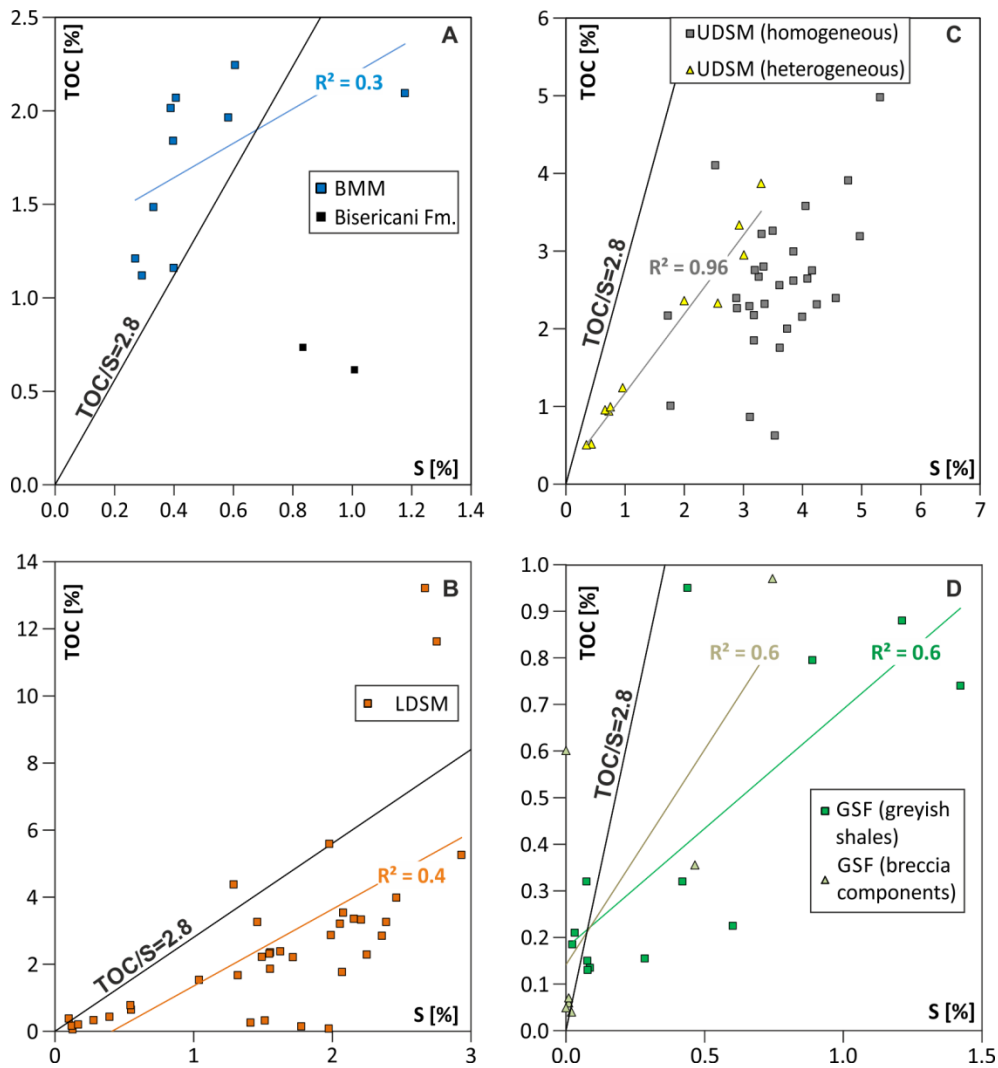


Figure 23: TOC/S cross plot for samples from the A) Bisericani Fm. and the Bituminous Marl Mbr., B) Lower Dysodilic Shale Mbr., C) Upper Dysodilic Shale Mbr. and D) Gura Soimului Fm.

#### 4.4.1 Bisericani Formation (BF)

Only two samples from the Bisericani Formation have been investigated within the frame of the present study. In order to enlarge the data base, data from **Amadori et al. (2012)** were used in addition (Table 5). Important to note, that data reported by these authors fit well with those from the present study.

Table 5: Bulk parameter for the Bisericani Fm. and the Lower Menilite Mbr. from Amadori et al. (2012)

	TOC (% rock)	S1 (mgHC/g rock)	S2 (mgHC/g rock)	T <sub>max</sub> (°C)	PP (S1+S2) (kgHC/trock)	HI (mgHC/g TOC)
Lower Menilite Mbr.	4.01	0.39	22.94	432	23.33	572
Bisericani Fm. (Middle Mbr.)	0.63 0.65	0.13 0.14	1.70 1.71	432 432	1.83 1.85	269 263

PP: Petroleum potential

Table 4 and Figure 21 show low carbonate (about 8 %) and TOC (0.62 - 0.74 %) contents. Relative high sulfur contents (0.83 - 1.01 %) result in TOC/S ratios below 2.8 (Figure 23 A). The HI ranges from 170 to 269 mg HC/g TOC (Table 4, Figure 21) suggesting the presence of kerogen type III-II (Figure 24).

## 4.4.2 Menilite Formation

### 4.4.2.1 Lower Menilite Member (LMM)

The only data from the LMM are from a single sample studied by Amadori (2012; Table 5). This sample has a high TOC (4.01 %), petroleum potential (23.33 kg HC/t rock) and HI value (572 mg HC/g TOC) suggesting the presence of hydrogen-rich kerogen type II.

### 4.4.2.2 Bituminous Marl Member (BMM)

Carbonate contents in the BMM are relatively high. The lower- and uppermost samples contain 84 % and 63 %, respectively. Samples in the middle part contain about 30 % calcite<sub>equiv.</sub> (Table 4 and Figure 21). The average TOC content is 1.7 % and the average sulfur content is 0.5 % (Table 4 and Figure 21). Sample 3 has a higher S value (1.2 %) and, therefore, a lower TOC/S ratio (1.8) than other samples (4.5 – 5.2).

With the exception of sample 3 (378 mg HC/g TOC), HI values typically range between 430 and 642 mg HC/g TOC (Table 4 and Figure 22), indicating the presence of hydrogen-rich type II kerogen (Figure 24). Remarkably the OI of sample 3 is higher than in other samples from the BMM. The S<sub>2</sub> values vary between 5 and 15 mg HC/g rock.

### 4.4.2.3 Lower Dysodilic Shale Member (LDSM)

Table 4 and Figure 21 show relative low CaCO<sub>3</sub> contents for samples from the LDSM. The average value is 1.2 % and only two samples from the uppermost part show values higher than 5 %. TOC values vary between 0.1 and 13.2 % (Table 4), but two samples have values exceeding 10 % (sample 37: 13.2 %; sample 38a: 11.6 %). Sandy layers (marked in the depth profiles in grey color; see Figure 21 and Figure 22) have low TOC values. According to the alternation of sandy layers and shale, sulfur contents and TOC/S ratios are strongly fluctuating (Figure 21). Most samples have a TOC/S ratio below 2.8 (Figure 23B).

HI values vary between 20-680 mg HC/g TOC (Table 4) and display a general upward decreasing trend. Sandy samples near the top of the LDSM (e.g. 45a to 48a) have especially low HI and high OI values (75 - 200 mg CO<sub>2</sub>/g TOC) (Table 4 and Figure 22). Consequently, these samples form distinct clusters in the HI-OI plot (Figure 24). The charts in Figure 24 show a dominance of kerogen type II. A single sample from the lower part of the LDSM plots into the type I field, whereas sandy samples contain kerogen type III.

### 4.4.2.4 Upper Dysodilic Shale Member (UDSM)

The carbonate content of the UDSM is low. Only two samples from the upper part (II-55, 80) show carbonate contents exceeding 10 %.

TOC values vary significantly, both in the lower heterogeneous part (samples II-45 to 70; 0.51-3.87 %) and in the overlying homogeneous part (samples II-54 to II-73; 0.63-13.39 %; Table 4). Above sample II-63 (7.36 % TOC), TOC contents show a general upward decrease.

Samples from the heterogeneous part contain less sulfur (0.35-3.38 % S) than samples from the upper part (1.67-7.18 % S). Whereas TOC contents decrease near the top of the UDSM, S contents remain high. TOC and S contents have a strong positive correlation only in the lower part of the UDSM (R<sup>2</sup>=0.96, Figure 23). All samples have TOC/S ratios below 2.8.

HI is about 350 to 400 mg HC/g TOC and OI is about 15 mg CO<sub>2</sub>/g TOC in the heterogeneous and middle part of the USDM (Figure 22). Slightly lower HI and slightly higher OI values are observed in the uppermost part (sample 80 to II-73, profile meter 510 to 520). The HI-OI plot shows the prevalence of kerogen type II (Figure 24). Rocks with kerogen type III occur mainly in the uppermost part of the USDM.

#### **4.4.3 Gura Soimului Fm. (GSF)**

The carbonate content of the GSF is low (< 3 %; Table 4 and Figure 21). Sulfur contents are low near the base of this formation, but reach 2.9 % in its upper part.

Both, samples from the greyish shales and from breccia components, have low TOC and S values with a moderate correlation (Figure 23D). Samples from the base of the GSF have TOC/S ratios significantly higher than 2.8.

The HI ranges from 0 to 310 mg HC/g TOC in the greyish turbidites and from 150 to 310 mg HC/g TOC) in breccia components (Figure 24). The OI varies between 10 and 180 mg CO<sub>2</sub>/g TOC in greyish shale samples and is around 30 mg CO<sub>2</sub>/g TOC in breccia components. Most of the samples plot near the border between kerogen type II and III.

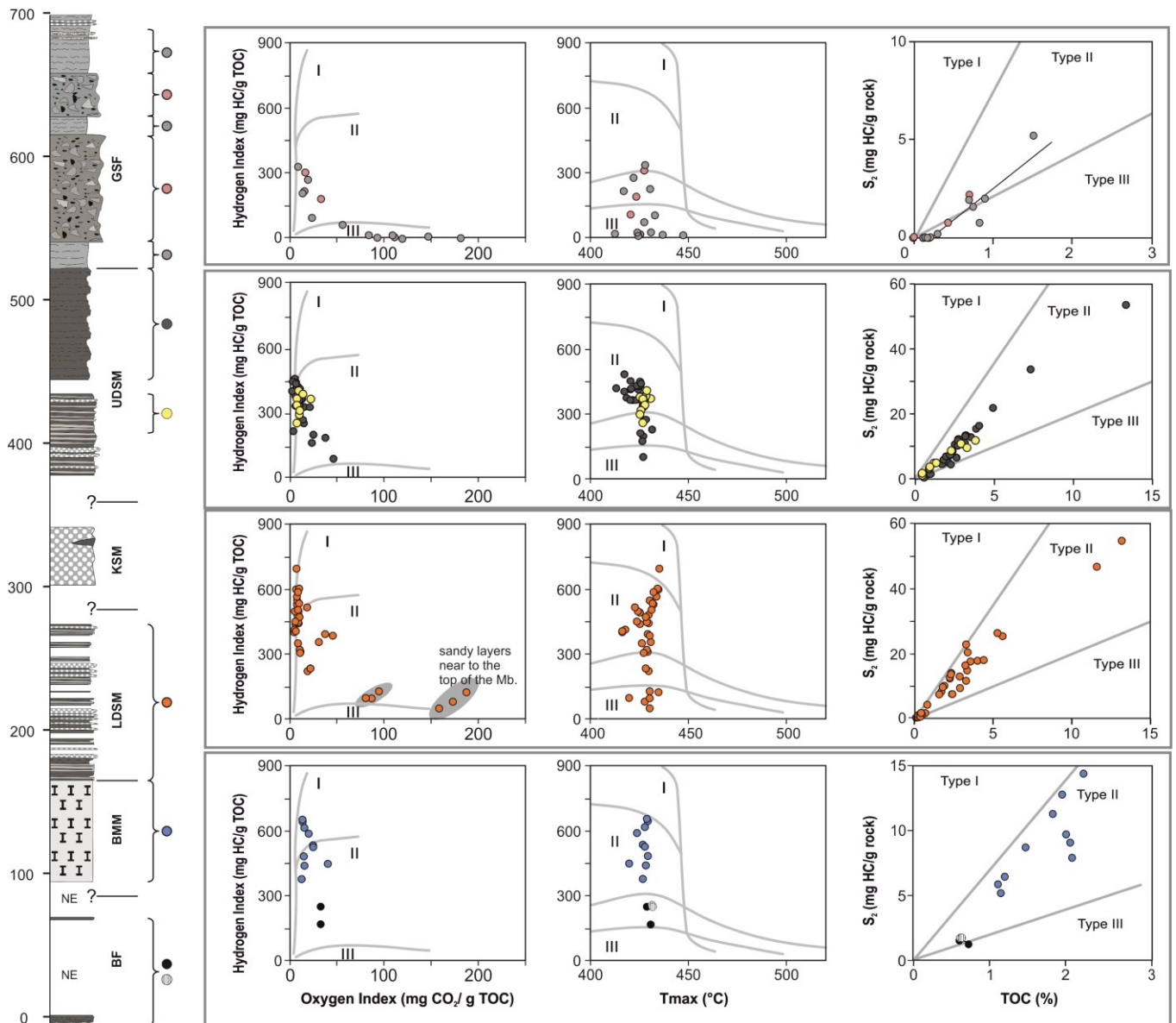


Figure 24: Plots of hydrogen index versus oxygen index and Tmax, S<sub>2</sub> versus TOC for different stratigraphic units. Hydrogen index, Tmax, S<sub>2</sub> and TOC data from samples from Bisericani Formation (grey symbol) and the Lower Menilite Member are taken from Amadori et al. (2012).

## 4.5 Biomarker

For biomarker analysis, 32 samples distributed over the whole profile were chosen based on bulk geochemical parameters and to include different sedimentary units.

Typical gas chromatograms of the saturated and aromatic hydrocarbon fractions are shown in Figure 25 and Figure 26.

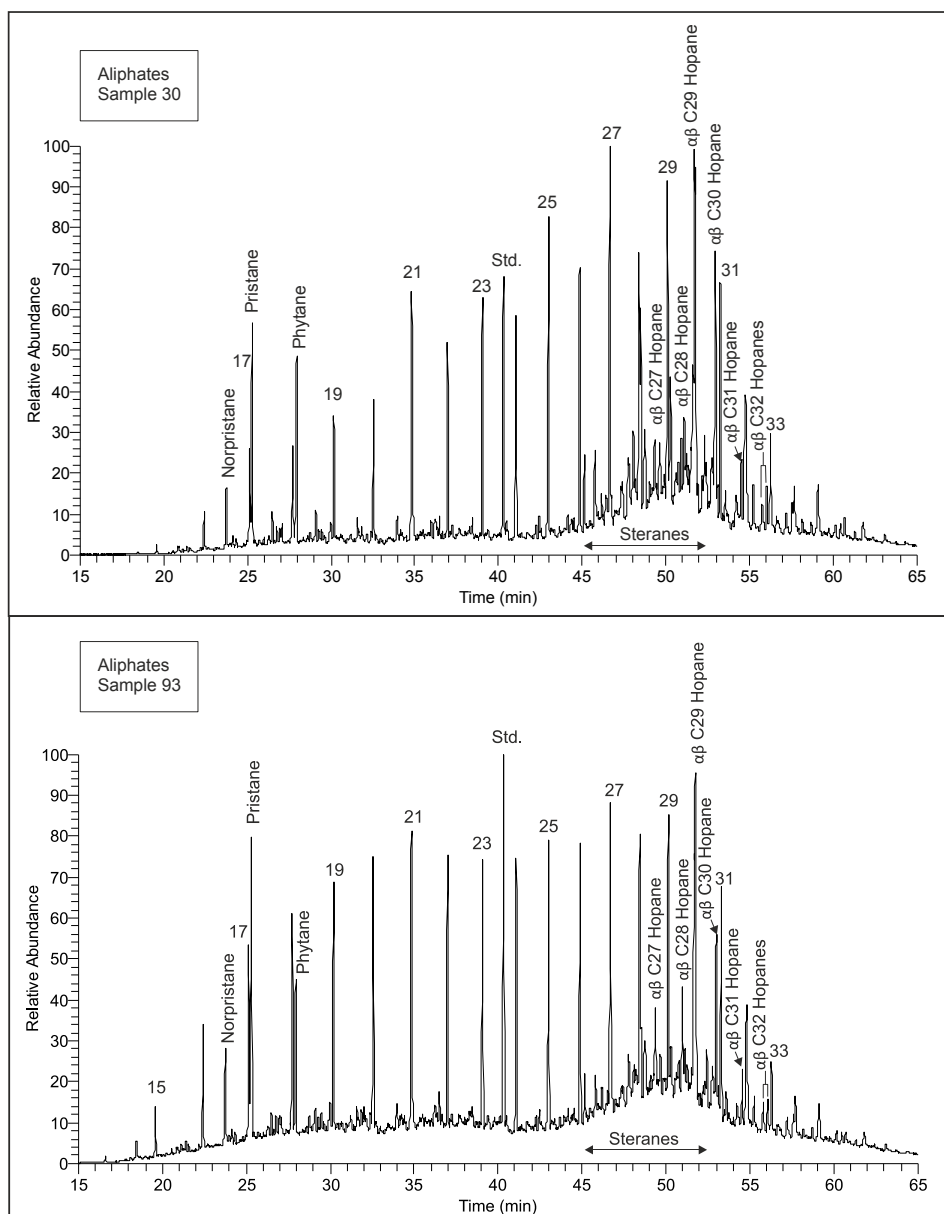


Figure 25: GC MS of the aliphatic hydrocarbon fractions of sample 30 (Lower Dysodilic Shale Mbr.) and sample 93 (Gura Soimului Fm.)

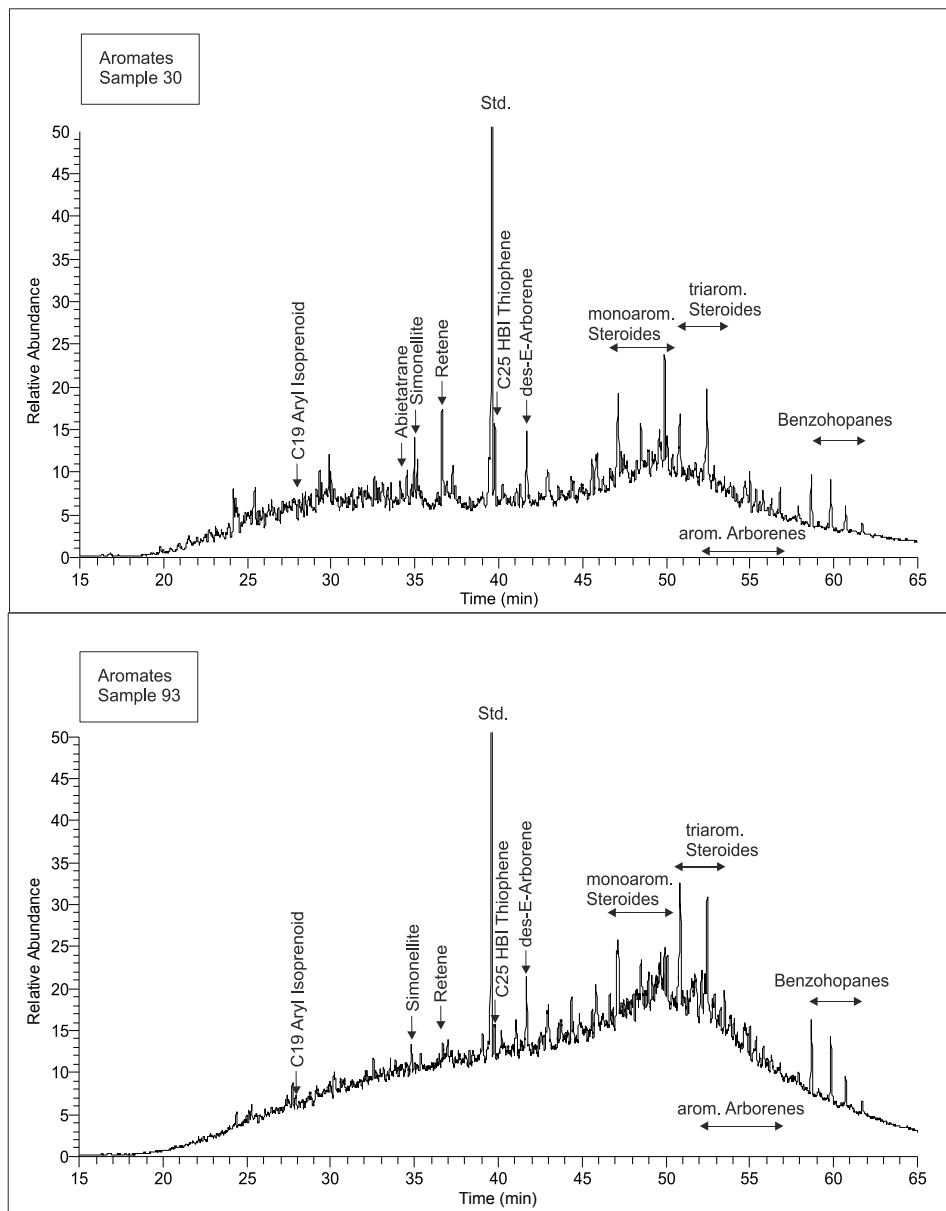


Figure 26: GC MS of the aromatic hydrocarbon fractions of sample 30 (Lower Dysodilic Shale Mbr.) and sample 93 (Gura Soimului Fm.)



#### 4.5.1 Chain Length Distribution

The relative proportions of short, middle and long chain *n*-alkanes are listed in Table 6. In general long chain *n*-alkanes (25-40 % of total *n*-alkanes; average: 35 %) predominate over the short chain *n*-alkanes (9-22 %; av. 16 %). *n*-Alkanes of intermediate molecular weight contribute to 29 % on average.

Table 6: Concentrations and concentration ratios of *n*-alkanes and isoprenoids as well as derived source- and facies-related parameters.

sample	meters to the base	TOC/S	Sum <i>n</i> -Alkane (µg/g TOC)	<i>n</i> -C <sub>15-</sub>	<i>n</i> -C <sub>21-</sub>	<i>n</i> -C <sub>27-</sub>	CPI	Pri/ <i>n</i> -C <sub>17</sub>	Phy/ <i>n</i> -C <sub>18</sub>	Pri/ Phy	MTTC ratio	C <sub>19</sub> -Aryl-Isoprenoids (µg/g TOC)	
				<i>n</i> -Alkane				Alkane					
GSF	97	0.70	625	0.16	0.35	0.28	1.27	2.39	0.95	1.75	0.84		
	96	0.55	1295	0.16	0.33	0.31	1.31	3.04	1.51	1.67	0.72	0.92	
	94	0.52	1382	0.14	0.37	0.30	1.25	1.79	1.82	1.05	0.59	1.12	
	93	0.80	5594	0.18	0.35	0.28	1.06	1.67	0.86	1.81	0.50	0.56	
UDSM	II-71	0.82	627	0.14	0.29	0.37	1.66	5.45	2.72	1.78	0.76	0.49	
	79	0.89	891	0.16	0.31	0.33	1.45	4.32	2.82	1.42	0.66	0.96	
	77	1.02	653	0.22	0.36	0.24	1.34	2.73	1.97	1.30	0.68	0.91	
	II-65	0.93	1197	0.18	0.33	0.30	1.34	4.09	2.43	1.67	0.65	1.54	
	II-63	0.94	1257	0.17	0.31	0.31	1.28	4.42	2.98	1.24	0.62	1.39	
	II-61	0.78	988	0.16	0.33	0.33	1.32	6.32	1.87	3.01	0.67	0.69	
	II-57	0.74	2020	0.18	0.32	0.33	1.19	3.02	2.43	1.39	0.61	1.45	
	71	3.37	415	0.19	0.33	0.30	1.49	3.30	1.54	2.04	0.74	0.38	
	70	1.40	1294	0.16	0.34	0.31	0.96	3.29	2.06	1.35	0.46	0.45	
	68	0.99	1915	0.17	0.31	0.34	1.20	2.62	1.88	1.33	0.67	0.95	
	67	1.02	2448	0.14	0.32	0.35	1.22	3.11	2.32	1.34	0.65	0.75	
	66	1.45	1185	0.13	0.32	0.34	1.20	2.92	2.17	1.17	0.36	0.35	
	LDSM	44	1.84	844	0.12	0.33	0.38	1.60	6.08	3.16	2.56	0.66	0.49
42b		1.44	726	0.17	0.28	0.36	1.40	3.59	2.42	2.14	0.64	0.33	
41a		1.47	1806	0.07	0.37	0.35	1.13	5.80	2.23	2.46	0.64	0.43	
37		239	4.95	567	0.10	0.34	0.39	1.51	3.48	1.62	2.33	0.72	0.00
36		237	1.62	643	0.11	0.33	0.37	1.34	1.60	1.35	1.15	0.74	0.37
33		231	1.20	1778	0.07	0.31	0.42	1.42	5.22	2.45	1.90	0.37	1.06
30		217	1.27	1885	0.08	0.30	0.41	1.21	2.47	2.15	1.14	0.39	1.94
27		211	2.83	768	0.08	0.34	0.39	1.39	2.98	1.90	1.62	0.68	0.81
25		207	1.11	300	0.05	0.27	0.45	1.03	1.03	2.44	0.37	0.37	0.15
21		197	3.40	1554	0.03	0.27	0.48	1.58	6.68	2.55	2.59	0.70	0.00
19		188	1.37	1832	0.08	0.31	0.42	1.24	3.20	2.21	1.28	0.45	1.15
16		182	1.14	1158	0.08	0.32	0.40	1.10	1.25	1.93	0.78	0.32	0.83
13		175	1.95	1527	0.14	0.32	0.35	1.15	1.73	2.15	0.88	0.52	3.88
9		167	1.56	5357	0.06	0.32	0.42	1.34	2.89	3.34	0.84	0.61	1.43
II-3b		164	6.22	481	0.24	0.29	0.25	1.33	1.00	1.42	0.63	0.74	1.92
BMM	II-3a	162	27.5	1028	0.21	0.31	0.27	0.87	6.09	2.68	1.47	0.43	3.18
	8	161	3.71	1279	0.07	0.27	0.41	0.91	17.5	8.85	1.51	0.85	1.34
	5	147	3.34	1062	0.24	0.32	0.25	0.95	2.44	1.06	1.69	0.32	0.85
BF	II-2	68	1.78	285	0.23	0.35	0.24	1.13	1.12	0.58	1.62	0.45	1.24

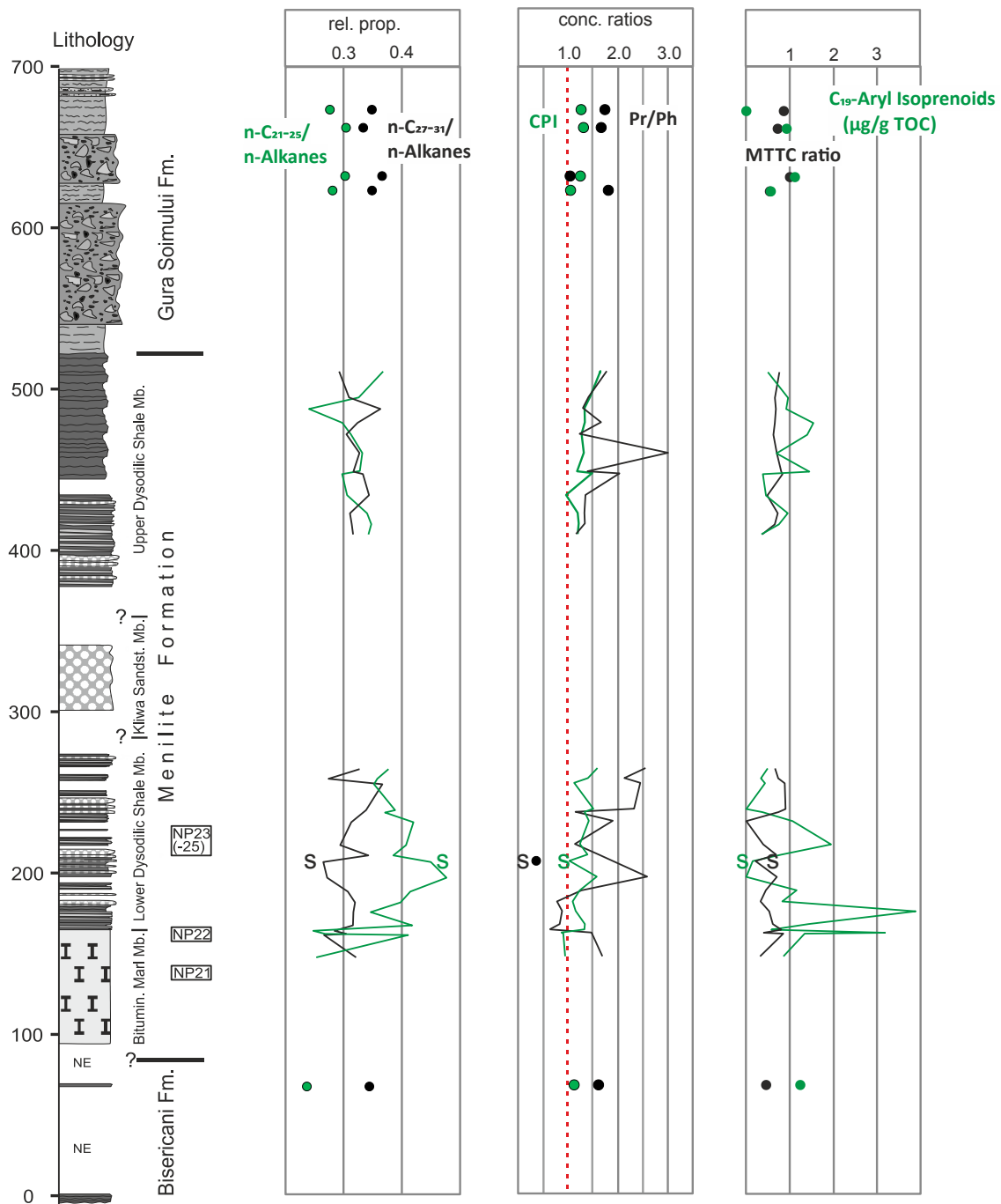


Figure 27: Variation of a) relative proportions of middle- and long-chain *n*-alkanes. b) CPI and Pr/Ph ratio and c) MTTC ratio and C19 Aryl Isoprenoids versus depth

Figure 28 shows the contribution of short and long chain *n*-alkanes for different stratigraphic units. Samples from the **BMM** contain between 25 and 40 % long chain *n*-alkanes and between 9 and 23 % for short chain *n*-alkanes. Samples from the **LDSM** have a wide range in both, short and long chain *n*-alkanes. In contrast to the LDSM, a relatively uniform amount of long (~ 35 %) and short chain *n*-alkanes (11 - 20 %) is found in the samples from the **UDSM**. The samples from the **GSF** include about 16 % short chain *n*-alkanes of and around 30 % long chain *n*-alkanes. In these samples the middle chain *n*-alkanes predominate over the long chain *n*-alkanes (Figure 27).

Figure 28 shows the ratio between long- and short-chain *n*-alkanes. It is striking, that samples from the LDSM and the UDSM correlate well according the long-versus short-chain *n*-alkanes.

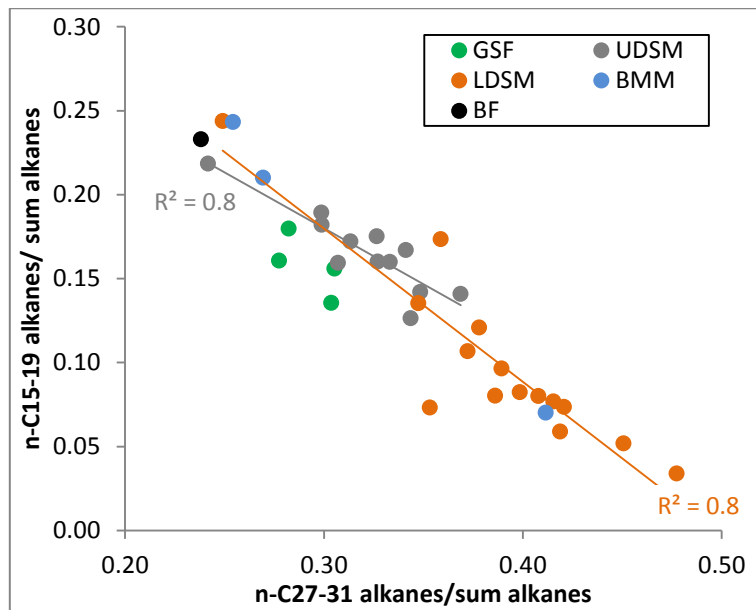


Figure 28: Cross plot of short and long chain *n*-Alkanes

#### 4.5.2 Carbon Preference Index (CPI)

The vertical trend of CPI is shown in Figure 27. CPI values range between 0.87 and 1.66. The average CPI of the entire sample set is 1.26.

All samples from the BMM show CPI values <1.0 (Figure 27). This may indicate a hypersaline environment and/or high input of microbial organic matter (Peters et al. 2005). In contrast, the rest of the samples (excluding sample 70) shows values >1.0. The detected CPI range is consistent with a maturity of 0.4 % vitrinite reflectance (see the following chapter).

#### 4.5.3 Pristane/Phytane ratio

Pr/Ph ratios vary between 0.4 and 3.0. Figure 29 shows a plot of Pr/Ph ratios versus CPI.

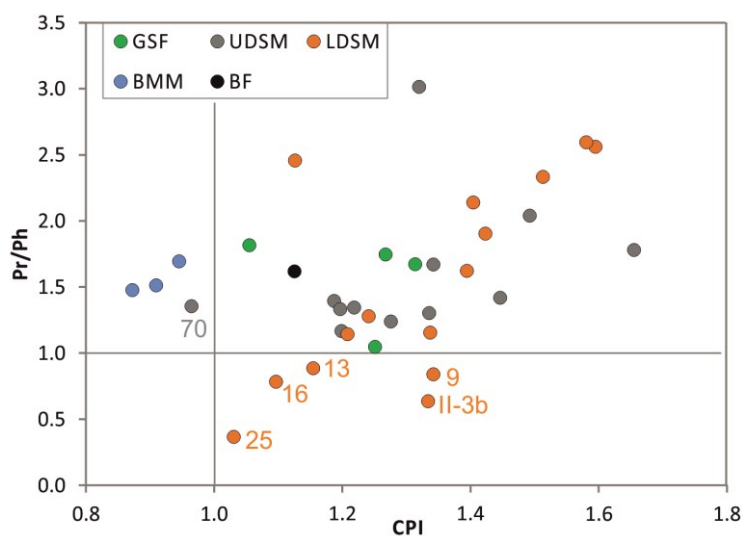


Figure 29: Pristane/Phytane-CPI

Five samples from the lower part of the **LDSM** have Pr/Ph ratios <1 indicating anoxic conditions. Two of these samples (II-3B, 25) are sandy and have TOC contents <0.5%. Most samples from the LDSM show a positive relation between CPI and Pr/Ph values.

Samples from all other units show Pr/Ph ratios between 1 and 3 indicating dysoxic conditions during organic matter accumulation. Some samples with enhanced pristane/phytane ratios also show high CPI values. This may be due to the influence of terrigenous organic matter input on both parameters.

Figure 30 shows the distribution of pristane/*n*-C<sub>17</sub> and phytane/*n*-C<sub>18</sub>. Most of the samples plot within the field characteristic for mixed (terrigenous-algal) organic sources. Samples from the lower part of the LDSM, characterized by Pr/Ph ratios <1, plot into the field for marine organic matter. Samples from the BMM plot near the border to terrestrial organic matter, which is in apparent contradiction to a high amount of microbial organic matter suggested by CPI values <1.

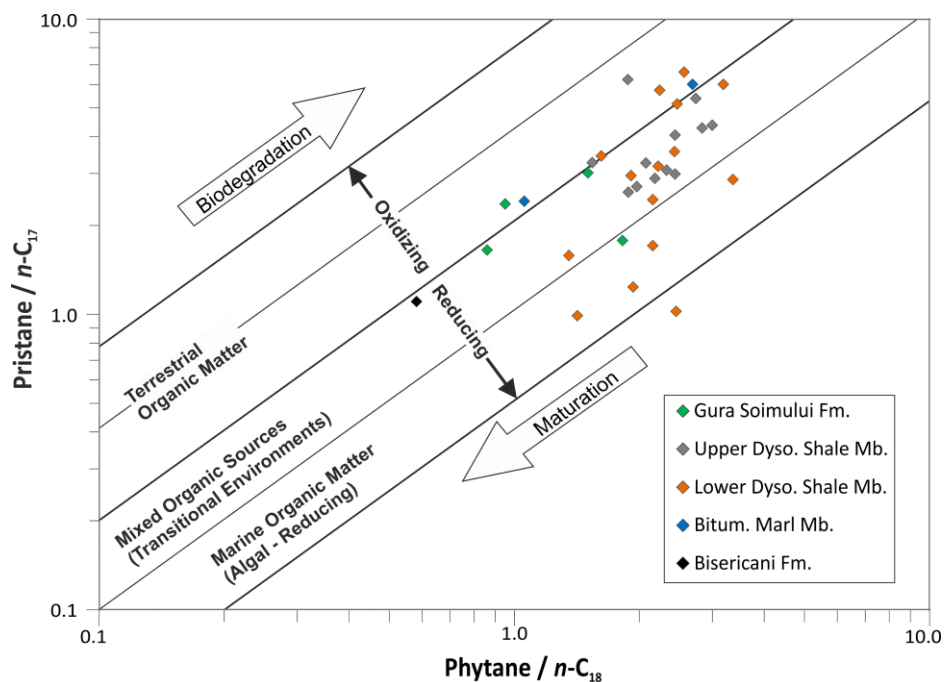


Figure 30: Pristane/*n*-C<sub>17</sub> versus Phytane/*n*-C<sub>18</sub> ratio (Peters, 1999)

#### 4.5.4 Aryl-Isoprenoids

The depth plot in Figure 27 shows that the concentration of C<sub>19</sub> aryl-isoprenoids reaches a maximum in the uppermost **BMM** and the lower part of the **LDSM**. As expected, samples with high concentrations in C<sub>19</sub> Arylisoprenoids are typically characterized by low Pr/Ph ratios (Figure 27 and Figure 29).

#### 4.5.5 MTTC ratio

MTTC ratios are plotted versus Pr/Ph ratios in Figure 31. According to this plot, salinity varied frequently between semi-saline to fresh-water and mesosaline. Frequent salinity variations occurred especially during deposition of the **BMM** and the **LDSM**. Relatively stable conditions with normal marine conditions persisted during deposition of the upper part of the **UDSM**.

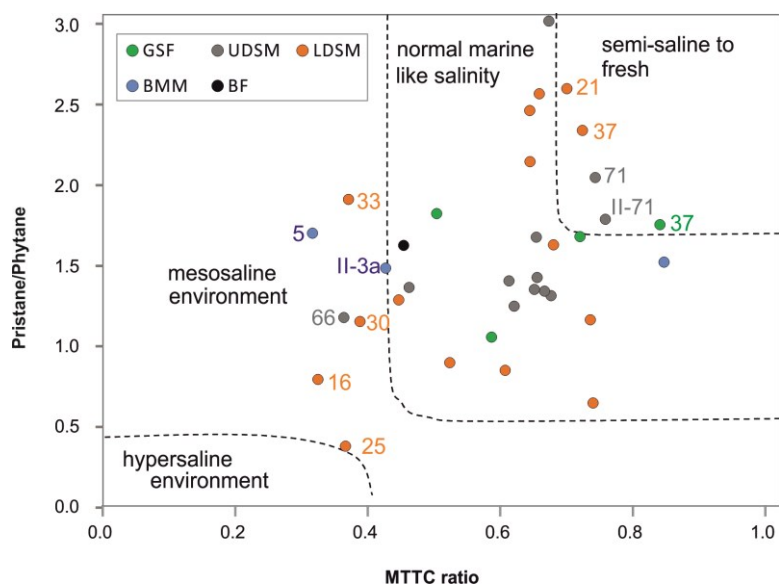


Figure 31: Pr/Phy versus MTTC ratio; for legend see Figure 30

#### 4.5.6 Steranes, Hopanes

Steranes and hopanes data are listed in Table 6. Depth profiles are shown in Figure 32.

In the **BMM** and the **LDSM** the relative proportions of steranes are fluctuating whereby the C<sub>29</sub> steranes dominate over the C<sub>28</sub> and C<sub>27</sub> steranes. The concentration of methylsteranes is generally higher than in other units of the Menilite Formation and shows an upward decreasing trend. Concentrations of benzohopanes are generally high and reach a maximum (80 µg/gTOC) in the LDSM. Both, the BMM (av. 6500 µg/g TOC) and the LDSM (2900 µg/g TOC) contain high concentrations in hopanes. The steroids/hopanoids ratio varies between 0.05 and 0.3.

In the **UDSM** C<sub>27</sub> steranes predominate over the C<sub>28</sub> and C<sub>29</sub> steranes. C<sub>28</sub> steranes show similar concentrations as in the LDSM. C<sub>29</sub> steranes are fluctuating, but occur in lower concentrations than in the underlying members. Regarding methylsteranes, steranes, benzohopanes, and hopanes concentrations, the upward decreasing trends in the LDSM continue in the UDSM. Therefore, their concentrations are lower than in the LDSM. Moreover, there is a remarkable lower variation in these values than in the LDSM. The steroids/hopanoid ratio is about the same as in the LDSM.

Samples from the **GSF** show a peak in the concentrations of methylsteranes, benzohopanes and hopanes. The remaining concentrations follow the trends from the UDSM.

The hopane isomerization (22S/(22S+22R)) ratios of the C-31 homohopanes range from 0.34 to 0.47 indicating a low thermal maturity of the entire sedimentary succession (equivalent to vitrinite of 0.4 to 0.5 % Rr). Maturity trends with stratigraphic position cannot be observed.

Table 7: Overview of steranes (Ster) and hopanes (Hop)

sample	meter to the base	TOC/S	Ster (µg/g TOC)	C <sub>27</sub> C <sub>28</sub> C <sub>29</sub> -Ster/Ster			C <sub>28</sub> /C <sub>29</sub> Ster	Methyl Ster	Hop	Benzo-hop	S/(S+R) C31 Hop.	Gamma-cerane Index	Ster/Hop	
				(µg/g TOC)										
GSF	97	673	0.70	56	0.44	0.29	0.27	1.07	28.3	608	18.2	0.42	0.26	0.00
	96	662	0.55	431	0.29	0.34	0.37	0.93	28.6	2093	32.8	0.42	0.00	0.00
	94	632	0.52	353	0.36	0.32	0.32	1.00	67.9	5400	74.2	0.47	0.16	0.27
	93	623	0.80	366	0.35	0.30	0.34	0.88	78.5	8393	112.8	0.44	0.18	0.19
UDSM	II-71	511	0.82	101	0.39	0.32	0.29	1.07	9.9	963	25.5	0.40	0.00	0.24
	79	495	0.89	187	0.40	0.32	0.29	1.09	11.6	1746	27.8	0.42	0.00	0.25
	77	488	1.02	295	0.34	0.35	0.32	1.09	10.8	1420	10.2	0.44	0.00	0.21
	II-65	479	0.93	285	0.33	0.31	0.36	0.88	13.6	1921	29.5	0.42	0.00	0.16
	II-63	472	0.94	449	0.39	0.31	0.31	1.00	13.7	2097	29.7	0.42	0.00	0.28
	II-61	460	0.78	107	0.33	0.30	0.37	0.81	13.7	1681	31.9	0.40	0.20	0.11
	II-57	449	0.74	90	0.40	0.32	0.29	1.11	19.9	2406	40.8	0.37	0.00	0.37
	71	447	3.37	58	0.31	0.28	0.41	0.68	6.2	1488	32.5	0.43	0.00	0.19
	70	434	1.40	286	0.38	0.29	0.33	0.88	14.0	2222	27.0	0.42	0.00	0.24
	68	423	0.99	221	0.35	0.31	0.34	0.92	19.4	1953	21.2	0.41	0.00	0.39
	67	416	1.02	268	0.39	0.30	0.31	0.95	17.6	2181	32.7	0.38	0.00	0.55
	66	410	1.45	425	0.30	0.31	0.39	0.78	11.9	1465	17.0	0.41	0.00	0.25
LDSM	44	264	1.84	199	0.27	0.31	0.42	0.73	13.3	2228	33.6	0.44	0.00	0.48
	42b	258	1.44	316	0.30	0.28	0.42	0.68	16.4	2526	32.8	0.44	0.00	1.77
	41a	255	1.47	254	0.33	0.29	0.38	0.75	17.7	2105	33.7	0.45	0.20	0.20
	37	239	4.95	71	0.27	0.30	0.42	0.72	7.0	1811	47.9	0.44	0.00	0.21
	36	237	1.62	309	0.29	0.30	0.40	0.74	11.4	2689	69.0	0.39	0.05	0.12
	33	231	1.20	350	0.32	0.30	0.38	0.78	28.0	3424	28.0	0.38	0.00	0.11
	30	217	1.27	1013	0.25	0.27	0.48	0.55	31.6	3179	36.1	0.41	0.11	0.53
	27	211	2.83	265	0.31	0.31	0.39	0.79	8.3	1782	20.8	0.39	0.07	0.29
	25	207	1.11	244	0.29	0.25	0.46	0.54	10.7	1341	90.8	0.34	0.09	0.45
	21	197	3.40	218	0.21	0.26	0.54	0.48	10.9	8177	47.8	0.38	0.03	0.17
	19	188	1.37	314	0.33	0.27	0.40	0.66	13.8	2073	16.6	0.35	0.00	0.43
	16	182	1.14	318	0.28	0.27	0.45	0.60	19.8	1683	21.1	0.38	0.00	1.06
	13	175	1.95	503	0.31	0.29	0.40	0.73	12.3	2268	32.2	0.38	0.07	1.30
	9	167	1.56	1214	0.27	0.32	0.41	0.78	16.8	5009	24.9	0.35	0.00	2.68
	II-3b	164	6.22	414	0.21	0.33	0.46	0.71	30.6	3419	36.3	0.45	0.17	0.11
BMM	II-3a	162	27.5	946	0.30	0.29	0.40	0.73	40.5	6866	60.3	0.41	0.11	0.11
	8	161	3.71	1349	0.33	0.32	0.35	0.90	21.4	7327	40.8	0.37	0.10	0.01
	5	147	3.34	768	0.27	0.32	0.40	0.80	22.5	5198	34.1	0.44	0.00	0.01
BF	II-2	68	1.78	46	0.30	0.32	0.37	0.87	6.0	300	26.4	0.44	0.11	0.00

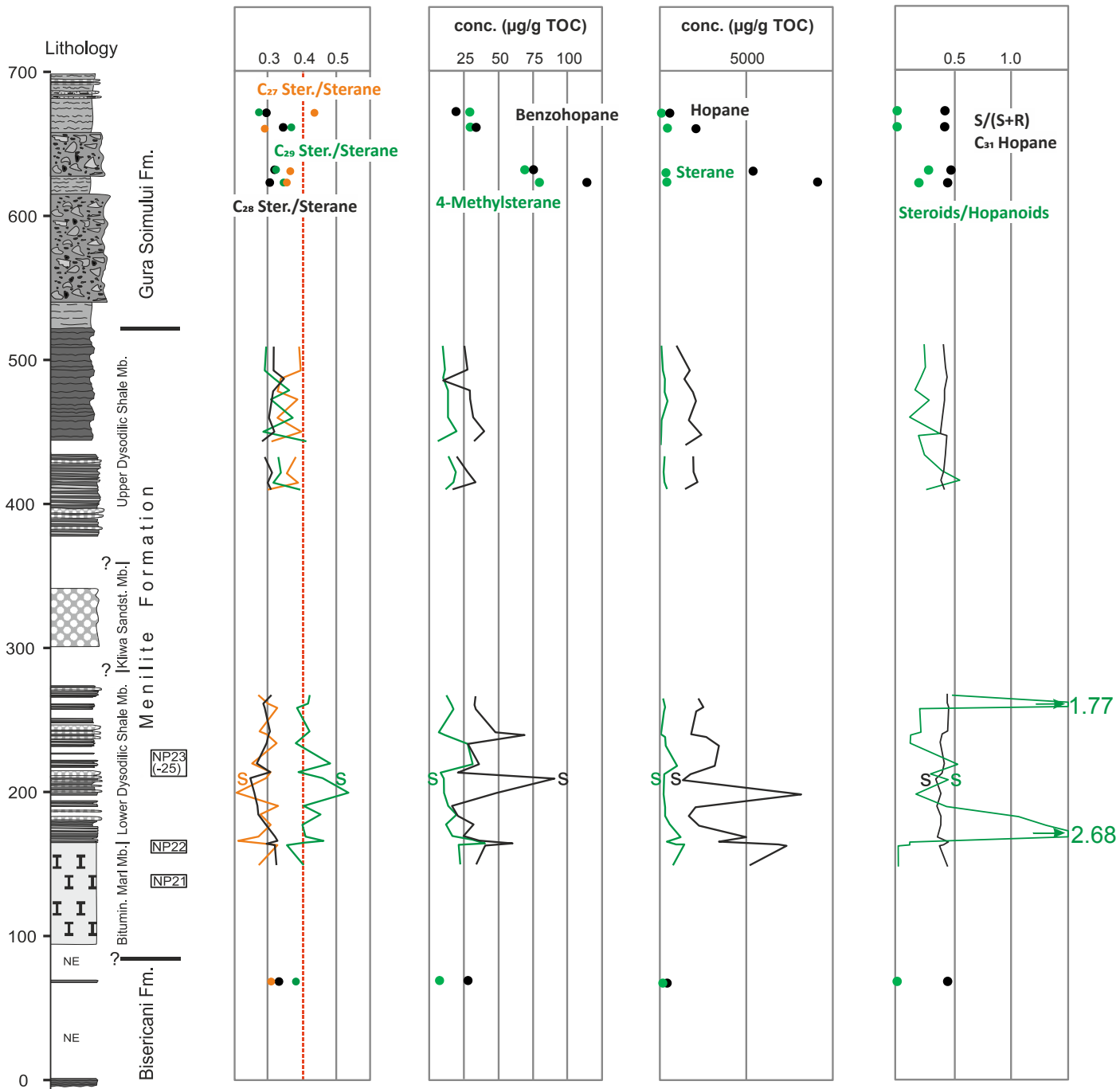


Figure 32: Depth profiles: a) C<sub>27</sub>, C<sub>28</sub> and C<sub>29</sub> Steranes/sum Steranes; b) hopanes and steranes; c) steroids/hopanooids and S/(S+R) hopanes; d) 4-Methylsteranes and Benzohopanes

Figure 33 shows the triangle diagram of C<sub>27</sub>, C<sub>28</sub> and C<sub>29</sub> steranes. Most samples plot into the bay/estuarine field.

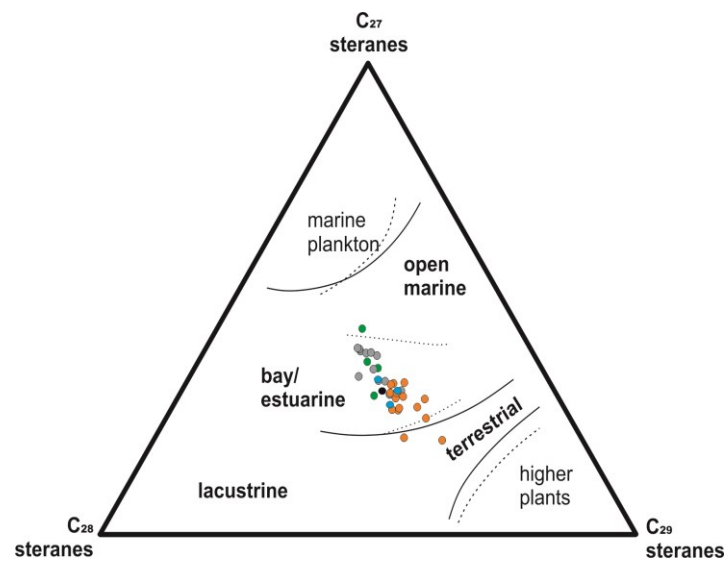


Figure 33: Distribution of steranes. Modified, (Huang & Meinschein 1979)

#### 4.5.7 Gammacerane Index

The GI is similar for samples from the **BF** and two samples from the **BMM** (~0.10). Samples from the **LDSM** have highly varying GI values (0 - 0.20). Gammacerane has not been detected in most samples from the **UDSM**; only sample II-61 has a relatively high GI (0.20). The GI of samples from the **GSF** is relative high and ranges between 0.16 and 0.26.

The Gammacerane Index (GI) is considered a proxy for water column stratification, which is often accompanied by reduced oxygen content in bottom waters. Therefore, a negative correlation between GI and Pr / Ph ratios is expected. This effect is not visible in our sample set (Figure 34).

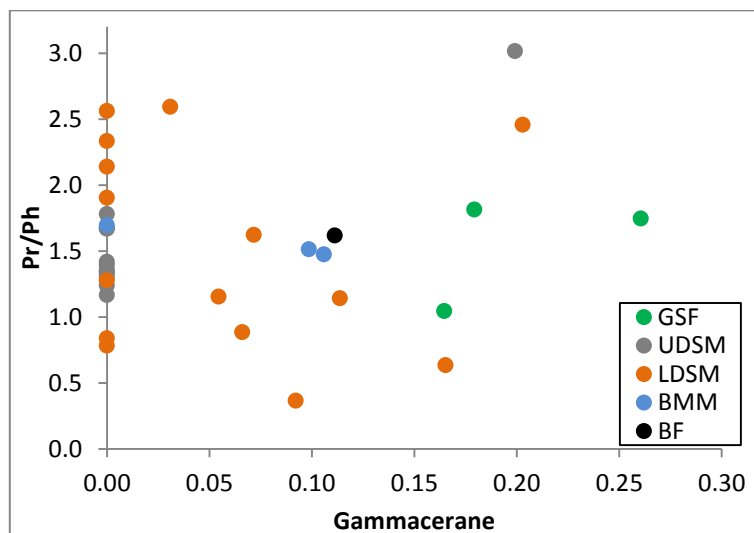


Figure 34: Pristane/Phytane (Pr/Ph) ratio versus Gammacerane Index



#### 4.5.8 Arboranes, Cadalenes, Diterpenoids, C<sub>25</sub> Thiophenes

Table 8 summarizes the concentrations of arboranes, cadalenes, diterpenoids and C<sub>25</sub> HBI thiophenes found in the samples, which are plotted versus depth in Figure 35.

Table 8: Arboranes. cadalenes. diterpenoids and C<sub>25</sub>thiophenes

	sample	meters to the base	TOC/S	Cadalene	Diterpenoids (Arom.)	Arboranes (Arom.)	C <sub>25</sub> HBI Thiophenes	DBT/Phen
(µg/g TOC)								
<b>GSF</b>	97	672.70	0.70	0.63	6.11	2.28	0.00	0.19
	96	661.70	0.55	3.74	12.86	15.86	0.00	0.40
	94	631.70	0.52	0.58	16.35	26.86	20.40	0.23
	93	622.70	0.80	0.00	15.20	79.72	21.47	0.00
<b>UDSM</b>	II-71	510.50	0.82	6.97	16.16	18.99	6.05	0.49
	79	494.50	0.89	6.15	11.50	17.60	6.87	0.47
	77	487.50	1.02	2.17	8.78	8.00	2.13	0.46
	II-65	478.90	0.93	11.19	14.64	33.19	4.63	0.37
	II-63	471.50	0.94	9.51	22.40	47.12	8.31	0.35
	II-61	460.00	0.78	18.40	23.58	26.82	3.50	0.35
	II-57	448.50	0.74	14.29	8.90	33.85	15.06	0.41
	71	447.00	3.37	35.60	86.39	21.17	6.11	0.38
	70	433.80	1.40	7.40	11.51	8.37	6.45	0.31
	68	422.70	0.99	5.90	11.81	13.37	8.33	0.42
	67	415.90	1.02	7.11	14.10	22.88	17.91	0.36
	66	409.60	1.45	3.18	7.36	7.10	4.30	0.30
<b>LDSM</b>	44	264.10	1.84	19.72	38.20	18.65	16.11	0.28
	42b	258.10	1.44	11.22	19.77	16.74	57.97	0.28
	41a	254.90	1.47	20.94	20.97	22.47	6.67	0.29
	37	238.90	4.95	30.68	53.71	49.96	9.98	0.42
	36	237.10	1.62	5.51	22.55	28.10	8.20	0.38
	33	231.40	1.20	9.50	34.73	29.10	18.13	0.33
	30	217.00	1.27	5.91	35.31	154.02	19.15	0.25
	27	210.60	2.83	8.07	34.26	16.59	6.11	0.35
	25	206.60	1.11	0.04	3.18	35.30	40.59	0.14
	21	196.80	3.40	19.53	69.87	131.76	7.90	0.45
	19	188.40	1.37	3.70	7.32	5.29	7.19	0.18
	16	181.50	1.14	2.41	10.07	8.44	22.42	0.42
	13	175.35	1.95	9.97	38.41	32.72	41.94	0.25
	9	167.40	1.56	0.78	8.93	17.71	66.70	0.25
	II-3b	164.00	6.22	2.58	7.46	24.23	4.03	0.17
<b>BMM</b>	II-3a	162.00	27.50	4.28	12.38	15.02	6.69	0.36
	8	161.40	3.71	1.52	18.03	7.08	0.39	0.39
	5	147.40	3.34	2.29	6.66	11.50	0.38	0.39
<b>BF</b>	II-2	67.50	1.78	1.28	5.54	22.95	0.00	0.13

Samples from the **BMM** contain low concentrations of landplant biomarkers (arboranes, cadalenes, diterpenoids). Biomarkers for diatoms (C<sub>25</sub> HBI thiophenes) occur in low amounts only in the uppermost sample (and are also missing in the single studied sample from the BF).

Samples from the **LDSM** show strongly fluctuating concentrations of landplant and diatom derived biomarkers. Arboranes vary in a wider range (10-160 µg/gTOC) than diterpenoids. Concentrations of

cadalenes vary between 1 and 30  $\mu\text{g/gTOC}$ . The concentration of  $\text{C}_{25}$  HBI thiophenes are significantly higher (4-67  $\mu\text{g/gTOC}$ , average: 22.2  $\mu\text{g/gTOC}$ ) than in any other unit. Maximum concentrations of this diatom-biomarker are found in samples 9 and 42B.

Biomarker abundances vary strongly between the lower heterogenous and the upper uniform part of the **UDSM**. Landplant-derived biomarker are low in the lower part, but reach a maximum above the base of the upper part (sample 71). The concentration of cadalenes decreases upwards within the upper part of the UDSM reflecting an upward decreasing contribution of resins from conifers to the biomass. Concentrations of  $\text{C}_{25}$  HBI thiophenes are relative low (<18  $\mu\text{g/gTOC}$ ).

The values of arboranes and diterpenoids in the **GSF** are similar to those found in the underlying members. Concentrations of cadalenes are low (<5  $\mu\text{g/gTOC}$ ).  $\text{C}_{25}$  HBI thiophenes are restricted to the two lowermost samples, but these samples show relatively high amounts (~20  $\mu\text{g/gTOC}$ ).

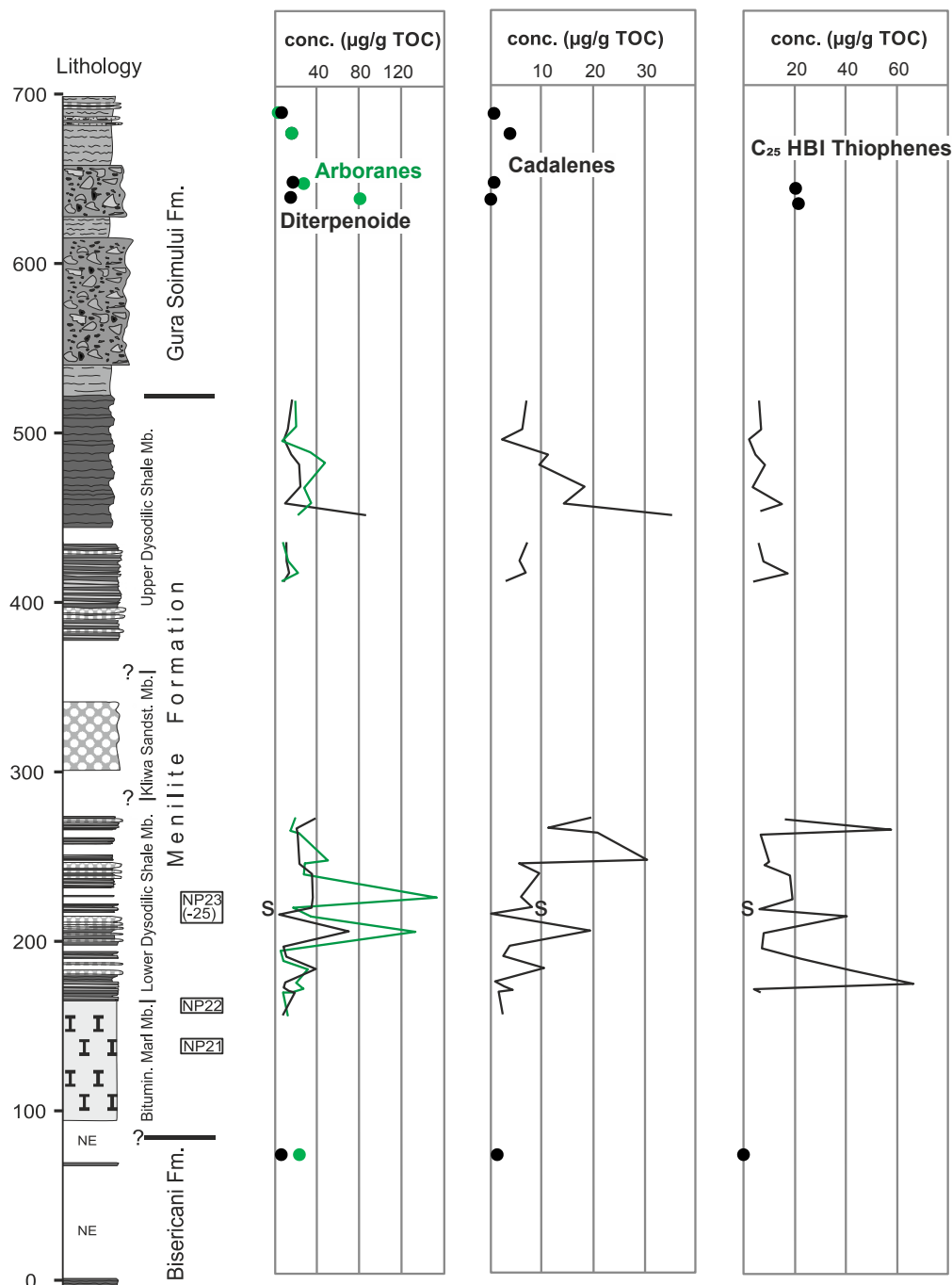


Figure 35: Depth profiles. a) arboranes and diterpenoids; b) cadalenes; c)  $\text{C}_{25}$  thiophenes

#### 4.5.9 DBT/Phenanthrene

Figure 36 shows the DBT/Phen versus Pr/Ph cross plot. All samples (including carbonate-rich samples from the **BMM**) have relative low DBT/Phen ratios (0.13-0.49), whereby samples from the **UDSM** yield the highest values.

The lowermost samples and sample 25 from the **LDSM** show Pr/Ph values below 1 (Figure 36). According to Hughes et al. (1995), those samples indicate a lacustrine (sulphate-poor) environment with a variable lithology. The remaining samples (Pr/Ph>1) would represent a marine and lacustrine environment, dominated by shale (Figure 36).

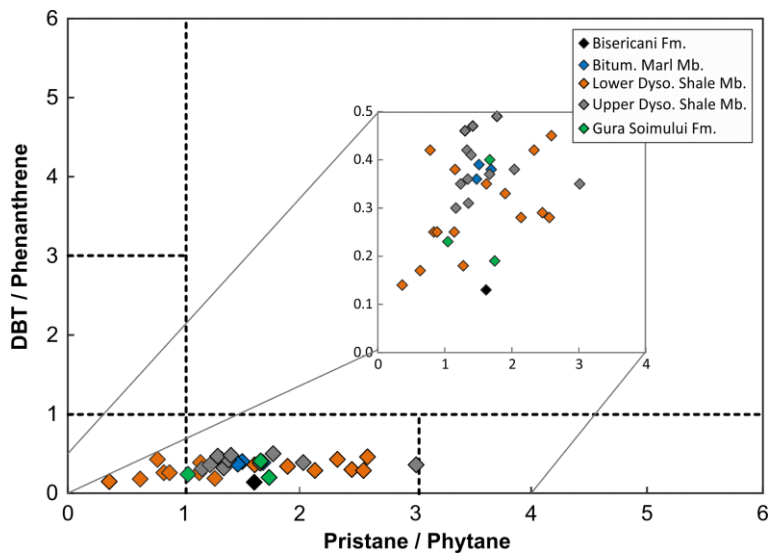


Figure 36: Dibenzothiophene/Phenanthrene versus Pristane/Phytane (Hughes et al. 1995)

## 4.6 Organic Petrology

The maceral composition of 10 samples is shown in Table 9 and Figure 41.

Analyzed samples have an average organic matter content of 8.4 vol.%  $\pm$  7.8 vol.%, a mineral matter content of 89.6 %  $\pm$  7.4 % and a pyrite content of 2.0 %  $\pm$  0.7 % (Table 9).

Table 9: Maceral percentages. The values are calculated on whole rock (light blue) and mineral matter free basis

Fm/Mbr	sample	Vitrinite	Inertinite	Lamalginitite	Telalginitite	Sporinite	Cutinite	Resinite	Liptodetrinite	Exsuda-tinite	Organic Matter	Mineral matter*	Pyrite
		[vol.%]										[vol.%]	[vol.%]
<b>GSF</b>	<b>97</b>	0.30		1.6	0.4	1.5			0.4		<b>4.2</b>	<b>94.3</b>	<b>1.5</b>
		7.1		38.1	9.5	35.7			9.5		<b>100</b>		
<b>Upper Dysodilic Shale Mbr</b>	<b>82</b>	0.6	0.1	1.4	0.1	0.8					<b>3.0</b>	<b>94.5</b>	<b>2.5</b>
		20.0	3.3	46.7	3.3	26.7					<b>100</b>		
	<b>78</b>	1.3	0.1	1.5	0.5	0.8					<b>4.2</b>	<b>93.7</b>	<b>2.1</b>
		31.0	2.4	35.7	11.9	19.0					<b>100</b>		
	<b>68</b>	0.8	0.1	0.9	0.1	0.7			1.2		<b>3.8</b>	<b>93.8</b>	<b>2.4</b>
		21.1	2.6	23.7	2.6	18.4			31.6		<b>100</b>		
<b>Lower Dysodilic Shale Mbr</b>	<b>44</b>	4.80		2.6	0.3	1.1			0.2		<b>9.0</b>	<b>89.5</b>	<b>1.5</b>
		53.3		28.9	3.3	12.2			2.2		<b>100</b>		
	<b>37</b>	7.6	0.3	2.1	0.3	2.0	0.5				<b>12.8</b>	<b>85.6</b>	<b>1.6</b>
		59.4	2.3	16.4	2.3	15.6	3.9				<b>100</b>		
	<b>27</b>	2.7	0.2	0.3		1.3			0.9		<b>5.4</b>	<b>91.9</b>	<b>2.7</b>
		50.0	3.7	5.6		24.1			16.7		<b>100</b>		
	<b>21</b>	21	0.6	3.1	0.6	2.2		0.1	1.2	0.1	<b>28.9</b>	<b>70.2</b>	<b>0.9</b>
		72.7	2.1	10.7	2.1	7.6		0.3	4.2	0.3	<b>100</b>		
	<b>9</b>			2.9	0.2	1.5	0.2		2.4		<b>7.2</b>	<b>89.5</b>	<b>3.3</b>
				40.3	2.8	20.8	2.8		33.3		<b>100</b>		
<b>BMM</b>	<b>4</b>			1.8	0.1	1			2.6		<b>5.5</b>	<b>93.2</b>	<b>1.3</b>
				32.7	1.8	18.2			47.3		<b>100</b>		
average											8.4	89.6	2.0
standard deviation											7.8	7.4	0.7

\* Excluding pyrite

Sample 4 from the **BMM** contains 35 vol.% alginite, 18 vol.% sporinite and 47 vol.% liptodetrinite. Altogether, this sample has 5.5 vol.% organic matter. Five samples from the **LDSM** contain between 5 (sample 27) and 29 vol.% (sample 21) microscopically visible organic matter. The organic matter in sample 21 is dominated by landplant-derived vitrinite. Three samples from the **UDSM** contain in average 3.7 vol.% organic matter. High percentages of sporinite (19 vol.%) and liptodetrinite (32 vol.%) have been observed in samples 78 and 68, respectively.

Sample 97 from turbiditic layers of the **GSF** consists of 4 vol.% organic matter.

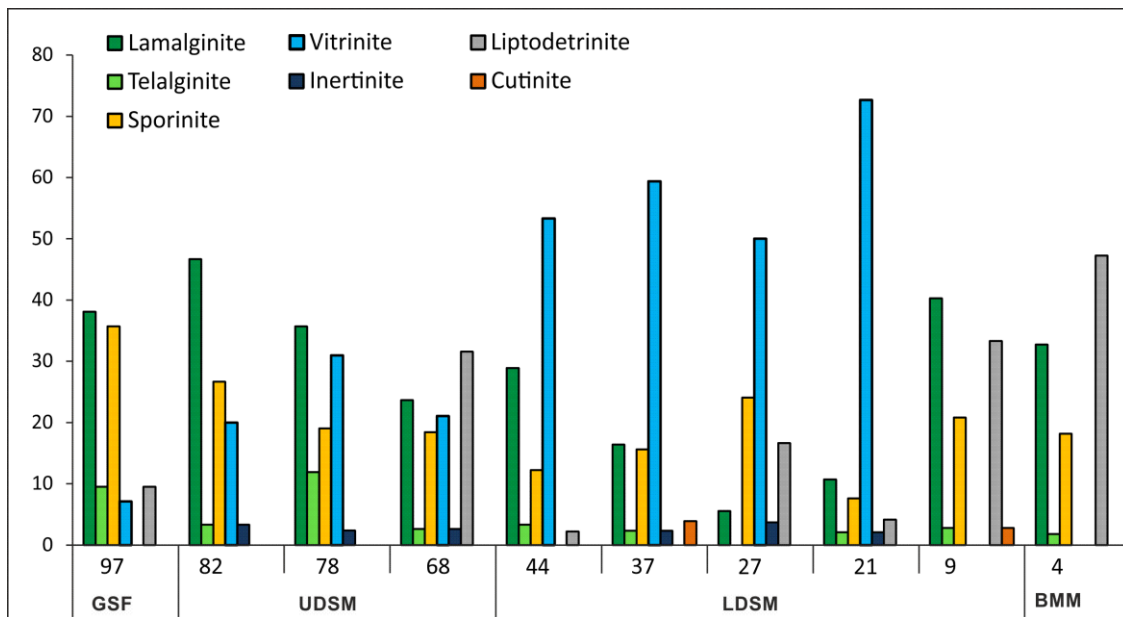


Figure 37: Contribution of various macerals. GSF=Gura Soimului Fm., UDSM=Upper Dysodilic Shale Mbr., LDSM=Lower Dysodilic Shale Mbr., BMM=Bituminous Marl Mbr.

There is an excellent correlation between vitrinite contents (mineral matter free) and diterpenoid concentrations ( $r^2=0.86$ ) suggesting that vitrinite is mainly derived from gymnosperms (Figure 38).

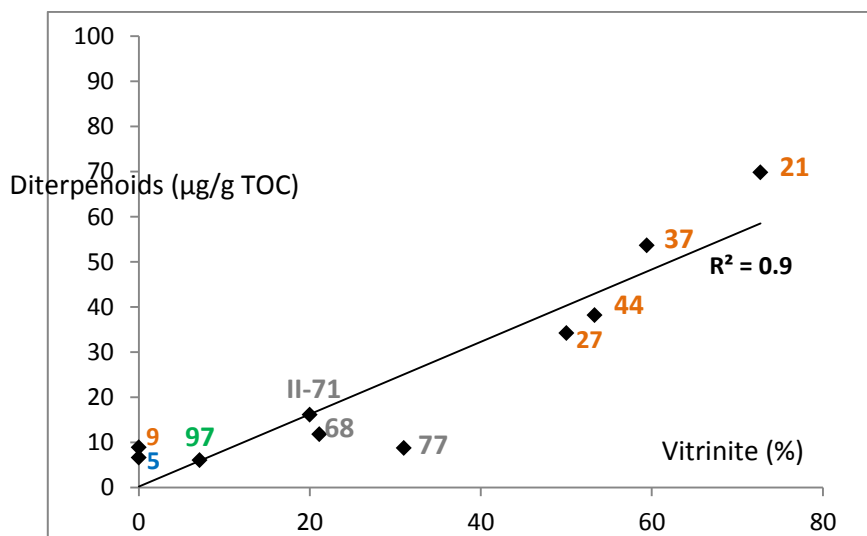


Figure 38: Diterpenoids versus Vitrinite

Vitrinite reflectance varies between 0.37 %Rr (samples 21, 44) and 0.42 %Rr (sample 78) proving that the organic matter is thermally immature.

## 4.7 Pyrolysis-GC

Eight samples representing the BMM, LDSM and UDSM were selected for pyrolysis gas chromatography. The TOC values of these samples vary between 1.24 (II-49) and 7.36 % (77). The HI varies from 311 (sample 66) to 603 mgHC/gTOC (sample 20).

Tables in the Appendix provide information on the individual components in the pyrolysate together with TOC content and hydrogen index

Figure 39 shows the kerogen classification established by Horsfield (1989), which considers the aliphatic fraction, i.e. *n*-alkyl-chain-length distribution versus total gas C1-5, from open-system pyrolysis experiments, in a ternary diagram. Horsfield (1989) defined petroleum type organofacies fields based on the observation that source kerogens of high wax oils have a high proportion of long-chain *n*-alkanes and *n*-alkenes in their pyrolysates, whereas major sources of gas are characterised by very short average *n*-alkyl chain length. Intermediate chain lengths were found to characterise anoxic marine shales, which generate low-wax crude oils in nature.

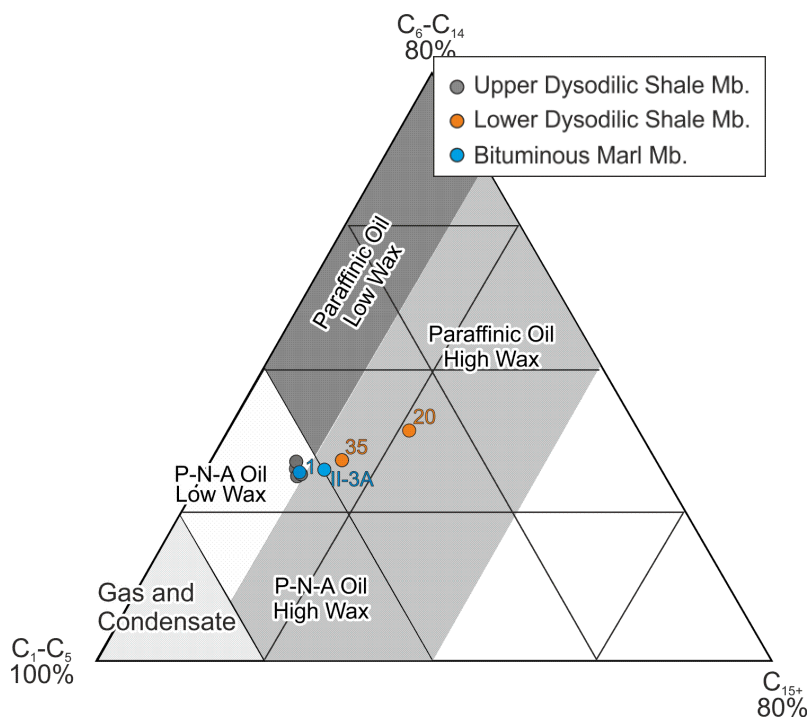


Figure 39: Characterisation of petroleum type organofacies based on carbon chain length distribution. (Horsfield 1989)

The samples from the **BMM** plot on the edges of the “Paraffinic-Naphthenic-Aromatic (P-N-A) Oil High Wax” facies. Sample 1 is close to the “Paraffinic Oil High Wax” field and sample II-3A plots close to the “P-N-A Low Wax” field. Two samples from the **LDSM** will generate “High Wax Paraffinic Oil”. Sample 20, characterized by the highest wax content, contains kerogen with the highest HI of all samples used for Py-GC. This fits well with the observation that high wax oils are mostly derived from autochthonous hydrogen-rich organic matter (alginate, liptodetrinite, (Mahlstedt 2012)). All samples from the UDSM have black oil potential. They plot into the “P-N-A Oil Low Wax” field.

The samples can be further characterized using two ternary diagrams, in which readily identifiable aliphatic, aromatic, oxygen- and sulfur-bearing compounds are employed.

Figure 40 shows Py-GC screening data based on the sulfur discriminator (Eglinton et al. 1990). As pyrolytic thiophenes were shown to be proportionally representative of kerogen-bond-sulfur molecules

(Eglinton et al. 1990), the use of 2,3-dimethylthiophene and o-xylene and n-C<sub>9:1</sub> in a ternary diagram (Eglinton et al. 1990) allows the discrimination of source rocks deposited in marine or hyper saline sedimentary environments and those deposited in freshwater lacustrine or terrestrial environments. All samples plot into the “type II intermediate” field in Figure 40, whereby samples from the UDSM (and sample 35 from the LDSM) yield slightly higher amounts of 2,3-dimethylthiophenes and o-xylenes and smaller amounts of n-C<sub>9:1</sub> in comparison to the remaining samples. Despite of these subtle differences, all samples will yield low sulfur oils.

The ternary diagram in Figure 41 (after (Larter 1984)) shows the relative proportions of phenol, n-octene and m,p-xylene in the pyrolysate. It can be used to evaluate the amount of kerogen representing land plant derived moieties and to distinguish between phenol-rich and phenol-poor Type III source rocks (Mahlstedt 2012). The samples from the BMM and sample 20 from the LDSM plot into the “aquatic” field in Figure 41. The remaining samples plot into the “terrestrial” field.

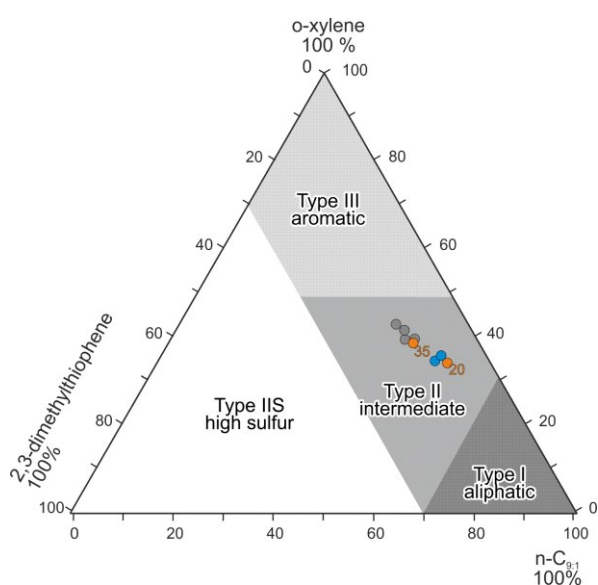


**Figure 40: Screening data from pyrolysis gas chromatography: sulfur discriminator (Eglinton et al. 1990)**

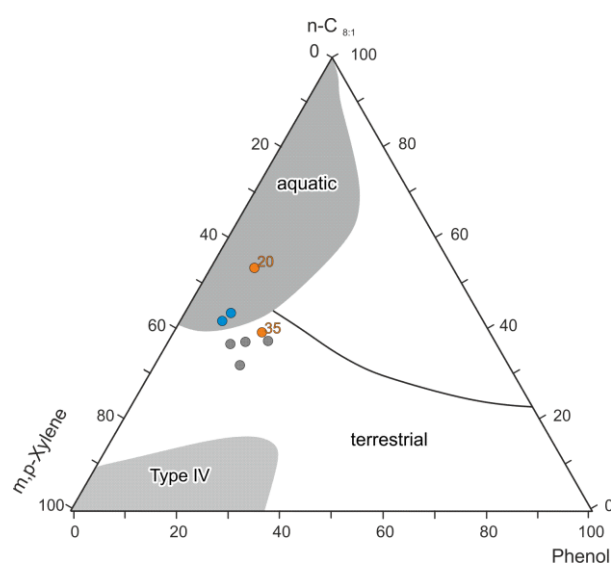


**Figure 41: Characterisation of petroleum type organofacies based on phenol content**

Marine source rocks such as black shales and carbonates of high petroleum potential display an enrichment in aromatic compounds such as alkylbenzenes and alkyl-naphthalenes, as well as sulfur containing compounds (Mahlstedt 2012). Their organic matter is derived from algal and bacterial inputs containing autochthonous material in abundance, as well as terrigenous debris. Most dominant aromatic hydrocarbons are toluene and xylenes, with amounts equalling or exceeding those of n-hydrocarbons in the same boiling range (Mahlstedt 2012). Aromatic compounds are products from the non-condensed aromatic structure of type II kerogen (Hartgers et al. 1994; Vandenbroucke 2003), which are released in the form of labile moieties during artificial and natural maturation (Horsfield 1989). Alkylthiophenes are formed during early diagenesis by intermolecular sulfur incorporation reactions involving functionalised lipids and hydrogen sulfide (Eglinton et al. 1990), and are released preferentially by thermal degradation of polysulfide bonded linear C5-C7 skeletons (Sinninghe Damsté et al. 1998).

## 4.8 Inorganic Geochemistry

Element concentrations of 43 samples have been determined using a handheld XRF instrument and are listed in Table 10.

**Table 10: Concentrations (in %) of elements and element oxides determined with a handheld XRF instrument (missing values are below the detection limit)**

Sample	Al	Al <sub>2</sub> O <sub>3</sub>	Ca	CaO	Cl	Cu	CuO	Fe	Fe <sub>2</sub> O <sub>3</sub>	K	K <sub>2</sub> O	Mn	MnO	Mo x10 <sup>-5</sup>	MoO <sub>3</sub> x10 <sup>-5</sup>	Ni	NiO
98	6.7	12.7	2.0	2.8	0.13	0.003	0.004	4.6	6.5	4.0	4.8	0.12	0.15	6.3	9.5		
II-80	8.0	15.0	1.1	1.6	0.13	0.006	0.008	6.2	8.8	3.6	4.3	0.45	0.58			0.010	0.013
II-79	7.5	14.2	0.6	0.8	0.13	0.008	0.010	4.8	6.9	3.7	4.4	0.17	0.22	4.0	5.9	0.009	0.011
II-78	7.7	14.5	1.0	1.3	0.13	0.004	0.005	5.5	7.8	3.5	4.3	0.27	0.35	3.3	5.0	0.012	0.015
85	7.5	14.2	0.7	1.0	0.14	0.019	0.024	3.6	5.2	3.1	3.7	0.19	0.25			0.014	0.018
II-77	8.4	15.9	0.9	1.2	0.14	0.009	0.011	4.5	6.4	3.5	4.2	0.31	0.40			0.011	0.014
II-75	8.7	16.4	0.9	1.2	0.13	0.012	0.015	4.8	6.9	3.3	4.0	0.12	0.15			0.012	0.015
84	8.4	15.9	1.0	1.4	0.15	0.011	0.014	4.9	7.1	3.5	4.2	0.47	0.61			0.011	0.014
II-74	8.9	16.8	0.6	0.8	0.13	0.016	0.020	4.0	5.8	3.5	4.3	0.07	0.09			0.009	0.011
83	8.1	15.3	1.1	1.5	0.13	0.009	0.011	5.3	7.6	3.4	4.1	0.48	0.61			0.010	0.013
II-73	7.7	14.6	0.7	1.0	0.15	0.008	0.010	5.4	7.7	3.0	3.6	0.09	0.12	18.9	28.4	0.013	0.017
II-72	8.6	16.3	0.8	1.1	0.14	0.007	0.009	4.8	6.8	3.2	3.8	0.08	0.11	13.6	20.5	0.009	0.011
II-71	8.9	16.7	0.7	0.9	0.14	0.010	0.013	5.3	7.6	3.0	3.6	0.06	0.07			0.011	0.014
81	7.4	14.0	0.8	1.1	0.14	0.007	0.009	6.0	8.5	2.6	3.2	0.08	0.10			0.014	0.018
II-70	7.4	14.0	0.7	1.0	0.15	0.005	0.006	4.7	6.8	3.2	3.8	0.12	0.15			0.005	0.006
80	8.0	15.2	1.4	2.0	0.14	0.006	0.008	7.9	11.4	2.6	3.1	0.19	0.24			0.011	0.014
78	7.7	14.5	0.7	0.9	0.15	0.008	0.010	4.6	6.6	2.9	3.5	0.06	0.08			0.009	0.011
II-69	6.9	13.1	0.5	0.7	0.14	0.005	0.006	4.7	6.7	2.8	3.4	0.06	0.08			0.007	0.009
II-68	7.6	14.3	0.6	0.8	0.13	0.004	0.005	4.7	6.8	3.0	3.6	0.05	0.07	17.5	26.3	0.005	0.006
II-67	6.5	12.2	0.5	0.7	0.13	0.004	0.005	4.4	6.3	2.8	3.4	0.07	0.09	10.8	16.1		
77	7.6	14.3	1.0	1.4	0.15	0.014	0.018	7.9	11.2	2.5	3.1	0.06	0.08			0.022	0.028
76	5.6	10.6	0.4	0.6	0.13	0.003	0.004	3.1	4.4	2.6	3.2	0.07	0.09				
II-64	6.8	12.8	0.5	0.6	0.14	0.005	0.006	4.7	6.7	2.9	3.4	0.08	0.10	9.9	14.9		
II-63	7.1	13.4	0.7	1.0	0.14	0.009	0.011	5.4	7.7	2.7	3.3	0.07	0.09	49.7	74.6	0.012	0.015
75	7.4	13.9	0.6	0.8	0.14	0.006	0.008	4.4	6.4	3.0	3.6	0.06	0.08			0.008	0.010
II-62	6.8	12.8	0.6	0.8	0.14	0.005	0.006	4.9	7.0	2.7	3.3	0.07	0.09	24.4	36.6	0.005	0.006
73	6.6	12.4	0.8	1.1	0.15	0.004	0.005	4.8	6.9	2.6	3.2	0.07	0.08	14.2	21.2	0.004	0.005
II-57	6.7	12.7	0.6	0.9	0.14	0.005	0.006	4.6	6.5	2.7	3.2	0.06	0.07	16.3	24.4		
II-54	6.4	12.0	0.5	0.7	0.13	0.005	0.006	4.3	6.1	2.7	3.3	0.06	0.08	11.0	16.5		
II-50	4.1	7.7	0.4	0.5	0.17	0.002	0.003	2.1	3.0	1.9	2.2	0.06	0.08	5.3	7.9		
II-49	5.2	9.8	0.4	0.5	0.15	0.003	0.004	2.3	3.3	2.4	2.8	0.06	0.08	8.4	12.6		
42b	7.1	13.5	0.5	0.8	0.13	0.005	0.006	4.0	5.8	2.9	3.5	0.05	0.06	9.9	14.8	0.006	0.008
42a	2.4	4.6	0.5	0.6	0.12			1.4	2.0	1.2	1.4	0.07	0.09	4.5	6.7		
35	7.1	13.5	0.5	0.7	0.13	0.005	0.006	4.2	6.0	3.2	3.9	0.05	0.06	11.3	16.9	0.004	0.005
33	5.6	10.6	0.4	0.6	0.13	0.003	0.004	3.3	4.8	2.7	3.3	0.05	0.06	9.1	13.6		
20	6.1	11.5	0.5	0.7	0.13	0.003	0.004	4.6	6.6	3.1	3.8	0.04	0.05	7.3	10.9	0.004	0.005
12	5.0	9.4	0.7	1.0	0.21	0.003	0.004	3.9	5.6	2.8	3.3	0.04	0.05	12.1	18.2	0.004	0.005
11	0.5	0.9	0.4	0.6	0.22	0.002	0.003	0.9	1.3	0.5	0.6	0.07	0.09	6.1	9.2		
II-3a	2.5	4.8	24.7	34.5	0.14			1.5	2.2	0.4	0.5	0.07	0.09	6.5	9.7		
1	2.7	5.1	14.5	20.2	0.11			1.1	1.6	0.8	1.0	0.05	0.06	4.4	6.6		
II-4	2.2	4.1	28.6	39.9	0.16			2.0	2.8	0.2	0.2	0.08	0.11	4.2	6.3		
II-2	6.1	11.5	3.3	4.6	0.13			3.4	4.9	2.6	3.1	0.04	0.05	3.5	5.3		
II-1	4.9	9.2	4.2	5.9	0.13			3.2	4.6	1.9	2.3	0.05	0.06	4.8	7.2		



**Table 11: Concentrations (in %) of elements and element oxides determined with a handheld XRF instrument (missing values are below the detection limit)**

Sample	P	P <sub>2</sub> O <sub>5</sub>	Rb	RbO <sub>2</sub>	Si	SiO <sub>2</sub>	Sr	SrO	Ti	TiO <sub>2</sub>	V	V <sub>2</sub> O <sub>5</sub>	Zn	ZnO	Zr	ZrO <sub>2</sub>
98	0.14	0.32	0.012	0.013	25.4	54.4	0.008	0.009	0.54	0.91	0.013	0.023	0.009	0.011	0.032	0.043
II-80	0.16	0.37	0.019	0.021	26.1	55.9	0.011	0.013	0.48	0.79	0.018	0.032	0.011	0.014	0.015	0.020
II-79	0.13	0.29	0.019	0.021	26.3	56.2	0.012	0.014	0.53	0.88	0.014	0.025	0.011	0.014	0.015	0.020
II-78	0.13	0.30	0.018	0.020	26.3	56.3	0.011	0.013	0.48	0.79	0.015	0.027	0.010	0.012	0.014	0.019
85	0.13	0.30	0.017	0.019	28.6	61.2	0.011	0.013	0.48	0.81	0.015	0.027	0.010	0.012	0.023	0.031
II-77	0.14	0.32	0.020	0.022	27.4	58.5	0.012	0.014	0.53	0.88	0.016	0.029	0.010	0.012	0.015	0.020
II-75	0.16	0.36	0.019	0.021	27.1	57.9	0.012	0.014	0.50	0.83	0.021	0.037	0.010	0.012	0.014	0.019
84	0.16	0.37	0.020	0.022	26.1	55.7	0.012	0.014	0.51	0.85	0.015	0.027	0.011	0.014	0.015	0.020
II-74	0.14	0.33	0.020	0.022	28.3	60.5	0.012	0.014	0.52	0.87	0.019	0.034	0.008	0.010	0.015	0.020
83	0.15	0.34	0.019	0.021	25.9	55.3	0.011	0.013	0.49	0.81	0.019	0.034	0.011	0.014	0.014	0.019
II-73	0.12	0.28	0.017	0.019	25.4	54.4	0.011	0.013	0.51	0.85	0.025	0.045	0.010	0.012	0.015	0.020
II-72	0.14	0.33	0.019	0.021	27.2	58.2	0.013	0.015	0.55	0.92	0.028	0.050	0.010	0.012	0.015	0.020
II-71	0.12	0.28	0.018	0.020	27.0	57.7	0.012	0.014	0.52	0.87	0.033	0.059	0.008	0.010	0.016	0.022
81	0.11	0.25	0.015	0.016	24.0	51.3	0.010	0.012	0.50	0.84	0.021	0.037	0.006	0.007	0.016	0.022
II-70	0.12	0.27	0.016	0.017	28.4	60.8	0.014	0.017	0.52	0.86	0.016	0.029	0.008	0.010	0.023	0.031
80	0.14	0.33	0.014	0.015	23.9	51.1	0.012	0.014	0.46	0.77	0.020	0.036	0.008	0.010	0.014	0.019
78	0.12	0.27	0.017	0.019	26.2	56.1	0.012	0.014	0.53	0.88	0.031	0.055	0.008	0.010	0.018	0.024
II-69	0.14	0.32	0.014	0.015	27.9	59.6	0.012	0.014	0.51	0.84	0.017	0.030	0.009	0.011	0.022	0.030
II-68	0.14	0.33	0.014	0.015	27.1	57.9	0.012	0.014	0.53	0.89	0.019	0.034	0.007	0.009	0.026	0.035
II-67	0.11	0.26	0.013	0.014	28.0	59.9	0.014	0.017	0.52	0.86	0.020	0.036	0.007	0.009	0.026	0.035
77	0.18	0.42	0.015	0.016	22.7	48.6	0.013	0.015	0.43	0.72	0.036	0.064	0.007	0.009	0.014	0.019
76	0.15	0.34	0.010	0.011	32.6	69.7	0.009	0.011	0.43	0.72	0.010	0.018	0.005	0.006	0.039	0.053
II-64	0.12	0.27	0.014	0.015	28.2	60.3	0.012	0.014	0.52	0.87	0.021	0.037	0.009	0.011	0.025	0.034
II-63	0.15	0.33	0.014	0.015	28.0	60.0	0.013	0.015	0.47	0.78	0.020	0.036	0.008	0.010	0.021	0.028
75	0.15	0.35	0.016	0.017	28.0	59.9	0.012	0.014	0.49	0.81	0.018	0.032	0.010	0.012	0.019	0.026
II-62	0.11	0.25	0.014	0.015	27.5	58.8	0.013	0.015	0.52	0.86	0.016	0.029	0.009	0.011	0.022	0.030
73	0.12	0.27	0.013	0.014	27.1	57.9	0.011	0.013	0.50	0.84	0.017	0.030	0.009	0.011	0.021	0.028
II-57	0.13	0.29	0.013	0.014	28.3	60.6	0.015	0.018	0.49	0.81	0.024	0.043	0.007	0.009	0.021	0.028
II-54	0.12	0.28	0.013	0.014	28.6	61.2	0.013	0.015	0.48	0.80	0.020	0.036	0.008	0.010	0.026	0.035
II-50	0.15	0.34	0.007	0.008	38.2	81.6	0.011	0.013	0.39	0.65	0.005	0.009	0.005	0.006	0.047	0.063
II-49	0.43	0.97	0.009	0.010	33.6	71.9	0.012	0.014	0.48	0.80	0.009	0.016	0.005	0.006	0.052	0.070
42b	0.16	0.36	0.014	0.015	29.0	62.1	0.010	0.012	0.56	0.93	0.016	0.029	0.012	0.015	0.044	0.059
42a	0.14	0.32	0.005	0.005	43.0	92.0	0.006	0.007	0.26	0.43			0.003	0.004	0.033	0.045
35	0.15	0.33	0.015	0.016	28.7	61.5	0.009	0.011	0.55	0.91	0.019	0.034	0.007	0.009	0.039	0.053
33	0.33	0.75	0.011	0.012	31.1	66.6	0.007	0.008	0.49	0.82	0.010	0.018	0.005	0.006	0.058	0.078
20	0.11	0.26	0.014	0.015	29.6	63.2	0.012	0.014	0.50	0.84	0.014	0.025	0.006	0.007	0.039	0.053
12	0.15	0.35	0.011	0.012	31.5	67.5	0.009	0.011	0.49	0.81	0.013	0.023	0.005	0.006	0.047	0.063
11	0.64	1.46	0.002	0.002	49.5	105.9	0.005	0.006	0.22	0.37			0.002	0.002	0.051	0.069
II-3a	0.18	0.41	0.002	0.002	16.3	34.8	0.045	0.053	0.07	0.12					0.003	0.004
1	0.178	0.408	0.004	0.004	26.3	56.2	0.053	0.063	0.14	0.23					0.007	0.009
II-4	0.167	0.383			9.4	20.1	0.035	0.041	0.03	0.05						
II-2	0.120	0.275	0.013	0.014	27.02	57.80	0.020	0.024	0.54	0.90	0.015	0.027	0.006	0.007	0.026	0.035
II-1	0.167	0.383	0.009	0.010	32.69	69.92	0.021	0.025	0.38	0.64	0.011	0.020	0.006	0.007	0.021	0.028

Element concentrations of three samples have been analyzed using a traditional calcination (Table 12) to test the reliability of the handheld instrument. Because the analytical results from both techniques fit well, the values yielded with the handheld instrument are considered reliable and used to establish the depth trends shown in Figure 42.

**Table 12: Concentrations (in ppm and %) of elements and element oxides of samples 98, II-67, II-79 using XRF technique and traditional pellets**

(ppm)	98	II-67	II-79
Ba	638.35	611.75	393.70
BaO	712.72	683.02	439.57
Ce	85.20	68.55	60.95
CeO <sub>2</sub>	104.66	84.21	74.87
Co	13.60	9.25	23.80
CoO	17.29	11.76	30.26
Cr	87.55	153.45	149.05
Cr <sub>2</sub> O <sub>3</sub>	127.95	224.27	217.84
Cu	34.85	44.80	78.45
CuO	43.63	56.08	98.20
Ga	19.55	21.25	26.00
Ga <sub>2</sub> O <sub>3</sub>	26.28	28.56	34.95
La	40.95	25.20	38.70
La <sub>2</sub> O <sub>3</sub>	48.03	29.55	45.39
Nb	18.45	18.80	18.65
Nb <sub>2</sub> O <sub>5</sub>	26.39	26.89	26.68
Ni	39.25	59.20	102.75
NiO	49.95	75.33	130.75
Pb	30.20	23.60	14.30
PbO	34.86	27.24	16.51
Rb	113.75	137.70	208.30
Rb <sub>2</sub> O	124.40	150.59	227.80
Sc	13.50	15.40	15.85
Sc <sub>2</sub> O <sub>3</sub>	20.71	23.62	24.31
Sr	100.05	146.35	127.05
SrO	118.32	173.07	150.25
Th	7.90	7.90	9.65
ThO <sub>2</sub>	8.45	8.45	10.32
V	181.35	282.80	226.05
V <sub>2</sub> O <sub>5</sub>	323.75	504.85	403.54
Y	38.35	25.85	28.95
Y <sub>2</sub> O <sub>3</sub>	48.70	32.83	36.76
Zn	75.40	71.85	106.50
ZnO	93.86	89.44	132.57
Zr	288.05	256.60	141.15
ZrO <sub>2</sub>	389.10	346.62	190.67

(%)	98	II-67	II-79
Al	9.09	8.75	11.30
Al <sub>2</sub> O <sub>3</sub>	17.18	16.53	21.36
Ca	1.90	0.44	0.53
CaO	2.66	0.62	0.74
Fe	4.62	5.08	5.03
Fe <sub>2</sub> O <sub>3</sub>	6.61	7.26	7.19
K	3.73	2.84	3.76
K <sub>2</sub> O	4.49	3.43	4.53
Mg	2.29	1.24	1.66
MgO	3.79	2.05	2.76
Mn	0.09	0.02	0.13
MnO	0.12	0.03	0.17
Na	1.40	0.69	0.55
Na <sub>2</sub> O	1.89	0.93	0.74
P	0.08	0.05	0.09
P <sub>2</sub> O <sub>5</sub>	0.19	0.11	0.21
S	0.22	0.18	0.00
SO <sub>3</sub>	0.56	0.45	-0.01
Si	29.17	31.65	28.99
SiO <sub>2</sub>	62.41	67.71	62.02
Ti	0.53	0.51	0.52
TiO <sub>2</sub>	0.88	0.85	0.86

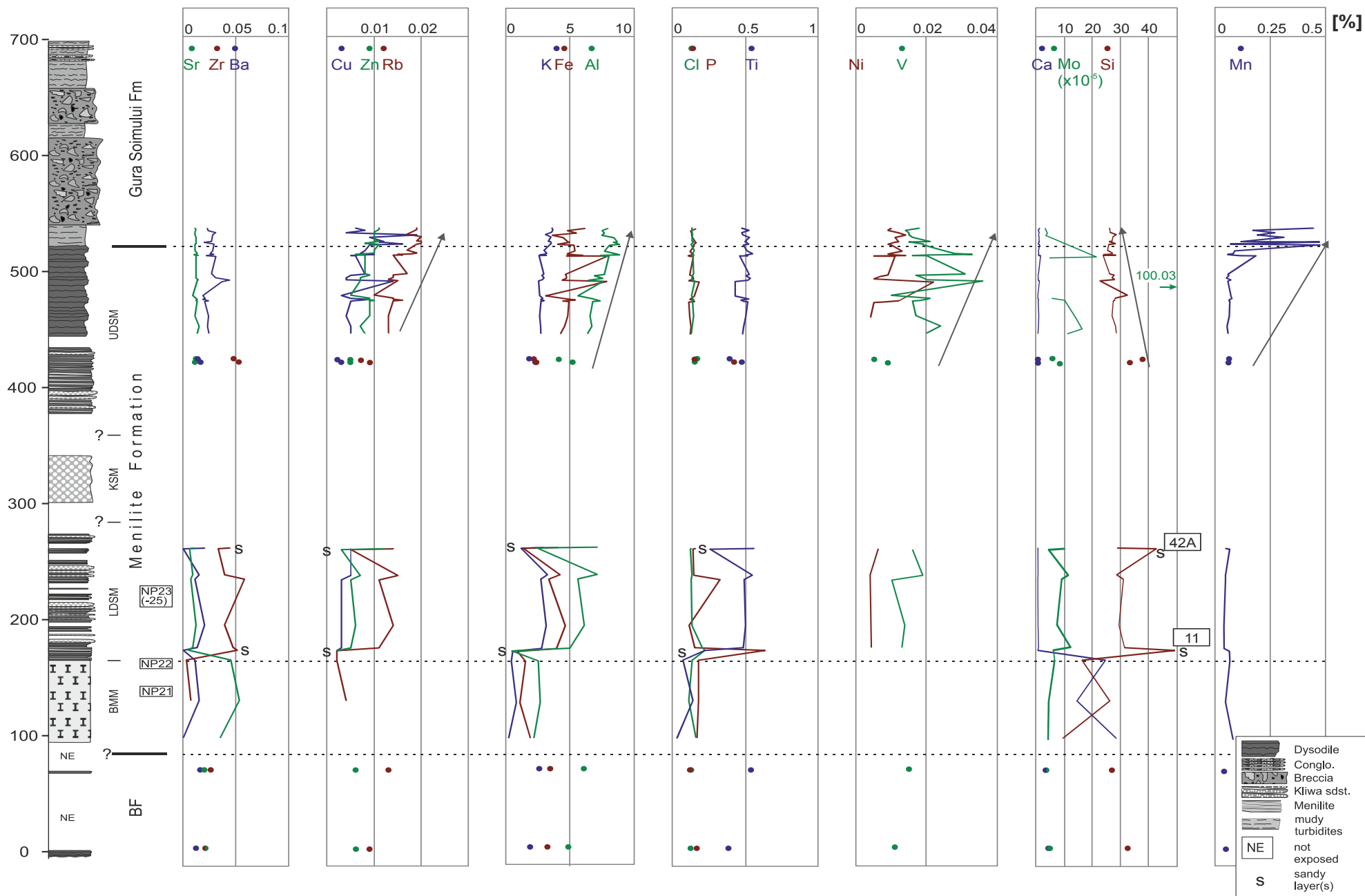


Figure 42: Element concentrations (%) versus depth

Concentrations of major element oxides are plotted in a triangular plot showing relative proportions of CaO (mostly carbonates), SiO<sub>2</sub> (quartz/opal and aluminosilicates) and Al<sub>2</sub>O<sub>3</sub> (aluminosilicates) (Figure 43). For comparison, average shale (AS, Wedepohl, 1971), K-feldspar and kaolinite are also plotted (Bunte 2009).

With the exception of samples from the BMM and the BF, all samples are low in carbonate. Most samples from the Menilite Formation have higher Al<sub>2</sub>O<sub>3</sub>/SiO<sub>2</sub> ratios than average shale or K-feldspar suggesting that quartz is a considerable detrital component. In addition, some SiO<sub>2</sub> may be of biogenic origin. In contrast, samples from the GSF plot close to K-feldspar/average shale. No sample plots near the kaolinite composition. This may indicate that weathering was not intense during the deposition.

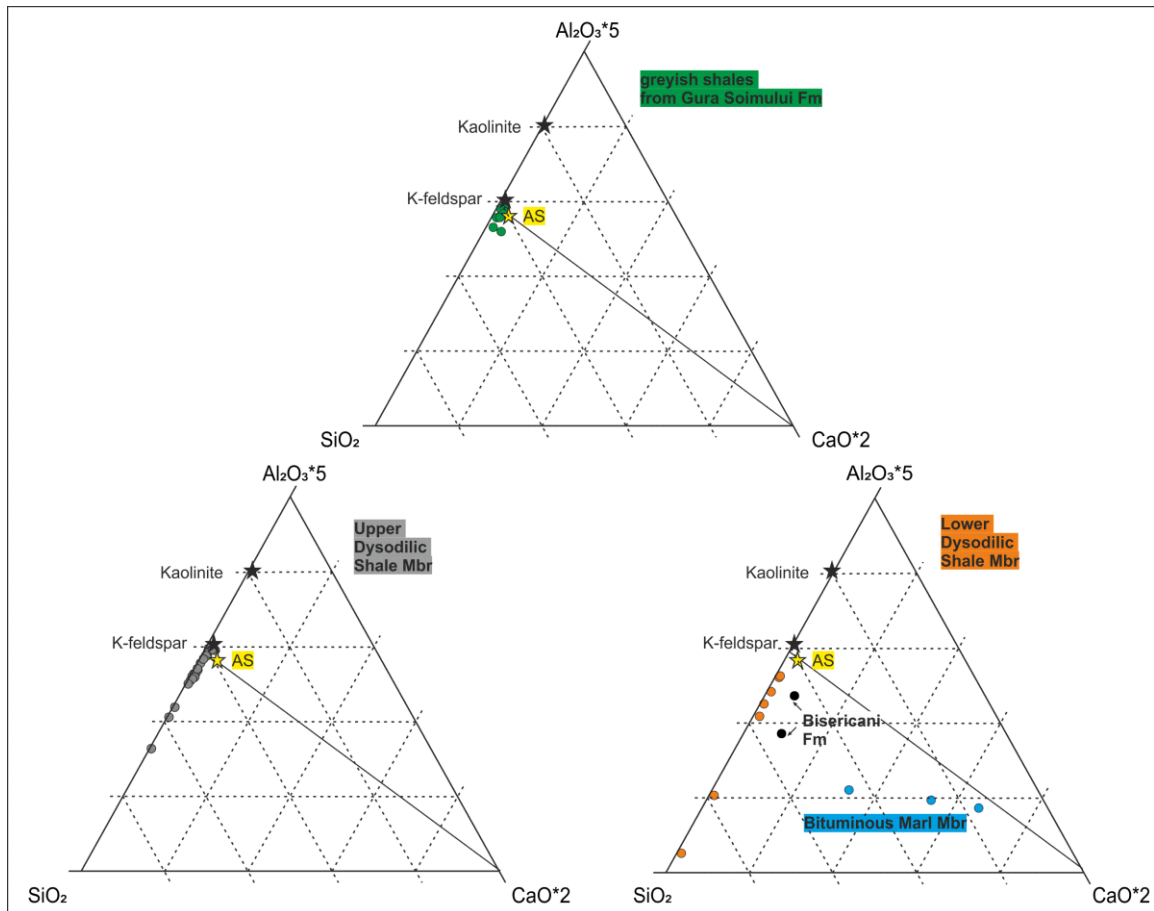


Figure 43: Plot of major element oxides (Al<sub>2</sub>O<sub>3</sub>\*5 – SiO<sub>2</sub> – CaO\*2). For comparison, average shale (AS), K-feldspar, and kaolinite are plotted as well (after Wedepohl, 1971).

CaO, Sr, and MnO concentrations are cross-plotted against TIC concentrations in Figure 44 A, B, C. TiO<sub>2</sub> versus Al<sub>2</sub>O<sub>3</sub> and Zr versus Al<sub>2</sub>O<sub>3</sub> is plotted in Figure 45.

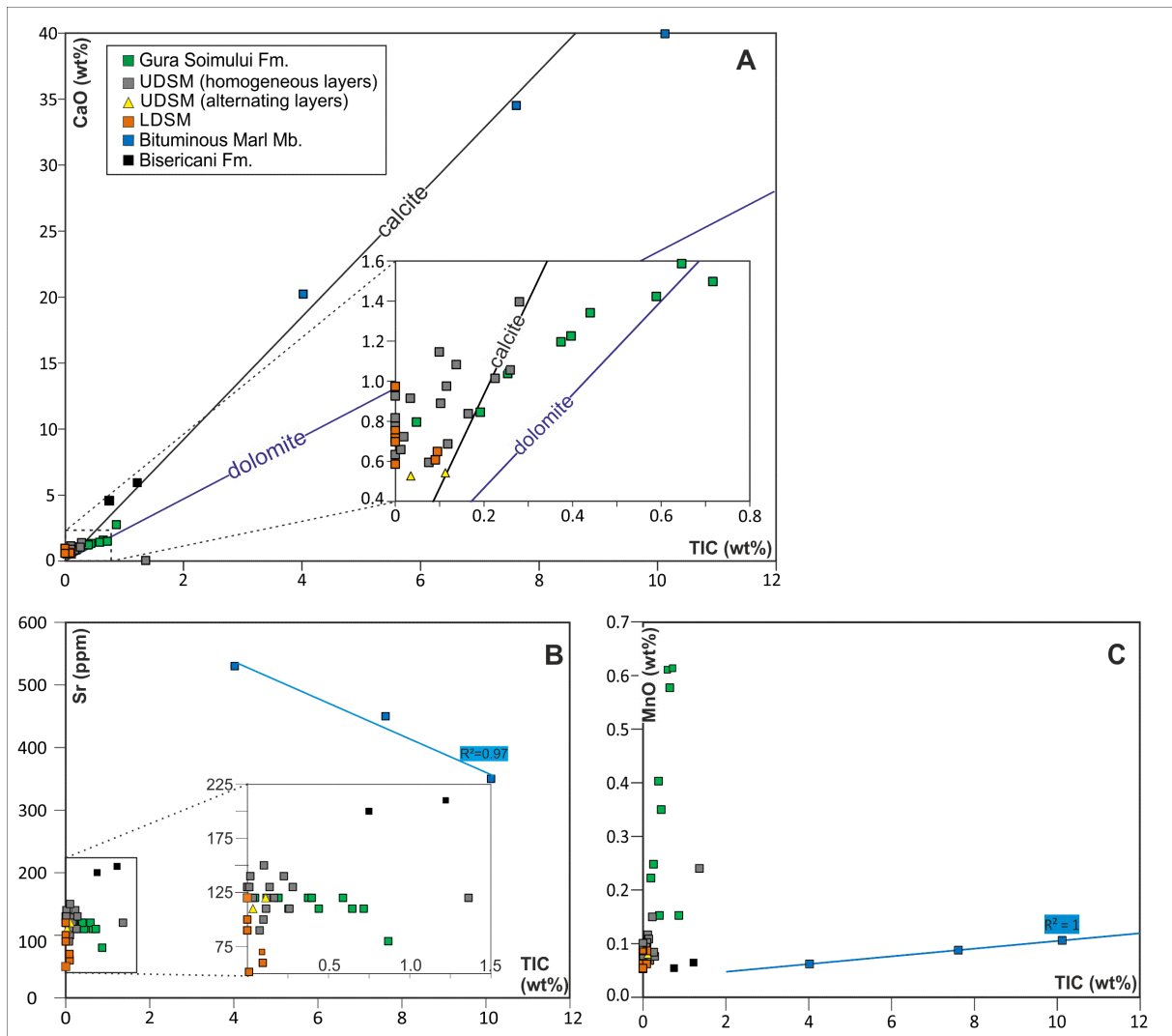


Figure 44: Plots of A) CaO, B) Sr and C) MnO versus total inorganic carbon (TIC)

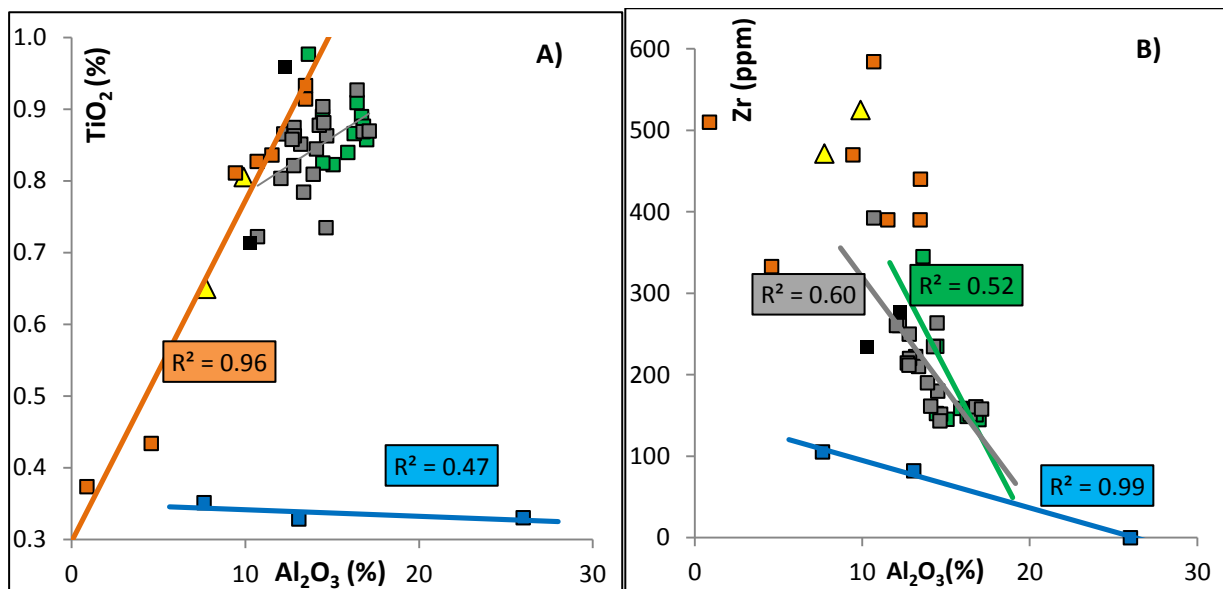


Figure 45: Plots of A) TiO<sub>2</sub> and B) Zr versus Al<sub>2</sub>O<sub>3</sub> (carbonate free). See Figure 44 for color-code

The detrital, non-carbonate fraction is investigated using cross-plots of TiO<sub>2</sub> and Zr versus Al<sub>2</sub>O<sub>3</sub> (Figure 45). In this diagram all concentrations were calculated on a “carbonate-free” basis to avoid simple dilution effects (Bunte 2009).

For example, Al<sub>2</sub>O<sub>3</sub> “carbonate-free” was calculated as follows:

$$Al_2O_3 \text{ "carbonate free"} = \frac{100 * Al_2O_3}{100 - CaCO_3}$$

$$Al_2O_3 = Al * 1.8895$$

$$CaCO_3 = TIC * 8.3331$$

Both, element concentrations and correlations between different oxides are discussed for each stratigraphic unit separately.

#### 4.8.1 Bisericani Formation

The carbonate content of the Bisericani Formation is lower than that of the BMM, but slightly higher than that of the LDSM and UDSM (Figure 44A). Consequently, the CaO and Sr contents also take medium values (Figure 42). The Mn content is low (<0.005 ppm).

#### 4.8.2 Menilite Formation

##### 4.8.2.1 Bituminous Marl Mbr.

In agreement with lithology, BMM samples contain the highest contents in calcium (av. 22.6 %) and strontium (av. 0.04 %; Figure 42). In contrast, aluminium (av. 2.5 %), potassium (0.45 %), silicon (av. 20 %) and iron contents (<2.0 %) are relatively low. V contents are below the detection limit. Mo contents are low (4-7 ppm). The high carbonate content is also visible in (Figure 43). All data points plot below the line for average shale indicating access SiO<sub>2</sub> (biogenic SiO<sub>2</sub> or detrital quartz).

As expected, there is a good fit between CaO and TIC ( $R^2=0.96$ ; Figure 44 A) and MnO and TIC ( $R^2=1.00$ ; Figure 44 C) indicating that most MnO is present in carbonate minerals. The ratio between CaO and TIC suggests that calcite is the main carbonate mineral. Sr is negatively correlated with TIC ( $R^2=0.97$ ; Figure 44 B). Hence, an additional non-carbonate source for Sr must be present.

Data points in Figure 45 show low TiO<sub>2</sub> (< 0.4 %) and Zr (0-100 ppm) concentrations, whereby the (carbonate-free) Al<sub>2</sub>O<sub>3</sub> value is moderate to high (7-28 %). Both, TiO<sub>2</sub> and Zr correlate negatively with Al<sub>2</sub>O<sub>3</sub> ( $R^2=0.47$  and  $0.99$ , respectively). This shows that Ti and Zr bearing phases other than clay minerals (e.g. heavy minerals) must be present (Bunte 2009).

#### 4.8.2.2 Lower Dysodilic Shale Mbr.

Strongly varying element concentrations reflect the different alternating lithologies.

The sandy samples 11 and 42A have high silicon (43 - 50 %), but low Ni, V, Ti, K, Fe, Al, Cu, Zn, Rb, Mn and Ba contents. Whereas, the concentration of P is high in the lower sample 11, the concentration of Zr is high in the upper sample 42A (Figure 42).

Fine-grained samples are characterized by lower silicon concentrations (Figure 42), but the diagram in Figure 43 shows that the SiO<sub>2</sub>/Al<sub>2</sub>O<sub>3</sub> ratio is still higher than in average shale. Zr contents are relative high.

Considering all LDSM samples, there is an excellent correlation between TiO<sub>2</sub> and Al<sub>2</sub>O<sub>3</sub> ( $R^2=0.96$ , Figure 45) suggesting that TiO<sub>2</sub> is more or less uniformly incorporated into the clay component. In contrast, there is no correlation between Zr and Al<sub>2</sub>O<sub>3</sub> (Figure 45).

#### 4.8.2.3 Upper Dysodilic Shale Mbr.

Samples from the lower heterolithic part of the UDSM show element concentrations similar to those from the LDSM. For example, the concentrations of Si, Zr are relative high. Whereas Si and Zr show an upward decreasing trend in the UDSM, Al and K concentrations increase upwards reflecting an increase in the shale component (see also Figure 43). Fe concentrations are typically higher in the UDSM than in the LDSM.

Trends visible in Figure 45 suggest that TiO<sub>2</sub> is incorporated into the clay component (weak positive correlation between TiO<sub>2</sub> and Al<sub>2</sub>O<sub>3</sub>;  $R^2= 0.24$ ), whereas Zr is probably present in heavy minerals (moderate negative correlation between Zr and Al<sub>2</sub>O<sub>3</sub>;  $R^2= 0.6$ ).

### 4.8.3 Gura Soimului Formation

Many trends observed in the UDSM continue in the lowermost part of the GSF. For example, Zn, Rb, K, and Al concentrations continue to increase upwards (Figure 42). Moreover, samples from the GSF plot close to average shale (Figure 43), similar to those from the upper part of the UDSM.

In contrast, trends of V, Mo and Mn show a break between the UDSM and the GSF. Whereas, V and Mo percentages are lower in the GSF than in the Menilite Fm., Mn contents are significantly higher. Mn percentages in the Menilite Fm. are <0.1 %, values up to 0.5 % occur in the GSF.

The TiO<sub>2</sub> and Al<sub>2</sub>O<sub>3</sub> contents are not correlated ( $R^2=0.07$ ; Figure 45A). In contrast, there is a moderate negative correlation ( $R^2=0.52$ ) between Zr and Al<sub>2</sub>O<sub>3</sub> (Figure 45B).

## 5 Discussion

### 5.1 Reliability of spectral gamma measurements

Because U and Th contents determined with the XRF instrument are mostly below the detection limit, only potassium contents can be compared with those from the spectral gamma ray tool.

The inset shows that K contents measured by the different approaches differ significantly. As values measured by the xrf tool are considered reliable (see chapter 4.8 Inorganic Geochemistry), the values from the gamma ray tool are rejected. Apart from a defect of the instrument, possible explanation for the disappointing result might be (1) weathering effects, (2) effects of rough, uneven surfaces, or (3) effects of adjacent layers in case of thin bedded, alternating lithologies.

Table 13: Potassium measured by xrf and gamma ray tool

sample	potassium [%]		$\Delta$ xrf-gamma
	xrf	gamma	
98	3.95	1.04	2.91
II-80	3.58	0.97	2.62
II-79	3.66	1.45	2.21
II-78	3.55	1.04	2.51
85	3.08	0.68	2.40
II-77	3.50	0.07	3.43
II-75	3.30	0.60	2.70
84	3.47	0.75	2.72
II-74	3.53	0.40	3.13
83	3.42	0.38	3.04
II-73	2.96	0.27	2.69
II-72	3.18	0.32	2.86
II-71	3.01	0.45	2.56
81	2.65	0.46	2.19
II-70	3.15	0.36	2.79
80	2.57	0.51	2.06
78	2.95	0.42	2.53
II-69	2.81	0.77	2.04
II-68	2.96	0.00	2.96
II-67	2.84	0.00	2.84
77	2.54	0.40	2.14
76	2.62	0.35	2.27
II-64	2.86	0.07	2.79
II-63	2.72	0.01	2.71
75	2.98	0.54	2.44
II-62	2.73	0.21	2.52
73	2.62	0.41	2.21
II-57	2.69	0.20	2.49
II-54	2.70	0.27	2.44
II-50	1.85	0.00	1.85
II-49	2.35	0.22	2.13

sample	potassium [%]		$\Delta$ xrf-gamma
	xrf	gamma	
42b	2.93	0.22	2.71
42a	1.17	0.21	0.96
35	3.23	1.20	2.03
33	2.71	0.89	1.82
20	3.13	1.01	2.12
12	2.77	0.31	2.46
11	0.51	0.55	-0.04
II-3a	0.40	0.00	0.40
1	0.79	0.01	0.79
II-4	0.15	0.00	0.16
II-2	2.60	0.00	2.60
II-1	1.88	0.00	1.88

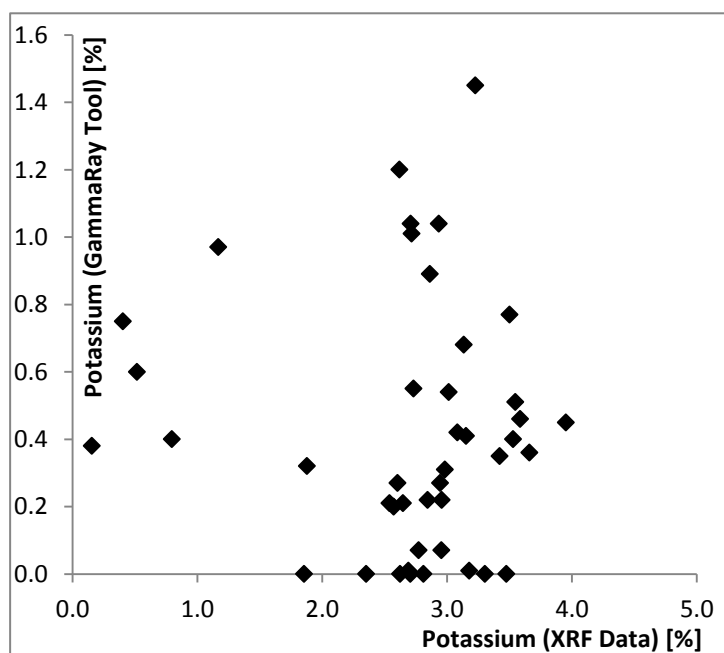


Figure 46: Gamma ray Potassium versus XRF Potassium



Because it is obvious that K contents measured with the gamma spectrometer are useless, U and Th contents are also not considered further.

## 5.2 Relation between TOC and gamma-ray response

One of the goals of the thesis is to investigate whether organic richness of the Menilite Formation can be determined by (spectral) gamma-ray tools, which would allow the estimation of the source potential of the Menilite Formation in boreholes.

A linear relationship between TOC and U has been reported in a few black shale systems (Bell et al. 1940; Bell et al. 1940). Further research was made by (Mann et al. 1986). They figured out, that the U/TOC ratio varies in black shale systems of different ages and in different regions. The U content in shales is determined by detrital and authigenic components within the shale. "Average non-bituminous shale" (Wedepohl 1971; Farrimond et al. 1998) contains about 4 ppm U, which is largely of detrital origin. Characteristic differences exist in relation on the detrital source material.

Source rocks are often enriched in authigenic U, which precipitates at the sediment-water interface under anoxic conditions and accumulates together with organic matter (Mann et al. 1986). The reduction and precipitation of authigenic U can lead to an increase in the total U content of organic-rich sediments, which may exceed by many times the detrital U component (Lüning & Kolonic 2003).

Lüning & Kolonic (2003) summarized factors controlling U/TOC ratios preserved in black shales. Amongst them are: (1) The primary concentration of dissolved U<sup>6+</sup> in the water column; (2) Low sedimentation rates favour higher U/TOC ratios, e.g. in abyssal compared to hemipelagic settings; (3) In alternating oxic and anoxic environments, U may be partly or fully oxidised, remobilised and released to solution; (4) Development of stable U/TOC ratios may be inhibited by shallow-marine, phosphate-, carbonate-, and sand-rich systems.

U values recorded with the gamma spectrometer along the Tazlau profile are questionable (see above). Therefore, the following diagrams (Figure 47) show the relation between dose rate (DR) and TOC for different stratigraphic units.

Because there are only two samples from the **BF**, it is impossible to assess the DR-TOC relation. DR values from the **BMM** are relative low, a result of high carbonate contents (Figure 19). Whereas DR and TOC in the **BMM** are not correlated, a moderate positive correlation ( $R^2=0.46$ ) exists for samples from the **LDSM**. In this unit DR values in coarse-grained layers (quartzarenites, conglomerates, Kliwa Sandstones) with low TOC contents vary considerably. Shale layers have strongly varying TOC values and low to moderate DR values. DR increases upwards in the **UDSM**. In its lower part (dysodile-sandstone alternations) DR is highly correlated ( $R^2=0.74$ ) with TOC contents. In its homogenous upper part there is no correlation. Strongly varying and partly remarkably high DR values are observed in the **GSF** despite of low TOC contents.

The study shows moderate correlations between DR and TOC in the LDSM ( $R^2=0.46$ ) and the lower part of the UDSM ( $R^2 =0.74$ ). However, the relation between DR and TOC is different in both units. Moreover, no relation exists for other units. This implies that DR is controlled rather by lithology (carbonate and sand content) and variations in the detrital U component, than by organic matter richness.

It remains unclear, whether U contents would show better correlations. However, as emphasized by Lüning & Kolonic (2003), stable U/TOC ratios are rarely developed in shallow-marine, carbonate and sand-rich systems. Therefore the applicability of the spectral gamma log to assess TOC contents in the Menilite Formation is probably limited.

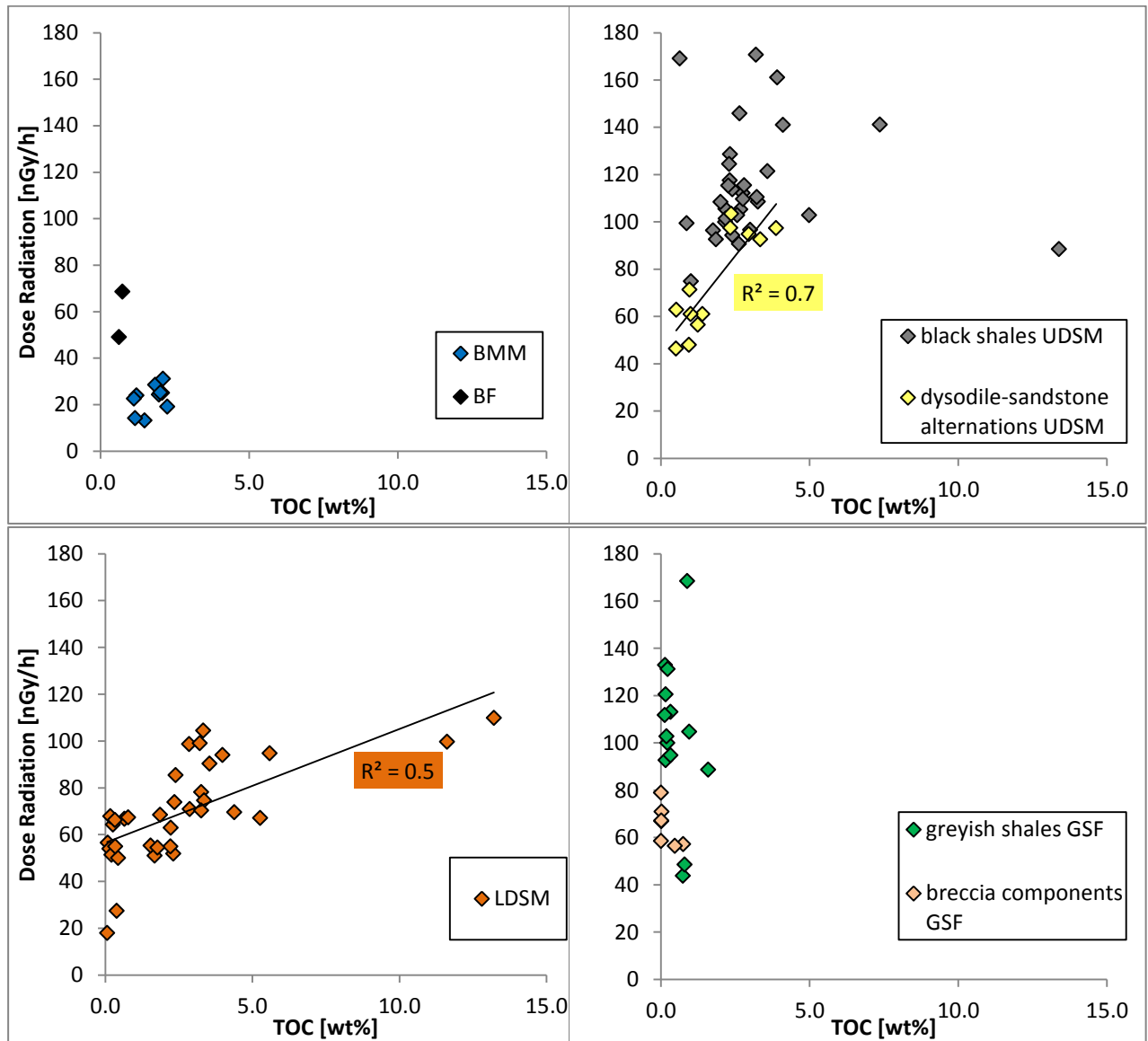


Figure 47: Plot of Dose Rate versus TOC for different stratigraphic units

### 5.3 Maturity

Vitrinite reflectance (c. 0.4 % R<sub>r</sub>), RockEval parameter T<sub>max</sub> (412-437 °C) and hopane isomerization ratios (0.35-0.47) show that the organic matter is thermally immature. The maturity parameters do not increase with stratigraphic depth indicating that maturation is syn- or post-orogenic.

The presence of oil fields 25 km south of Tazlau in the Comanesti-Moinesti area (Stefanescu 2006) shows that the Menilite Formation in this area is within the oil window.

### 5.4 Depositional Environment

The Late Eocene-Oligocene depositional environment of the study area has been reconstructed by Miclaus et al. (2009). According to these authors, the sediments accumulated in a forebulge depocenter (Figure 48). The pelitic background sediments interrupted by coarse-grained deposits are grouped in seven facies associations (FA 1-7; Figure 48)

In the present chapter the depositional environment of each stratigraphic unit is discussed based on the environmental indicators discussed in chapter 3 and the sedimentological model of Miclaus et al. (2009).

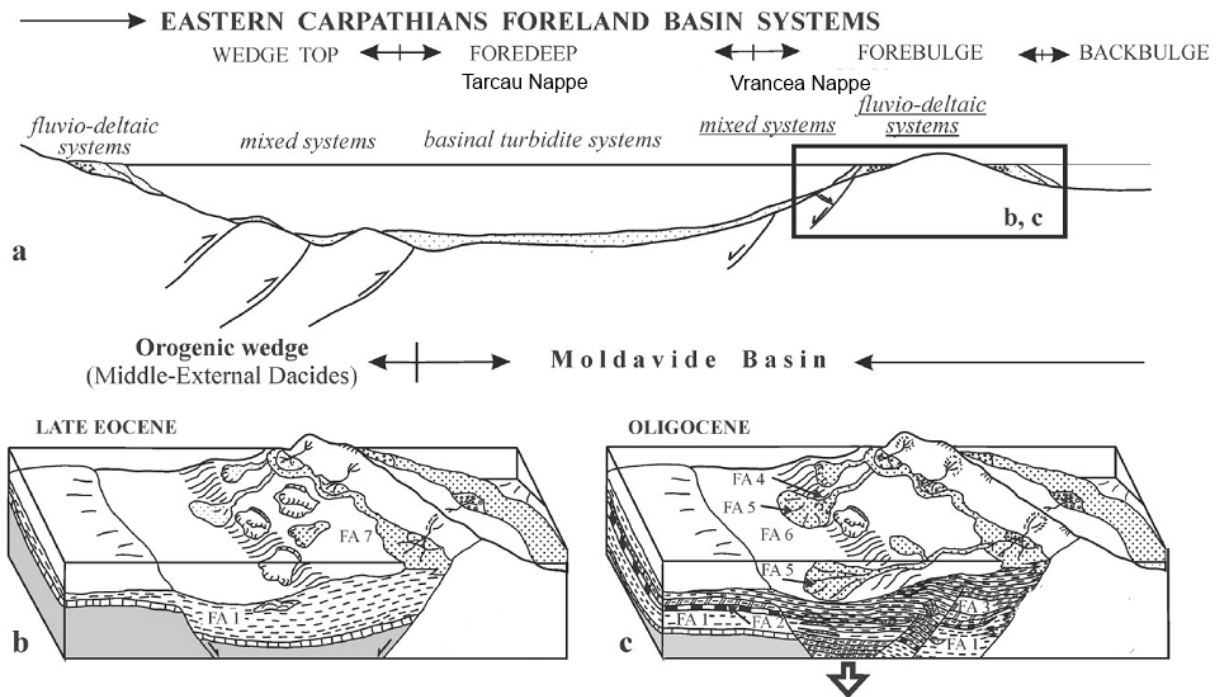


Figure 48: Paleogeographic interpretation of the Late Eocene-Oligocene depositional system within the Bistrita half-window (modified from Miclaus et al., 2009; 2010). The sketch suggests that the study area is located west of a forebulge in an area with active faulting.

- FA 1 - Greenish-grey pelites with slumps facies association of mud-rich slope apron system;
- FA 2 - Black shales with bedded cherts and sandstones facies association of shallow channels;
- FA 3 - Bituminous marls facies association of anoxic shelf;
- FA 4 - Sandstone and conglomerate facies association of channels with levee;
- FA 5 - Arenaceous-pelitic facies association of depositional lobes;
- FA 6 - Bituminous pelites with slumps and debrites facies association of fringe fans;
- FA 7 - Whitish marl with debrite facies association of oxic shelf.

### **5.4.1 Bisericani Fm**

The Bisericani Fm. includes approximately 300-m-thick greenish-grey mudstones, which are mainly unstructured, with sporadic thin- to medium-bedded sandstone beds and frequent slump deposits (Miclaus et al. 2009). These authors postulate that the Bisericani Fm. formed a mud-rich slope apron system.

Only few samples from the Bisericani Fm. have been investigated. TOC/S ratios of these samples are below 2.8 suggesting oxygen-deficient conditions (see also Amadori et al., 2012). Nevertheless TOC contents are low indicating low organic productivity, strong bacterial sulphate reduction or poor conditions for organic matter accumulation.

### **5.4.2 The Menilite Formation**

The Oligocene to Early Miocene Menilite Fm. includes “Lower Menilite Member”, “Bituminous Marl Member”, “Lower Dysodilic Shale Member”, “Kliwa Sandstone Member”, and “Upper Dysodilic Shale Member, which accumulated in the external Moldavian Basin (Miclaus et al. 2009).

#### **5.4.2.1 Lower Menilite Mbr.**

The LMM was not exposed during the sampling campaign. According to Amadori et al. (2012) the LMM is very rich in organic matter with a high HI. This indicates an environment with high bioproductivity and excellent preservation conditions. The high silica content typical for menilite shales points to a significant contribution of siliceous organisms. Thus, the lower boundary of the LMM represents a change from pelitic sedimentation in a (sub-)oxic environment to pelitic sedimentation in a strongly oxygen-depleted environment (see also Miclaus et al., 2009).

#### **5.4.2.2 Bituminous Marl Mbr.**

The BMM (FA 3 of Miclaus et al., 2009) forms a prominent carbonate-rich marker bed in the Romanian Carpathians. It has been considered equivalent to the “Dynow Formation” in the Alpine Foreland Basin (Schulz et al. 2002) and the Polish Carpathians (e.g. Miclaus & Schieber, 2014). The Dynow Formation has been dated into NP zone 23. The same age has been determined for the BMM (Micu & Gheța 1986; Ionesi & Mészáros 1989). Whereas Lebenzon (1973) dated the BMM into NP22. New nannoplankton data reported in this thesis, suggest NP 21 to 22 for the BMM exposed in the Tazlau profile. In contrast, Amadori et al. (2012) and Guerrero (2012) assume a Chattian age. Hence it remains unclear, if the BMM is a time-equivalent of the Dynow Formation.

The thickness of the BMM is often in the range of 10 to 30 m (e.g. Miclaus et al. (2009); Belayouni et al. (2009); Guerrero et al. (2012)), but reaches about 70 m near Tazlau. Probably, the high thickness is a result of intense slumping near an active fault system (Figure 48).

The carbonate content of the BMM is generally high (up to 83 wt.%). Part of the carbonate is provided by calcareous nannoplankton. Relative low TOC contents (average 1.7 %) are due to dilution by carbonate minerals. The low gamma radiation reflects the high carbonate content.

According to Miclaus et al. (2009), the most remarkable sedimentary feature of the BMM is the presence of true cross-bedding with sigmoidal foresets that dip at 10-15 degrees. These cross-bedded marls occur either as thin (5-10 cm) or thick to very thick (1-1.2 m) bed sets. Fine lamination of

quartzarenites might be an indicator for fallout from suspension. Fine sandstone interlayers can be attributed to storms, floods or turbidite currents (Miclaus et al. 2009).

Based on sandy channel fillings with wave ripple cross-lamination, a shallow to moderate water depth with strong terrestrial input and high transport energy (“distal shelf, fed during storms or by hyperpycnal flows from shoreline sources”) has been postulated by (Miclaus et al. 2009). In contrast, Amadori et al. (2012) assume a (hemi-)pelagic depositional environment. A relative deep environment with strong bottom current activity has also been proposed by Miclaus & Schieber (2014).

The mineralogical composition of quartzarenites is a strong argument for detrital input from the Eastern European Platform (Miclaus et al. 2009). This is supported by the presence of a polygenic conglomerate with extra-basinal clasts (Amadori et al. 2012).

#### *Redox conditions*

Rare bioturbation indicates that the water column was at least temporarily (dys-)oxic and allowed life of organisms beneath the sediment surface. Despite moderate TOC contents (~1.7 %), TOC/S ratios are relatively high (~4). This argues against an anoxic environment (and for sulfur limitation; see below).

Oxygen depleted, but not strictly anoxic, conditions are suggested by Pr/Ph ratios varying between 1.5 and 1.7. At the same time strongly varying concentrations of C<sub>19</sub> aryl isoprenoids indicate short periods with photic zone anoxia. Strongly restricted conditions are also suggested by low Mo/TOC ratios (Figure 49).

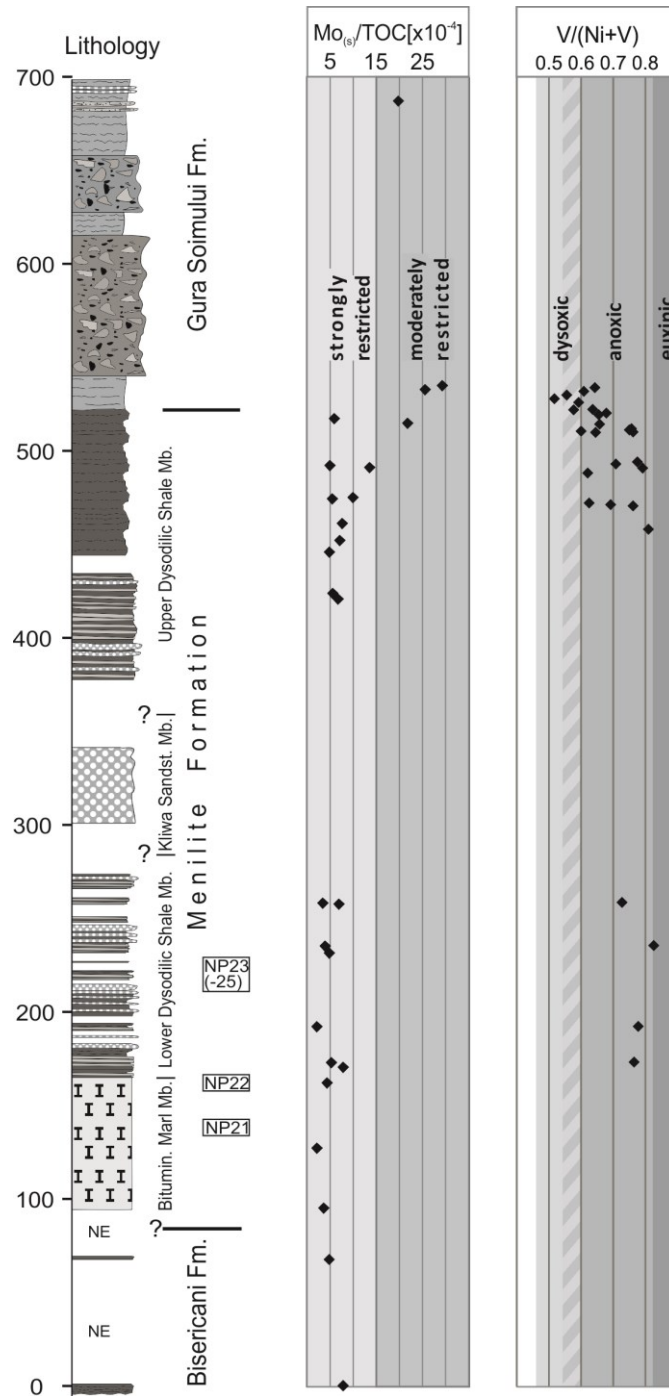


Figure 49: Depth profiles of Mo/TOC (after Algeo & Lyons 2006) and V/(V+Ni) ratios (after Hatch & Leventhal 1992) and their paleoenvironmental interpretation

### Salinity

High TOC/S ratios (~4) argue for sulphate limitation for the activity of sulphate reducing bacteria, as usually seen in environments with reduced salinity (Berner 1984). Sulfur limitation is also visible in a triangular plot of Fe/TOC/S (Figure 50). At the same time, reactive Fe is often a limiting factor for pyrite formation in carbonate environments. This may explain the relatively high organic sulfur content reflected by DBT/Ph ratios in the order of 0.4 (Figure 36).

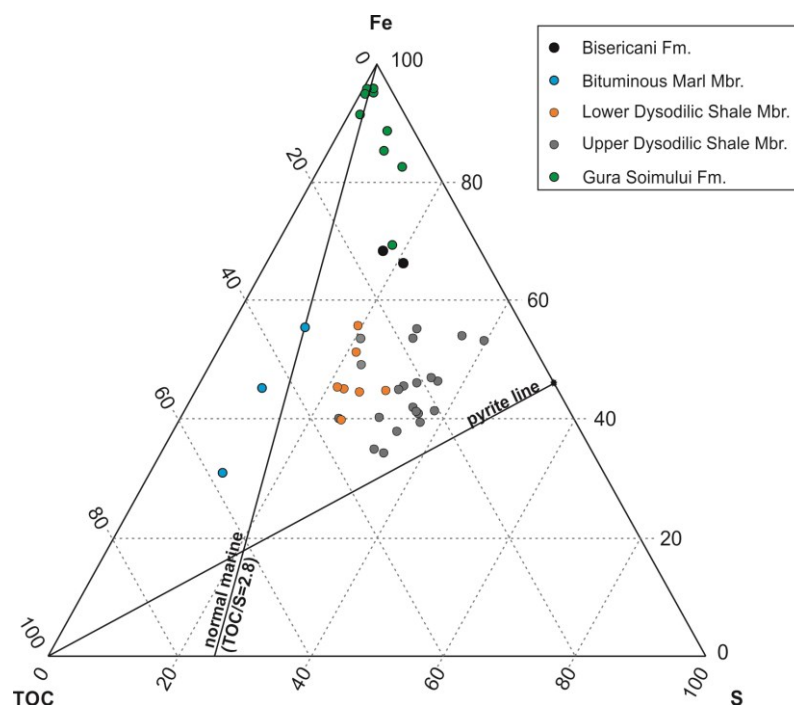


Figure 50: Fe-S-TOC ternary diagram

The MTTTC ratio suggests salinity conditions widely varying between reduced (sample 8) and enhanced salinity (samples 5, II-3a). Gammacerane is considered a proxy for a stratified water column, often related to salinity stratification. Thus, the presence of gammacerane in the upper two samples argues against a pure freshwater environment, at least in the uppermost part of the BMM.

Summarizing, it is obvious that the salinity proxies do not yield consistent results. Whereas TOC/S ratios and the MTTTC ratio of sample 8 indicate reduced salinity, MTTTC ratios of two other samples and the presence of gammacerane argue against it. If the BMM is coeval with the Dynow Fm. (NP23), reduced salinity should be expected.

#### Organic matter source

High HI values of organic matter (430 to 642 mg HC/g TOC) indicate the presence of well-preserved, hydrogen-rich type II kerogen. This is supported by the maceral composition of sample 4, characterized by dominant liptodetrinite (47 vol.%) and the absence of vitrinite and inertinite. Sporinite (18 vol.%) is the only terrestrial maceral present. CPI values  $<1$  suggest hypersaline environments and/or strong microbial activity. In the present case hypersaline conditions are unlikely (see above). Thus the data probably reflect strong microbial activity.

*N*-alkane distribution shows no clear predominance. Concentrations of long and short chain *n*-alkanes show a similar range. Whereby short chain alkanes, indicating algae and microorganisms, show the smallest amounts (7-24 %). Middle chain *n*-alkanes (25-32 %) indicate macrophyten, algae and bank vegetation. Highest concentrations of long chain *n*-alkanes (25-40) are found in sample 8. High concentrations are often found in organic matter derived from higher plants. In the present case, maceral composition and CPI argue against a major contribution of higher plants. Instead, long-chain hydrocarbons may be derived from microbial or algal biomass.

$C_{29}$  steranes dominate (35-40 vol.%). Similar to long-chain hydrocarbons, they pretend a high amount of landplants. However, low concentrations of landplant-derived biomarkers (cadalenes, diterpenoids,

arboranes), which are lower than in any other stratigraphic unit argues against a significant contribution of terrestrial organic matter. C<sub>28</sub> steranes occur in significant amounts. Part of the C<sub>28</sub> steranes may be derived from calcareous nannoplankton and diatoms, which have been detected in this study and by Miclaus & Schieber (2014).

Highest concentrations of hopanes and benzohopanes are found in the BMM. Hopanes are derived from prokaryotes (bacteria and archaea). High concentrations of benzohopane agree with the carbonatic environment (Peters et al., 2006).

Methylsteranes, derived from (marine and non-marine) dinoflagellates exist in moderate amounts in samples 5 and 8 (~22 µg/gTOC) and in high amounts (~40 µg/gTOC) in sample II-3a from the top of the BMM.

#### 5.4.2.3 Lower Dysodilic Shale Mbr.

The LDSM consists of alternations of thin-bedded sandstones (up to 1.5 m) and bituminous shales, which is also reflected by strong variations in the outcrop gamma ray log. Following the model of Miclaus et al. (2009), the LDSM has been deposited in fan lobes (FA 5 of Miclaus et al., 2010). The mineral composition of the turbiditic sandstones classifies them as quartzarenites suggesting a provenance from the Eastern European Platform (= Kliwa depositional system; Amadori et al., 2012).

#### *Redox*

Most shaly samples have TOC/S ratios below 2.8 (1.0 – 2.0) (Figure 21). These ratios argue for anoxic conditions in the bottom water (Berner 1984). Higher ratios are limited to samples with TOC contents exceeding 4 %. Probably, sulphur availability in the pore water was a limiting factor for pyrite formation in these samples with very high organic matter contents. Figure 50 shows that Fe was probably not a limiting factor for pyrite formation (Hofmann et al. 2000).

Pr/Ph ratios near the base of the LDSM are below 1 and increase upwards to values around 2.5. This trend suggests a change from anoxic to dysaerobic conditions. The presence of aryl-isoprenoid in significant amounts in the lowermost part of the LDSM indicates photic zone anoxia during the transition from the BMM to the LDSM. Similar, but opposite, vertical trends of aryl-isoprenoid concentrations and Pr/Ph ratios support an upward increase in the availability of oxygen.

The change in redox conditions is reflected by HI values of shaly samples. HI values between 500 and 600 (max. 700) mgHC/gTOC prevail in the anoxic lower part of the LDSM, whereas HI decreases to 300 mgHC/gTOC in the dysoxic upper part. This suggests that HI variations are caused at least partly by changes in preservation conditions.

However, Pr/Ph ratios (and HI) may also be influenced by the input of terrestrial plants. This is supported by good correlations between Pr/Ph with CPI (Figure 29) and with cadalene, a conifer biomarker (Figure 51).



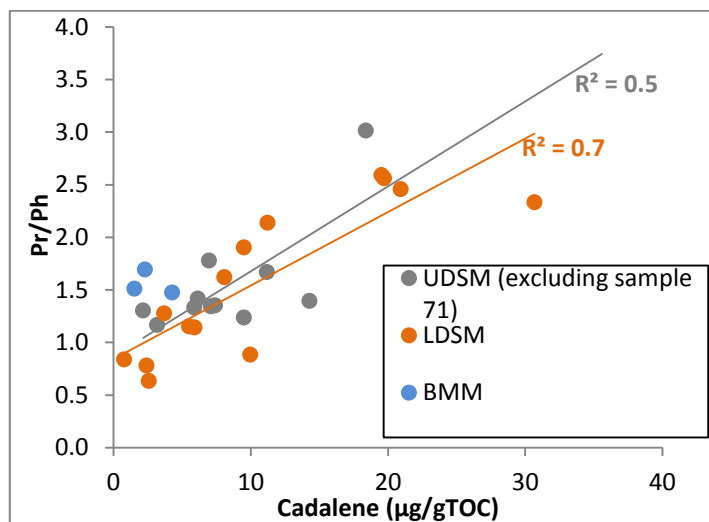


Figure 51: Pr/Ph versus Cadalene

Figure 49 shows that the postulated changes in redox conditions were not strong enough to influence Mo/TOC and V(V+Ni) ratios. Both parameters indicate strongly oxygen-depleted conditions.

The DBT/Ph ratio is a proxy for free H<sub>2</sub>S in the water column, which can be incorporated in the organic matter. In the sample set the ratio is relatively low (0.15 - 0.45, Figure 36), probably because any H<sub>2</sub>S was fixed by iron (Figure 50).

#### Salinity

MTTC ratios (Figure 31) indicate frequent changes in salinity between semi-saline and mesosaline.

#### Organic matter source

Although HI values are high (300 – 700 mgHC/gTOC), the organic matter of the LDSM includes significant amounts of landplants. This is evident from high vitrinite percentages (Figure 37). Cutinite, another landplant-derived maceral, occurs in significant amounts only in the LDSM (samples 9, 37). Further support for strong terrestrial input is provided by high concentrations of landplant-derived biomarkers, moderately high CPI values up to 1.6, high percentages of long-chain *n*-alkanes and C<sub>29</sub> steranes (Figure 27). Several of these parameters point to an increase of terrestrial organic matter in the upper part of the LDSM.

Note, that sandy samples are characterized by low HI values pretending the presence of kerogen type III (Figure 24). However, this classification is mainly due to low TOC contents (<1 %) and a strong mineral matrix effect (Langford & Blanc-Valleron 1990), Figure 24).

The concentration of 4-methylsteranes is generally higher than in other units of the Menilite Fm. and shows an upward decreasing trend. 4-methylsteranes are characteristic for marine and non-marine dinoflagellates or bacteria.

The LDSM shows high concentrations of diatom derived C<sub>25</sub> HBI thiophenes (4-67 µg/gTOC, average: 22.2 µg/g TOC; Figure 35). Maximum concentrations of this diatom-biomarker are obtained in samples 9 and 42B. Diatoms have also been detected in a nanoplankton sample (20) from the LDSM.

Interestingly, the concentrations of the diatom biomarker correlates positively ( $r^2=0.82$ ) with the steroids/hopanoids ratio, which also reaches maxima (>2) near the base and the top of the LDSM.

However, in most samples the steroids/hopanoids ratio is low (0.2 – 0.5). According to Mackenzie (1984), a high steranes/hopanes ratio is indicative of a marine, algal-dominated organic facies. Low ratios indicate a dominance of cyanobacteria and heterotrophic bacteria (Figure 52).

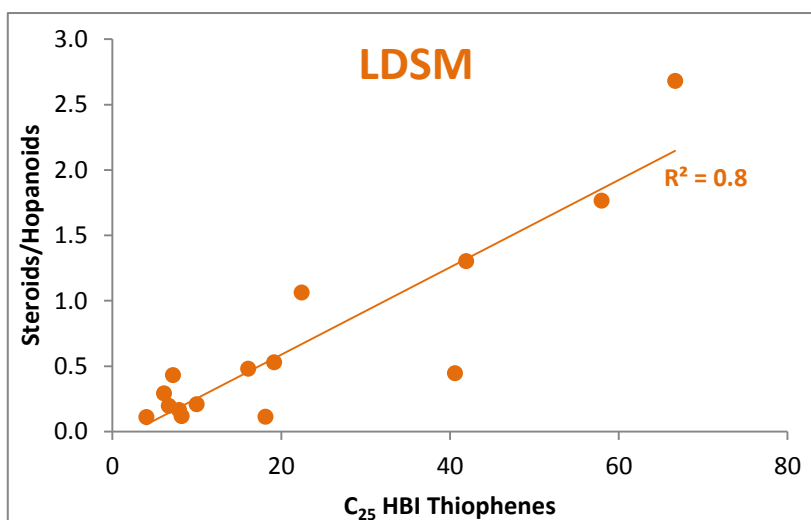


Figure 52: Steroid/Hopanoid ratio versus C<sub>25</sub> HBI Thiophenes

#### 5.4.2.4 Kliwa Sdst Mbr.

The KSM is composed of thick sandstone, characterized by low gamma radiation. Thin shale beds are rare. Single sandstone beds are typically 1 to 2 m thick. Following the model of Miclaus et al. (2009), the sand-dominated succession has been deposited in a channel (FA 4; Figure 55).

Whereas, a deep marine environment is favored, it should be mentioned that a near-shore environment has been postulated for the Kliwa sandstone (Melinte-Dobrinescu & Brustur 2008).

The TOC/S ratio of a single sample from the upper part of the KSM is significantly below 2.8. This value suggests that oxygen-depletion continued during deposition of the KSM. However, as TOC/S ratios may be influenced by different processes, this statement needs independent verification.

#### 5.4.2.5 Upper Dysodilic Shale Mbr.

The UDSM in the Tazlau section shows a clear fining upward trend (Figure 21) reflecting a transition from sedimentation on a depositional lobe (FA 5) to sedimentation in an outer-fan fringe or in basin plain environment (FA 6; Figure 55; Miclaus et al., 2009).

(Amadori et al. 2012) The deposits of the UDSM are marked by a decrease in clastic supply, although it presents yet a double origin (sub-arkoses and quartzarenites). Black shales followed, indicating the onset of restricted conditions after the former changing period.

According to Guerrero et al. (2012), the UDSM show a regressive (progradational) trend with an evolution from pelagic (basal black shale) to hemipelagic environments (coarse facies in the upper part of the member).

## Redox

All samples (with the exception of sample 71 with >13 %TOC) have TOC/S ratios significantly below 2.8 arguing for anoxic conditions (Bernier 1984). The observed upward decrease in TOC/S ratios from 1.5 to 0.5 may be influenced by the changes in the reactivity of organic matter. Most samples from the UDSM plot close to the pyrite line in Figure 50, suggesting a minor amount of Fe, which is incorporated in minerals other than pyrite (Hofmann et al. 2000).

Pr/Ph ratios are typically between 1 and 2, but reach 3 in the middle part of the member. A subtle increase in Pr/Ph ratios is visible in the uppermost part of the UDSM. The data indicate oxygen-depleted, but not strictly anoxic conditions. In contrast, varying contents of the C<sub>19</sub> aryl isoprenoid (0.3 – 1.5 µg/gTOC) indicate that even photic zone anoxia were established temporarily (Figure 27).

The inorganic redox proxies (Mn, Mo/TOC, V/(V+Ni) ratios show strongly restricted conditions. However, similar to the Pr/Ph ratio, the inorganic redox proxies indicate a subtle trend towards less reducing conditions in the uppermost part of the UDSM (Figure 49).

Pr/Ph ratios (and HI) may also be influenced by the input of terrestrial plants. This is supported by a good correlations between Pr/Ph with with CPI (Figure 29) and with cadalene, a conifer biomarker (Figure 51).

## Salinity

MTTC ratios vary significantly between 0.3 and 0.7 in the lower heterogenous part of the UDSM and are more uniform in the upper homogenous part (0.6 – 0.8). This shows normal marine to slightly enhanced salinity during deposition of the lower part and normal to slightly reduced salinity during deposition of the upper part.

A cross plot of aryl-isoprenoids versus MTTC ratios (Figure 53) suggests that the best conditions for the development of photic zone anoxia prevailed during times with normal marine salinity.

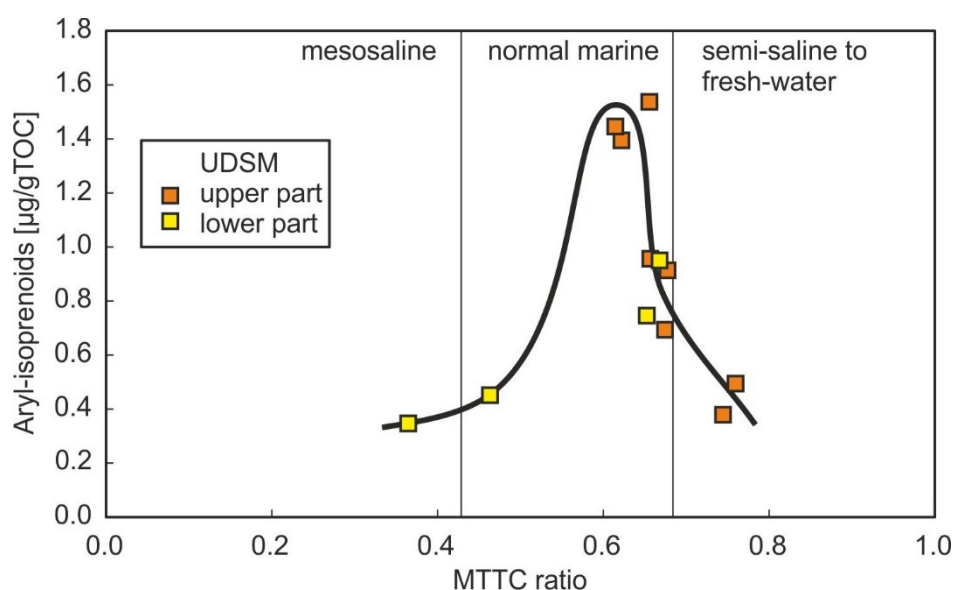


Figure 53: Cross plot of C<sub>19</sub> aryl-isoprenoids versus MTTC ratio for samples from the Upper Dysodilic Shale Member

### *Organic matter source*

High amounts of organic matter (2 – 4 %; max. 13.3 %) with HI values typically between 350 and 450 mgHC/gTOC accumulated during deposition of the UDSM. Lower HI values are a result of the mineral matrix effect, mainly in samples with a high sand content (Figure 24).

The maceral composition of three samples (68, 78, 82) is dominated by alginite (mainly lamalginite, but also telalginite). Vitrinite occurs in significant percentages (20 – 30 vol.%) in the studied samples, but is less abundant than in the LDSM (Figure 38).

Maceral data from sample 71 are not available, but high amounts of diterpenoids (which show a good correlation with cadalene in the UDSM;  $r^2=0.84$ ) suggest that the high TOC content of sample 71 (13.3 %) is due to a significant contribution of gymnosperms. In other samples, landplant-derived biomarkers are less abundant. A negative correlation between diterpenoids and HI is expected, but cannot be observed in the dataset.

In general the input of landplants in the UDSM is lower than in the LDSM. This is visible not only in the maceral percentages and the amount of diterpenoids, but also in relative low percentages of long-chain *n*-alkanes and  $C_{29}$  steranes.

Despite of low hopanoid contents, steroids/hopanoids ratios are low indicating strong microbial activity.

The  $C_{25}$  thiophenes occur in lower amounts than in the LDSM. This indicates that distinct diatom blooms are missing in the UDSM. 4-methylsteranes, biomarker for dinoflagellates also occur in low amounts.

### **5.4.3 Gura Soimului Fm**

The uppermost unit of the Vrancea Nappe is the GSF, early Burdigalian in age (Tabara & Popescu 2012). A change in color of pelitic rocks from dark grey to greenish across the UDSM/GSF boundary shows a change towards oxic conditions.

Chaotic polygenic conglomerates with clasts, exceeding 1 m in diameter, and a green-greyish fine sandy matrix are interpreted as mega-olistostromes. Both sedimentary (limestone, shales, calcarenite) and metamorphic clasts (green phyllites, schists, quartzites) are present (Amadori et al. 2012). In addition, clasts reworked from the underlying Menilite Fm. are also present. Amadori et al. (2012) link the deposition of the GSF with exhumation and erosion of rising areas in the eastern foreland.

### *Redox*

The transition from the UDSM to the shales in the lower part of the GSF is characterized by a change from anoxic to (sub)oxic conditions. This is evident from different datasets:

- Change in sediment color from dark grey to greenish bright grey
- Decrease in TOC content and a significant increase in TOC/S ratios
- Changes in inorganic redox-proxies (Mo/TOC and V/(V+Ni) ratios, Figure 49) including an increase in Mn concentrations (Figure 42)

## Salinity

MTTC ratios are only available for the upper part of the GSF. They suggest a normal marine to fresh-water depositional environment (Figure 31).

## Organic matter source

Most of the samples plot near the boundary between kerogen type III and II. Fig. x shows a significant mineral matrix effect for samples with low TOC contents. The relative low HI values point to poor preservation conditions for organic matter.

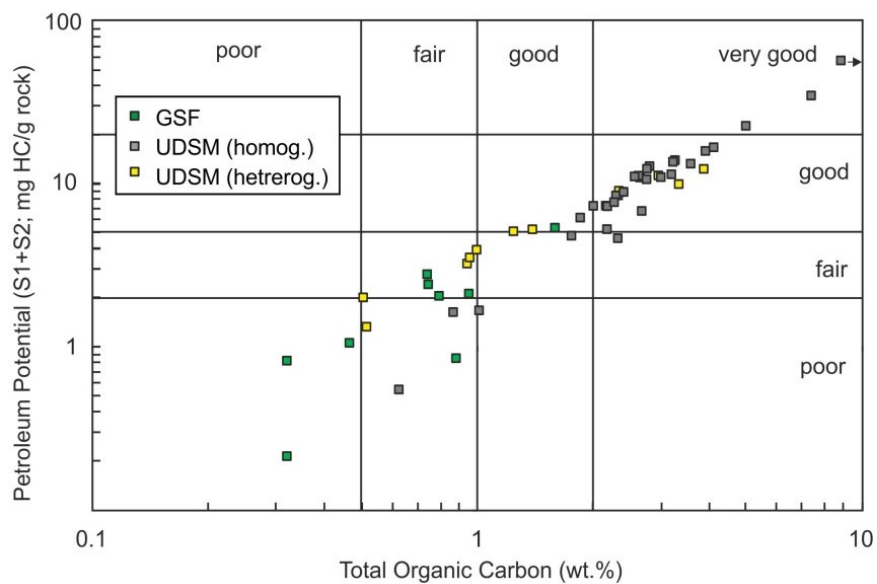
## 5.5 Hydrocarbon Potential

The estimation of the source rock potential and type of kerogen, considers Table 14.

**Table 14: Generative potential of source rocks** (Peters & Cassa 1994)

Type of kerogen generated					
Kerogen type	HI [mg HC/g rock]	S2/S3		TOC [%]	
I	>600	>15	Oil	<0.5	Poor
II	300-600	10-15	Oil	0.5-1	Fair
II/III	200-300	5-10	Mixed	1-2	Good
III	50-200	1-5	Gas	>2	Very good

**Figure 54** shows the source potential for each stratigraphic unit.



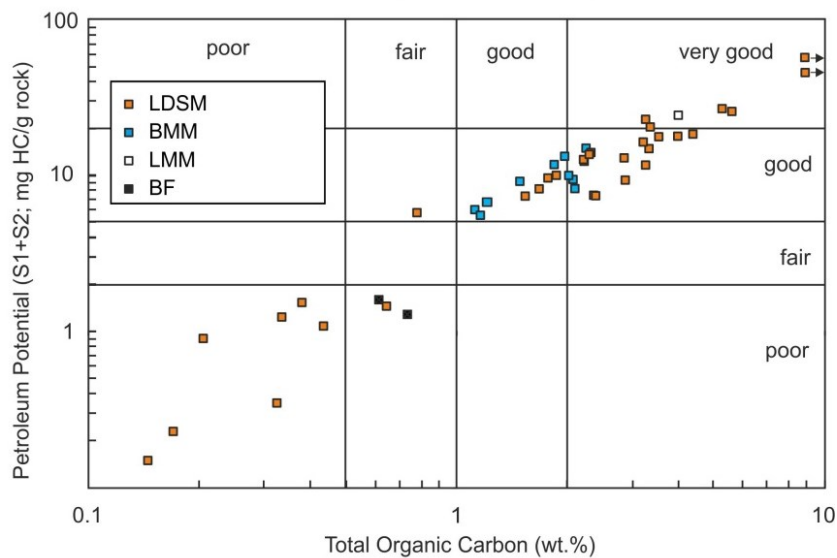


Figure 54: Genetic Potential versus TOC for different stratigraphic units

The petroleum potential (S1+S2), thickness and the density of the rock can be used to calculate the Source Potential Index (SPI). It is defined as the quantity of hydrocarbons that can be generated in a column of source rock under one square meter of surface area (Demaison & Huizinga 1991). It is applied for characterizing the source rock productivity. The SPI is calculated as follows:

$$SPI = \frac{\left( \overline{S1+S2} \right)^{*}h*\rho}{1000}$$

$\overline{S1+S2}$  : Average petroleum potential for pelitic samples  
 h: Thickness,  
 ρ: Density  
 Net/Gross: Shale thickness/total thickness

Table 15 shows the SPI for different stratigraphic units exposed in the Tazlau profile.

Table 15: Calculation of the Source Potential Index (SPI) for the Tazlau section

Unit		$\overline{S1+S2}$ [mg HC/g rock]	Total thickness [m]	Net/Gross [%]	Estimated Density [g/cm <sup>3</sup> ]	SPI [tHC/m <sup>2</sup> ]
Upper Dysodilic Shale Mbr.	Upper part	11.7	71	100	1.8	1.50
	Lower part	7.3	47	50	2.2	0.32
Lower Dysodilic Shale Mbr.		17.5	107	67	1.9	2.38
Bituminous Marl Member		9.5	67	100	2.4	1.53
Lower Menilite Shale Mbr.		23.3	6	100	2.0	0.28
<b>Σ Lower Oligocene</b>						<b>6.01</b>

The low TOC contents of the BF and the GSF and their low S1 and S2 values show that these formations do not host a significant source rock potential (Figure 54). The following discussion, therefore, focusses on the Menilite Fm.

- **Lower Menilite Mbr.:** Source rock data from a single sample from the Lower Menilite Member (Amadori et al., 2012) show that this member has a very good oil potential (Figure 54). However, because of the low thickness of the Lower Menilite Member in the Tazlau section, its SPI is low (c. 0.3 tHC/m<sup>2</sup>).
- **Bituminous Marl Mbr.:** A good genetic potential is indicated by the average TOC content (1.72 %) and the average petroleum potential (9.5 mg HC/g rock). The high HI, the S<sub>2</sub>/S<sub>3</sub> ratio (30) and Py-GC data indicate a potential to generate a “Paraffinic-Naphthenic-Aromatic (P-N-A) High Wax Oil”. The SPI is 1.5 tHC/m<sup>2</sup>.
- **Lower Dysodilic Shale Mbr.:** The petroleum potential of pelitic samples is high (average: 17.5 gHC/grock). High HI values, S<sub>2</sub>/S<sub>3</sub> ratios (30.5 – 120) and Py-GC data show the good to very good potential to generate a “Paraffinic High Wax Oil”. Considering that the LDSM contains about 33 % sand, the SPI is calculated as 2.4 tHC/m<sup>2</sup>. This shows that the LDSM is the most important source rock unit within the Menilite Fm.
- **Upper Dysodilic Shale Mbr.:** Pelitic samples from the lower and upper part of the UDSM contain a good (av. 7.8 and 12.4 mgHC/grock, respectively) to very good (av. 2.2 and 3.2 %TOC, respectively) source rock potential. High HI values and S<sub>2</sub>/S<sub>3</sub> ratios (lower part: 26.3 - 47.6; av. 40.2; upper part: 6.6 - 116.7, av. 42.2), as well as Py-GC data show that all samples have black oil potential and will generate a P-N-A Oil Low Wax, whereby they are close to the border to the P-N-A Oil High Wax facies. The SPI is calculated at 0.3 and 1.5 tHC/m<sup>2</sup> for the lower and upper part.

Table 15 shows that the total SPI of the Menilite Formation is 6 tons of hydrocarbons per m<sup>2</sup> surface area. For comparison, the SPI of the Oligocene source rock interval in the Alpine Foreland Basin is only 1 tons of hydrocarbons per m<sup>2</sup> surface area (Schulz et al. 2010).

## 5.6 Parameters for the distinction of oil generated from different members

One of the tasks of this study is to explore the possibility to distinguish oils generated from different members within the Menilite Formation. Therefore, average values and (excluding sandy samples with low petroleum potential) for each relevant member have been calculated (Table 16). Those biomarkers and biomarker ratios are defined in the following, which show the greatest differences.

Table 16: Average values and standard deviation of biomarker ratios for different members (sandy samples without hydrocarbon potential are neglected)

		UDSM		LDSM		BMM	
		average	standard deviation	average	standard deviation	average	standard deviation
<b><i>n</i>-Alkane</b>	( $\mu\text{g/g TOC}$ )	1241	612	1573	1242	1123	136
<i>n</i> -C <sub>15-19</sub> /		0.17	0.02	0.09	0.04	0.17	0.09
<i>n</i> -C <sub>21-25</sub> /		0.32	0.02	0.32	0.03	0.30	0.03
<i>n</i> -C <sub>27-31</sub> /		0.32	0.03	0.39	0.04	0.31	0.09
<b>CPI</b>		1.30	0.18	1.34	0.17	0.91	0.04
<b>Steranes</b>	( $\mu\text{g/g TOC}$ )	231	128	411	329	1021	298
C <sub>27</sub> Steranes/		0.36	0.04	0.29	0.03	0.30	0.03
C <sub>29</sub> Steranes/		0.33	0.04	0.42	0.04	0.39	0.03
C <sub>28</sub> /C <sub>29</sub>		0.94	0.14	0.69	0.09	0.81	0.08
<b>Methylsteranes</b>	( $\mu\text{g/g TOC}$ )	13.53	3.96	15.95	7.18	28.14	10.69
<b>ba Hopanes</b>	( $\mu\text{g/g TOC}$ )	249	153	278	153	436	123
<b>Hopanes</b>	( $\mu\text{g/g TOC}$ )	1795	414	2997	1798	6463	1120
<b>Cadalene</b>	( $\mu\text{g/g TOC}$ )	10.7	9.1	11.4	8.8	2.7	1.4
<b>Diterpenoids</b>	( $\mu\text{g/g TOC}$ )	19.8	21.6	30.3	18.2	12.4	5.7
<b>Arboranes</b>	( $\mu\text{g/g TOC}$ )	21.5	12.2	40.9	46.9	11.2	4.0
<b>C<sub>25</sub> HBI Thiophenes</b>	( $\mu\text{g/g TOC}$ )	7.5	4.6	22.2	20.4	2.5	3.6
<b>Benzohopanes</b>	( $\mu\text{g/g TOC}$ )	27.1	8.0	34.2	14.1	45.1	13.6
<b>C<sub>19</sub> Aryl-Isoprenoids</b>	( $\mu\text{g/g TOC}$ )	0.86	0.42	0.98	1.04	1.79	1.23
<b>Steroids/Hopanooids</b>		0.27	0.12	0.72	0.78	0.04	0.06

Oil generated from the **BMM** is unique in having a CPI <1. Moreover, it will be characterized by high amounts of steranes, 4-methylsteranes and hopanes. In contrast, amounts of landplant (especially cadalene, diterpenoids, arboranes) and diatom biomarkers (C<sub>25</sub> HBI thiophenes) will be low.

Specific characteristics for LDSM oil include high percentages of long-chain *n*-alkanes, a fact which is also reflected by **Figure 39**, where LDSM samples plot into the "Paraffinic Oil, High Wax" facies. Steranes pattern will be characterized by high percentage of C<sub>29</sub> steranes and a low C<sub>28</sub>/C<sub>29</sub> steranes ratio. Furthermore it is expected that C<sub>25</sub> HBI thiophenes will be abundant.

Oil generated from the **UDSM** will have low amounts of steranes, hopanes and benzohopanes. Within the steranes, percentages of C<sub>27</sub> steranes will be relative high. In contrast, concentrations of aryl-isoprenoids will be low.



## 6 Conclusions

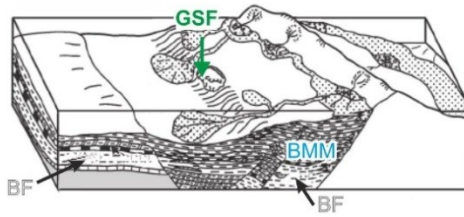
The study provided important new results on the depositional environment and hydrocarbon potential of the Menilite Formation in the Vrancea Nappe of the Eastern Carpathians. Major outcomes of the study are summarized in Figure 55, which is based on cartoons of the evolution of the study area published by Miclaus et al. (2009).

### Depositional environment

- The Bisericani Formation accumulated in late Eocene time in a slope apron system (FA 1 (Miclaus & Schieber 2014)). TOC contents and HI values are low 0.7 %.
- Deposition of the Menilite Formation starts with the Lower Menilite Member and marks a change towards strongly oxygen-deficient conditions. These, together with high paleoproductivity, caused accumulation of organic matter-rich rocks.
- The Bituminous Marl Member is the only carbonate-rich unit within the Menilite Formation. Calcareous nannoplankton dates the BMM into nannoplankton zones NP21-22. Thus, it is probably younger than the Dynow Marlstone in the Alpine Foreland Basin and the western Carpathians. Whereas Miclaus et al. (2009) favor a relative shallow depositional environment, Miclaus & Schieber (2014) argue for a deep marine setting (Figure 55). The organic matter, mainly derived from autochthonous marine organisms including bacterial biomass, is diluted by carbonate material. Salinity and redox conditions varied significantly from reduced to slightly enhanced and from strictly anoxic to dysoxic, respectively.
- The Lower Dysodilic Shale Member contains black shale and a significant number of sandstone beds deposited in a depositional lobe. Anoxic environments caused accumulation of abundant organic matter with hydrogen-rich kerogen type II. Despite of high HI values, landplants form a significant part of the organic matter and occur in minor amounts only near the base of the LDSM. A decrease in HI in the upper part of the LDSM is due to the combined effect of increasing contributions of terrestrial organic matter and increased oxygen contents. Similar to the BMM, salinity varied significantly.
- The Kliwa Sandstone Member represents a channel fill. Data from a shale bed suggest that oxygen-reduced conditions continued during deposition of the KSM.
- The Upper Dysodilic Shale Member shows a fining upward trend and represents the transition from a depositional lobe within frequent sandstone beds to a basin plain setting. MTTC ratios increase upwards and reflect a trend from slightly enhanced to slightly decreased normal marine salinities. Whereas oxygen-depleted, but not strictly anoxic conditions are indicated by Pr/Ph ratios, the presence of aryl-isoprenoids suggests temporary photic zone anoxia controlled by salinity variations. Anoxic conditions are also suggested by inorganic proxies. All parameters suggest a subtly upward increase in the availability of oxygen within the UDSM. Both autochthonous marine organic matter and landplants contributed to the organic matter. The organic matter is classified as kerogen type II, but it is less hydrogen-rich than that in the LDSM.
- A major change towards oxic conditions occurred at the boundary between the UDSM and the Gura Soimului Formation. The GSF in the Tazlau profile is characterized by thick megalolithes.

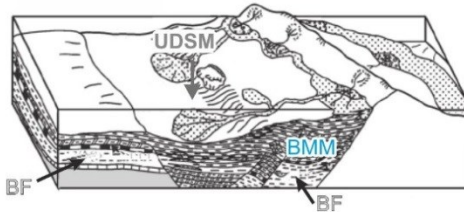
early Miocene  
 Oligocene  
 late Eocene

**Gura Soimului Fm.**



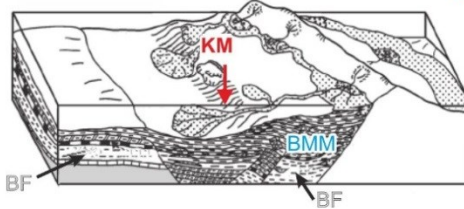
chaotic polygenic conglomerates  
 mega-olistostromes  
 oxic (to dysoxic)  
 low TOC

**Upper Dysodilic Shale Mbr.**



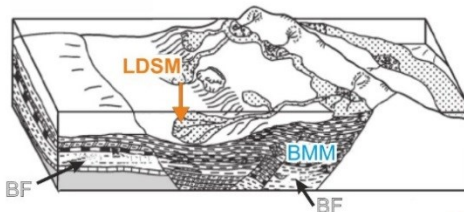
upper part: basin plain environment  
 TOC: 3.2 %; HI 300-400  
 anoxic  
 lower part: lobe  
 TOC: 2.2 %; HI 300-400

**Kliwa Mbr.**



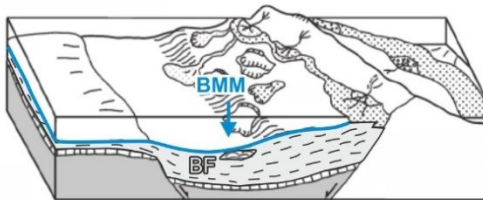
channel fill

**Lower Dysodilic Shale Mbr.**



deposited in fan lobes  
 TOC 2.6 % (max. 13 %)  
 TOC/S ratio: < 2.8  
 uppermost part: dysoxic (HI: 300-500)  
 lower part: anoxic (HI: 500-700)  
 frequent landplants

**Bituminous Marl Mbr.**

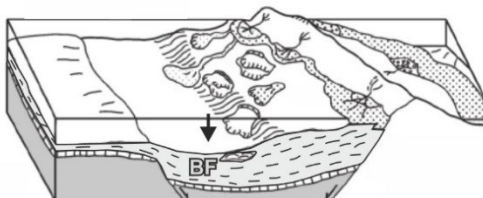


calcareous nannoplankton  
 TOC: 1.7 %, HI 400-600  
 TOC/S ratio: ~4  
 anoxic (temporarily (dys-)oxic)  
 CPI < 1 (microbial biomass)  
 very little landplants

**Lower Menilite Mbr**

TOC: 4.0 %, HI 570

**Bisericani Fm.**



greenish-grey mudstones  
 frequent slump deposits  
 TOC < 0.7 %  
 TOC/S ratios < 2.8  
 (dys?)oxic conditions

Menilite Formation (SPI ~ 6 t HC/m<sup>2</sup>)

Figure 55: Cartoons showing depositional systems of the Tazlau area during Eocene to early Miocene time (slightly modified after Miclaus et al., 2009). The position of the Tazlau section is indicated by an arrow. Explanations of the depositional environment and hydrocarbon potential are added

## Hydrocarbon potential

- The entire section is thermally immature.
- TOC contents and HI values of the Bisericani and Gura Soimului formations show that these are poor hydrocarbon source rocks. However, redeposited Menilite rocks within the olistolithes in the GSF may increase the overall hydrocarbon potential.
- The Source Potential Index of the Menilite formation is about 6 tons of hydrocarbons per square meter. This value shows the very high petroleum potential of the Eastern Carpathians. The largest contribution is from the Lower Dysodilic Shale Member (2.4 tHC/m<sup>2</sup>) and the Upper Dysodilic Shale Member (1.8 tHC/m<sup>2</sup>)
- All members are oil prone and will generate a low sulphur oil. The Lower Dysodilic Shale Member will generate a “Paraffinic High Wax Oil”, other members will generate a “Paraffinic-Naphthenic-Aromatic High Wax Oil”.
- Biomarker ratios can help to distinguish oil from different members: Oil from the **BMM** is unique in having a CPI <1 and will be rich in steranes, 4-methylsteranes and hopanes, whereas amounts of landplant and diatom biomarkers will be low. **LDSM** oil will include high amounts of long-chain *n*-alkanes, C<sub>29</sub> steranes and landplant biomarkers. Furthermore it is expected that C<sub>25</sub> HBI thiophenes will be abundant. Oil generated from the **UDSM** will have low amounts of steranes, hopanes and benzohopanes, but relative C<sub>27</sub> steranes percentages. Concentrations of aryl-isoprenoids will be low.
- The gamma log is mainly controlled by variations in lithology. However, pelitic rocks with similar TOC contents are characterized by highly different gamma radiation. For example, gamma radiation in the Upper Dysodilic Shale Member is higher than in the Lower Dysodilic Shale Member, despite of lower TOC contents. Moreover, pelites in the Gura Soimului Formation are high despite of very low TOC contents. Consequently, TOC contents cannot be determined using the gamma log alone.

## 7 References

- Algeo & Lyons, 2006.** Mo-total organic carbon covariation in modern anoxic marine environments: Implications for analysis of paleoredox and paleohydrographic conditions. In: *Paleoceanography*, Vol. 21 (1). Wiley Online Library.
- Amadori, Belayouni, Guerrera, Martin-Martin, Martin-Rojas, Miclaus & Raffaelli, 2012.** New data on the Vrancea Nappe (Moldavidian Basin, Outer Carpathian Domain, Romania): paleogeographic and geodynamic reconstructions. In: *International Journal of Earth Sciences*, Vol. 101 (6). Springer, pp. 1599–1623.
- Bechtel, Hámor-Vidó, Gratzner, Sachsenhofer & Püttmann, 2012.** Facies evolution and stratigraphic correlation in the early Oligocene Tard Clay of Hungary as revealed by maceral, biomarker and stable isotope composition. In: *Marine and Petroleum Geology*, Vol. 35 (1). Elsevier, pp. 55–74.
- Behar, 2001.** Rock-Eval 6 technology: performances and developments. In: *Oil & Gas Science and Technology*, Vol. 56 (2). IFP, pp. 111–134.
- Bell, Goodman & Whitehead, 1940.** Radioactivity of sedimentary rocks and associated petroleum. In: *AAPG Bulletin*, Vol. 24 (9). American Association of Petroleum Geologists, pp. 1529–1547.
- Bernard, Bernard & Brooks, 2004.** Determination of total carbon, total organic carbon and inorganic carbon in sediments.
- Berner, 1970.** Sedimentary pyrite formation. In: *American Journal of Science*, Vol. 268 (1). American Journal of Science, pp. 1–23.
- Berner, 1984.** Sedimentary pyrite formation: an update. In: *Geochimica et Cosmochimica Acta*, Vol. 48 (4). Elsevier, pp. 605–615.
- Bray & Evans, 1961.** Distribution of n-paraffins as a clue to recognition of source beds. In: *Geochimica et Cosmochimica Acta*, Vol. 22 (1). Elsevier, pp. 2–15.
- Brumsack, 1986.** The inorganic geochemistry of Cretaceous black shales in comparison to modern upwelling sediments from the Gulf of California. In: *Geological Society, London, Special Publications*, Vol. 21 (1). Geological Society of London, pp. 447–462.
- Brumsack & Gieskes, 1983.** Interstitial water trace-metal chemistry of laminated sediments from the Gulf of California, Mexico. In: *Marine Chemistry*, Vol. 14 (1). Elsevier, pp. 89–106.
- Bunte, 2009.** Geochemical signatures of black shales deposited during Oceanic Anoxic Event 2 (Cenomanian/Turonian) in the tropical Atlantic (Demerara Rise, ODP Leg 207) and in northern Germany (Wunstorf). Phd thesis. Universität Oldenburg.
- Burchfiel, 1980.** Eastern European Alpine system and the Carpathian orocline as an example of collision tectonics. In: *Tectonophysics*, Vol. 63 (1). Elsevier, pp. 31–61.
- Crusius, Calvert, Pedersen & Sage, 1996.** Rhenium and molybdenum enrichments in sediments as indicators of oxic, suboxic and sulfidic conditions of deposition. In: *Earth and Planetary Science Letters*, Vol. 145 (1). Elsevier, pp. 65–78.
- Csontos, 1995.** Tertiary tectonic evolution of the Intra-Carpathian area: a review. In: *Acta Vulcanol.*, Vol. 7. pp. 1–13.

- Csontos, 2004.** Mesozoic plate tectonic reconstruction of the Carpathian region. In: *Palaeogeogr. Palaeoclimatol. Palaeoecol.*, Vol. 210. pp. 1–56.
- Dean & Arthur, 1989.** Iron-sulfur-carbon relationships in organic-carbon-rich sequences; I, Cretaceous Western Interior Seaway. In: *American Journal of Science*, Vol. 289 (6). American Journal of Science, pp. 708–743.
- Demaison & Huizinga, 1991.** Genetic Classification of Petroleum Systems (1). In: *AAPG Bulletin*, Vol. 75 (10). American Association of Petroleum Geologists, pp. 1626–1643.
- Didyk, Simoneit, Brassell & Eglinton, 1978.** Organic geochemical indicators of palaeoenvironmental conditions of sedimentation. In: *Nature*, Vol. 272 (5650). Nature Publishing Group, pp. 216–222.
- Eglinton & Hamilton, 1967.** Leaf epicuticular waxes. In: *Science*, Vol. 156 (3780). American Association for the Advancement of Science, pp. 1322–1335.
- Eglinton, Sinninghe Damsté, Kohnen & de Leeuw, 1990.** Rapid estimation of the organic sulphur content of kerogens, coals and asphaltenes by pyrolysis-gas chromatography. In: *Fuel*, Vol. 69 (11). Elsevier, pp. 1394–1404.
- Emerson & Huested, 1991.** Ocean anoxia and the concentrations of molybdenum and vanadium in seawater. In: *Marine Chemistry*, Vol. 34 (3). Elsevier, pp. 177–196.
- Espitalie, Deroo & Marquis, 1985.** La pyrolyse Rock-Eval et ses applications. Deuxième partie. In: *Oil & Gas Science and Technology*, Vol. 40 (6). IFP, pp. 755–784.
- Espitalie, Madec, Tissot, Mennig, Leplat & others, 1977.** Source rock characterization method for petroleum exploration. In: *Offshore Technology Conference*.
- Farrimond, Taylor & Telnaes, 1998.** Biomarker maturity parameters: the role of generation and thermal degradation. In: *Organic Geochemistry*, Vol. 29 (5). Elsevier, pp. 1181–1197.
- Ficken, Li, Swain & Eglinton, 2000.** An n-alkane proxy for the sedimentary input of submerged/floating freshwater aquatic macrophytes. In: *Organic geochemistry*, Vol. 31 (7). Elsevier, pp. 745–749.
- Golonka, Gahagan, Krobicki, Marko, Oszczytko & Slalczka, 2006.** Plate-tectonic evolution and paleogeography of the Circum-Carpathian Region. In: Golonka, J and Picha, FJ (Ed.), *The Carpathians and their foreland: geology and hydrocarbon resources. Special issue of AAPG Memoir*, Vol. 84. pp. 11–46.
- Goossens, de Leeuw, Schenck & Brassell, 1984.** Tocopherols as likely precursors of pristane in ancient sediments and crude oils. In: *Nature*, Vol. 312 (5993). Nature Publishing Group, pp. 440–442.
- Grasu, Catana, Miclaus & Bobos, 1999.** East Carpathian molasse. Petrography and sedimentogenesis. Editura Tehnica Bucuresti.
- Hartgers, Sinninghe Damsté, Requejo, Allan, Hayes, Ling, Xie, Primack & de Leeuw, 1994.** A molecular and carbon isotopic study towards the origin and diagenetic fate of diaromatic carotenoids. In: *Organic geochemistry*, Vol. 22 (3). Elsevier, pp. 703–725.
- Hatch & Leventhal, 1992.** Relationship between inferred redox potential of the depositional environment and geochemistry of the Upper Pennsylvanian (Missourian) Stark Shale Member of the Dennis Limestone, Wabaunsee County, Kansas, USA. In: *Chemical Geology*, Vol. 99 (1). Elsevier, pp.

- Hauke, Graff, Wehrung, Trendel, Albrecht, Schwark, Keely & Peakman, 1992.** Novel triterpene-derived hydrocarbons of arborane/fernane series in sediments. Part I. In: *Tetrahedron*, Vol. 48 (19). Elsevier, pp. 3915–3924.
- Hofmann, Ricken, Schwark & Leythaeuser, 2000.** Carbon-sulfur-iron relationships and  $\delta^{13}\text{C}$  of organic matter for late Albian sedimentary rocks from the North Atlantic Ocean: paleoceanographic implications. In: *Palaeogeography, Palaeoclimatology, Palaeoecology*, Vol. 163 (3). Elsevier, pp. 97–113.
- Hollander, Sinninghe Damsté, Hayes, de Leeuw & Huc, 1993.** Molecular and bulk isotopic analyses of organic matter in marls of the Mulhouse Basin (Tertiary, Alsace, France). In: *Organic geochemistry*, Vol. 20 (8). Elsevier, pp. 1253–1263.
- Horsfield, 1989.** Practical criteria for classifying kerogens: some observations from pyrolysis-gas chromatography. In: *Geochimica et Cosmochimica Acta*, Vol. 53 (4). Elsevier, pp. 891–901.
- Huang & Meinschein, 1979.** Sterols as ecological indicators. In: *Geochimica et Cosmochimica Acta*, Vol. 43 (5). Elsevier, pp. 739–745.
- Hughes, Holba & Dzou, 1995.** The ratios of dibenzothiophene to phenanthrene and pristane to phytane as indicators of depositional environment and lithology of petroleum source rocks. In: *Geochimica et Cosmochimica Acta*, Vol. 59 (17). Elsevier, pp. 3581–3598.
- Ionesi & Mészáros, 1989.** Sur la limite Oligocène-Miocène dans le flysch externe Carpatique. In: *The Oligocene from the Transylvanian Basin Romania*. Univ. of Cluj Napoca, Cluj Napoca, pp. 133–141.
- Koopmans, Köster, Van Kaam-Peters, Kenig, Schouten, Hartgers, de Leeuw & Sinninghe Damsté, 1996.** Diagenetic and catagenetic products of isorenieratene: Molecular indicators for photic zone anoxia. In: *Geochimica et Cosmochimica Acta*, Vol. 60 (22). Elsevier, pp. 4467–4496.
- Kotarba, Wieclaw, Koltun, Marynowski, Kusmieriek & Dudok, 2007.** Organic geochemical study and genetic correlation of natural gas, oil and Menilite source rocks in the area between San and Stryi rivers (Polish and Ukrainian Carpathians). In: *Organic geochemistry*, Vol. 38 (8). Elsevier, pp. 1431–1456.
- Köster, Kotarba, Lafargue & Kosakowski, 1998.** Source rock habitat and hydrocarbon potential of Oligocene Menilite Formation (Flysch Carpathians, Southeast Poland): an organic geochemical and isotope approach. In: *Organic geochemistry*, Vol. 29 (1). Elsevier, pp. 543–558.
- Köster, Rospondek, Schouten, Kotarba, Zubrzycki & Sinninghe Damsté, 1998.** Biomarker geochemistry of a foreland basin: the Oligocene Menilite Formation in the Flysch Carpathians of Southeast Poland. In: *Organic Geochemistry*, Vol. 29 (1). Elsevier, pp. 649–669.
- Langford & Blanc-Valleron, 1990.** Interpreting Rock-Eval Pyrolysis Data Using Graphs of Pyrolizable Hydrocarbons vs. Total Organic Carbon (1). In: *AAPG Bulletin*, Vol. 74 (6). American Association of Petroleum Geologists, pp. 799–804.
- Larter, 1984.** Application of analytical pyrolysis techniques to kerogen characterization and fossil fuel exploration/exploitation. In: *Analytical pyrolysis*. Butterworths, London, pp. 212–275.

- Lebenzon, 1973.** Calcareous nannoplankton of Oligocene and Early Miocene deposits from the Tarcau Upper Drainage Basin. In: *DS Inst. Geol. Geofiz.* pp. 101–102.
- Lewan, 1984.** Factors controlling the proportionality of vanadium to nickel in crude oils. In: *Geochimica et Cosmochimica Acta*, Vol. 48 (11). Elsevier, pp. 2231–2238.
- Lüning & Kolonic, 2003.** Uranium Spectral Gamma-Ray Response as a Proxy for Organic Richness in Black Shales: Applicability and Limitations. In: *Journal of petroleum geology*. Scientific Press, pp. 153–174.
- Mackenzie, Brassell, Eglinton & Maxwell, 1982.** Chemical fossils: the geological fate of steroids. In: *Science*, Vol. 217 (4559). American Association for the Advancement of Science, pp. 491–504.
- Mahlstedt, 2012.** Evaluating the late gas potential of source rocks stemming from different sedimentary environments. Phd thesis. Technische Universität Berlin.
- Mann, Leythaeuser & Müller, 1986.** Relation between source rock properties and wireline log parameters: An example from Lower Jurassic Posidonia Shale, NW-Germany. In: *Organic geochemistry*, Vol. 10 (4). Elsevier, pp. 1105–1112.
- Matenco & Bertotti, 2000.** Tertiary tectonic evolution of the external East Carpathians (Romania). In: *Tectonophysics*, Vol. 316 (3). Elsevier, pp. 255–286.
- Melinte-Dobrinescu & Brustur, 2008.** Oligocene-Lower Miocene events in Romania. In: *Acta Palaeont. Romaniae*, Vol. 6. pp. 203–215.
- Miclaus, Loiacono, Puglisi & Baciu, 2009.** Eocene-Oligocene sedimentation in the external areas of the Moldavide Basin (Marginal Folds Nappe, Eastern Carpathians, Romania): sedimentological, paleontological and petrographic approaches. In: *Geologica Carpathica*, Vol. 60 (5). Versita, pp. 397–417.
- Miclaus & Schieber, 2014.** A Hierarchy of Current-Produced Bedforms in a Source Rock from the Eastern Carpathians Points to Predominant Bedload Deposition of an Organic-Rich Mudstone. In: *AAPG Annual Convention and Exhibition*.
- Micu & Gheța, 1986.** Eocene-Oligocene Boundary in Romania on the Calcareous Nannoplankton. In: *D. S. Inst. Geol. București*, Vol. 70 – 71 (4). pp. 283 – 287.
- Morford & Emerson, 1999.** The geochemistry of redox sensitive trace metals in sediments. In: *Geochimica et Cosmochimica Acta*, Vol. 63 (11). Elsevier, pp. 1735–1750.
- Ourisson, Albrecht, Rohmer & others, 1979.** The hopanoids. Paleochemistry and biochemistry of a group of natural products. In: *Pure Applied Chemistry*, Vol. 5. pp. 709–729.
- Peters & Cassa, 1994.** Essential Elements. In: *Applied Source Rock Geochemistry*. AAPG Special Volumes.
- Peters, Walters & Moldowan, 2005.** The biomarker guide: biomarkers and isotopes in the environment and human history, Cambridge University Press.
- Radulescu & Sandulescu, 1973.** The plate-tectonics concept and the geological structure of the Carpathians. In: *Tectonophysics*, Vol. 16. pp. 155–161.

- Raiswell & Canfield, 1998.** Sources of iron for pyrite formation in marine sediments. In: *American Journal of Science*, Vol. 298 (3). pp. 219–245.
- Ratschbacher, Linzer, Moser, Strusievcz, Bedeleian, Har & Mogocs, 1993.** Cretaceous to Miocene thrusting and wrenching along the central South Carpathians due to a corner effect during collision and orocline formation. In: *Tectonics*, Vol. 12 (4). Wiley Online Library, pp. 855–873.
- Sabel, 2006.** Geochemische Untersuchungen an Schwarzpeliten des Eozänen Eckfelder Maeres zur Rekonstruktion der Paläoumweltbedingungen. Phd thesis. Universitäts-und Landesbibliothek Bonn.
- Sabel, Bechtel, Püttmann & Hoernes, 2005.** Palaeoenvironment of the Eocene Eckfeld Maar lake (Germany): implications from geochemical analysis of the oil shale sequence. In: *Organic geochemistry*, Vol. 36 (6). Elsevier, pp. 873–891.
- Sachsenhofer, Stummer, Georgiev, Dellmour, Bechtel, Gratzer & Coric, 2009.** Depositional environment and hydrocarbon source potential of the Oligocene Ruslar Formation (Kamchia Depression; Western Black Sea). In: *Marine and Petroleum geology*, Vol. 26 (1). Elsevier, pp. 57–84.
- Sandulescu, 1980.** Sur certain problèmes de la corrélation des Carpathes orientales Roumaines avec les Carpathes Ukrainiennes. In: *D. S. Inst. geol. geofiz.*, Vol. LXV (5). pp. 163–180.
- Sandulescu, 1990.** Paleogeography of the Romanian Carpathians and foreland. In: Rakus, M and Dercourt, J and Naim, AEM (Ed.), *Evolution of the northern margin of Tethys. Special issue of: Mem. Soc. geol. Fr., Nouvelle Serie, Paris*, Vol. 154 (III). pp. 91–100.
- Sandulescu & Micu, 1989.** Oligocene paleogeography of the East Carpathians. In: Ghergari L. et al. (Ed.), *The Oligocene from the Transylvanian Basin*. Cluj-Napoca, p. 79–86.
- Schmid, Bernoulli, Fügenschuh, Matenco, Schefer, Schuster, Tischler & Ustaszewski, 2008.** The Alpine-Carpathian-Dinaridic orogenic system: correlation and evolution of tectonic units. In: *Swiss Journal of Geosciences*, Vol. 101 (1). Springer, pp. 139–183.
- Schulz, Horsfield & Sachsenhofer, 2010.** Shale gas in Europe: a regional overview and current research activities. In: *Petroleum Geology Conference Series*, Vol. 7. Geological Society of London, pp. 1079–1085.
- Schulz, Sachsenhofer, Bechtel, Polesny & Wagner, 2002.** The origin of hydrocarbon source rocks in the Austrian Molasse Basin (Eocene-Oligocene transition). In: *Marine and petroleum geology*, Vol. 19 (6). Elsevier, pp. 683–709.
- Sinninghe Damsté, Kock-van Dalen, de Leeuw, Schenck, Guoying & Brassell, 1987.** The identification of mono-, di- and trimethyl 2-methyl-2-(4, 8, 12-trimethyltridecyl) chromans and their occurrence in the geosphere. In: *Geochimica et Cosmochimica Acta*, Vol. 51 (9). Elsevier, pp. 2393–2400.
- Sinninghe Damsté, Kohnen & Horsfield, 1998.** Origin of low-molecular-weight alkylthiophenes in pyrolysates of sulphur-rich kerogens as revealed by micro-scale sealed vessel pyrolysis. In: *Organic Geochemistry*, Vol. 29 (8). Elsevier, pp. 1891–1903.
- Sinninghe Damsté, Köster, Baas, Koopmans, van Kaam-Peters, Geenevasen & Kruk, 1995.** Cyclisation and aromatisation of carotenoids during sediment diagenesis. In: *J. Chem. Soc. Chem. Commun.* pp. 187–188.



- Stach, 1982.** The macerals of coal, *Stach's Textbook of Coal Petrology*. Stach, E. and Mackowsky, M. and Teichmuller, M. and Taylor, G.H. and Chandra, D. and Teichmuller, R. (Ed.), Gebruder Borntraeger Berlin, pp. 87–150.
- Stefanescu, 2006.** Hydrocarbon Geology of the Romanian Carpathians, Their Foreland, and the Transylvanian Basin. In: *AAPG Memoir*, Vol. 84. pp. 521–567.
- Sweeney, 1980.** Stable isotope composition of dissolved sulfate and hydrogen sulfide in the Black Sea. In: *Mar. Chem.*, Vol. 9 (145-152).
- Tabara & Popescu, 2012.** Palynology and Palynofacies of Gura Soimului Formation from Bistrita Half-Window (Eastern Carpathians, Romania). In: *Acta Palaeontologica Romaniae*, Vol. 8. pp. 23–31.
- Tischler, Matenco, Filipescu, Gröger, Wetzel & Fügenschuh, 2008.** Tectonics and sedimentation during convergence of the ALCAPA and Tisza-Dacia continental blocks: the Pienide nappe emplacement and its foredeep (N. Romania). In: *Geological Society, London, Special Publications*, Vol. 298 (1). Geological Society of London, pp. 317–334.
- Tissot & Welte, 1984.** Petroleum formation and occurrence. Springer-Verlag, New York.
- Tribovillard, Riboulleau, Lyons & Baudin, 2004.** Enhanced trapping of molybdenum by sulfurized marine organic matter of marine origin in Mesozoic limestones and shales. In: *Chemical Geology*, Vol. 213 (4). Elsevier, pp. 385–401.
- Vandenbroucke, 2003.** Kerogen: from types to models of chemical structure. In: *Oil & gas science and technology*, Vol. 58 (2). IFP, pp. 243–269.
- Wedepohl, 1971.** Environmental influences on the chemical composition of shales and clays. In: Ahrens, L.H. and Press, F. and Runcorn, S.K. and Urey, H.C. (Ed.), *Physics and Chemistry of the Earth*, Vol. 8. pp. 305–333.




## 8 Appendix

### List of samples and applied methods




Sample Code	Field Work		Petrom	MU Leoben						Nannoplankton (S. Coric)		Py-GC (GFZ Potsdam)
	Gamma-Ray Spectrometry	Strike & Dip		TOC/RockEval	Leco	Biomarker	XRF	Maceral Analysis	Vitrinite Reflectance	Nannoplankton (S. Coric)	Py-GC (GFZ Potsdam)	
II-85	x											
II-84	x											
98	x		x	x		x						
97	x		x	x	x		x					
II-82	x											
II-81	x											
96	x		x	x	x							
95	x		x	x								
94	x		x	x	x							
93	x		x	x	x							
II-81	x											
92	x		x	x								
91	x		x	x								
90	x		x	x								
89	x		x	x								
88	x		x	x								
87	x		x	x								
II-80	x		x	x		x						
II-79	x	x	x	x		x						
II-78	x		x	x		x						
85	x		x	x		x						
II-77	x			x								
II-76	x		x	x		x						
II-75	x		x	x		x			x			
84	x		x	x		x			x			
II-74	x		x	x		x			x			
83	x		x	x		x						
II-73	x	x	x	x		x						
82	x		x	x		x			x			
II-72	x	x	x	x	x	x						
II-70	x		x	x		x			x			
80	x	x	x	x		x						
79	x		x	x		x						
78	x		x	x	x				x			
II-69	x		x	x		x						x
II-68	x		x	x		x			x			
II-67	x		x	x		x	x	x				
77	x		x	x	x	x			x			x
II-66	x		x	x								x
II-65	x		x	x	x							x
76	x		x	x		x						x
II-64	x		x	x	x	x						x
II-63	x		x	x		x			x			x
75	x		x	x		x			x			x
II-46	x		x	x								
II-45	x		x	x								
II-44	x	x										
II-43	x											x
II-42	x											x
II-41	x											x
II-40	x	x										x
56	x											x
55	x		x									
54	x			x								
53	x											
52	x											
51	x											
50	x											
49	x											
48a	x		x	x								
47	x		x	x								
46a	x		x	x								x
45a	x		x	x								x
44	x		x	x	x		x	x				x
43	x		x	x								x
42b	x		x	x	x	x						x
42a	x		x	x			x					x
41b	x		x	x								x
41a	x		x	x	x							x
40	x		x	x								x
39	x		x	x								x
38b	x											x
38a	x		x	x								x
37	x		x	x	x		x					x
34	x		x	x								x
33	x		x	x	x	x						x
32	x	x	x	x								
31	x											
30	x		x	x	x							x
29	x		x	x								
28	x											
27	x		x	x	x		x					x
26	x	x	x	x								x
25	x		x	x	x							x
24	x											x
23	x		x	x								x
22	x		x	x								x
21	x		x	x								x

Sample Code	Field Work		Petrom	MU Leoben				Nannoplankton (S. Coric)	Py-GC (GFZ Potsdam)	
	Gamma-Ray Spectrometry	Strike & Dip	TOC/RockEval	Leco	Biomarker	XRF	Maceral Analysis	Vitrinite Reflectance		
II-62	x	x	x	x		x			x	
74	x		x	x					x	
II-61	x		x	x	x				x	
73	x		x	x						
II-60	x		x	x						
II-59	x		x	x		x			x	
72	x	x	x	x						
II-58	x		x	x	x	x			x	
II-57	x		x	x					x	
71	x		x	x						
II-56	x		x	x						
II-55	x		x	x	x				x	
II-54	x	x	x	x		x			x	
70	x		x	x	x				x	
II-53	x	x	x	x					x	
69	x		x	x					x	
68	x		x	x	x		x		x	
II-50	x		x	x		x			x	
II-49	x		x	x		x				x
67	x		x	x	x				x	
II-48	x	x	x	x					x	
II-47	x		x	x					x	
66	x		x	x	x				x	x

**Legend**

	Gura Soimului Fm
	Upper Dysodilic Shale Mbr
	Kliwa Sandstone Mbr

Sample Number	Field Work		Petrom	MU Leoben				Nannoplankton (S. Coric)	Py-GC (GFZ Potsdam)	
	Gamma-Ray Spectrometer	Strike & Dip	TOC/RockEval	Leco	Biomarker	XRF	Maceral Analysis	Vitrinite Reflectance		
20	x		x	x		x			x	x
19	x		x	x	x				x	x
18	x								x	x
17	x	x							x	x
16	x		x	x	x				x	x
15b	x								x	x
15a	x		x	x					x	x
14	x								x	x
13	x		x	x	x				x	x
12	x	x	x	x		x			x	x
11	x		x	x		x			x	x
10a	x		x	x					x	x
9	x		x	x	x		x		x	x
II-3b	x	x	x	x	x	x				
II-3a	x		x	x	x	x				x
8	x		x	x	x				x	x
5	x		x	x	x				x	x
4	x		x	x			x		x	x
3	x		x	x					x	x
2	x		x	x					x	x
1	x		x	x		x			x	x
II-4	x		x	x		x				
II-2	x		x	x	x	x				
II-1	x		x	x		x				

	Lower Dysodilic Shale Mbr
	Bituminous Marl Mbr
	Bisericani Fm

**Photo Documentation**

Printed on CD

**Measurement Results**

Next Pages

sample	meters to base	U	K	Th	DR	S1	S2	S3	Tmax	TOC	HI	OI	TC	S	TOC/S	TIC	CaCO <sub>3</sub>	
		[ppm]	[%]	[ppm]	[nGy/h]	[mgHC/g rock]			[°C]	[%]	[mgHC/gTOC]	[mgCO <sub>2</sub> /gTOC]	[%]		[%]			
Gura Soimului Fm.	II-85	697.7	14.38	0.52	4.89	100.59												
	II-84	695.7	6.56	0.00	1.68	41.44												
	II-83	687.7	8.90	0.00	2.92	57.77												
	98	687.1	14.80	1.04	6.22	113.17	0.01	0.21	0.18	427	0.32	64	56	1.19	0.44	0.73	0.87	7.23
	97	672.7	14.73	0.58	5.46	104.75	0.05	2.08	0.15	430	0.95	218	16	1.09	1.37	0.70	0.14	1.17
	II-82	666.7	12.16	0.00	3.81	78.51												
	96	661.7	11.98	0.72	4.51	88.70	0.11	5.26	0.15	428	1.59	331	9	1.74	2.88	0.55	0.15	1.25
	95	641.7	10.14	0.13	3.07	66.93	0.01	0*	0.07	354*	0.01	0		0.06	0.06	0.17	0.05	0.38
	94	631.7	8.23	0.25	2.90	57.18	0.15	2.27	0.13	427	0.75	305	17	0.75	1.42	0.52	0.01	0.08
	93	622.7	6.41	0.08	2.53	43.79	0.79	2.01	0.15	422	0.74	271	20	1.27	0.93	0.80	0.53	4.41
	II-81	617.2	8.68	0.19	2.07	56.88												
	92	611.7	7.05	0.13	2.71	48.52	0.40	1.66	0.11	417	0.80	209	14	0.79	0.87	0.91	0.00	0.00
	91	604.2	7.49	0.50	3.20	56.41	0.21	0.85	0.16	423	0.47	183	33	0.43	0.36	1.31	0.00	0.00
	90	591	10.62	0.56	4.55	78.91	0.00	0*	0.12	261*	0.00	0		0.03	0.05	0.00	0.03	0.22
	89	562	11.20	0.04	2.74	70.94	0.02	0*	0.11	261*	0.02	0		0.15	0.04	0.50	0.13	1.10
	88	554	8.57	0.03	3.83	58.49	0.00	0*	0.11	404*	0.00	0		0.23	0.60	0.00	0.23	1.91
	87	541.7	10.37	0.00	3.33	67.14	0.035	0.045	0.13	420	0.01	100		0.11	0.07	0.14	0.10	0.84
	II-80	533.2	16.24	0.97	6.32	120.54	0.01	0.015*	0.22	412*	0.15	10	147	0.80	0.08	1.95	0.65	5.39
	II-79	531.2	17.04	1.45	7.01	132.89	0.00	0.01*	0.15	425*	0.14	7	111	0.33	0.09	1.57	0.19	1.60
	II-78	529.2	14.53	1.04	6.31	111.76	0.00	0*	0.16	424*	0.13	0	119	0.57	0.08	1.67	0.44	3.66
	85	527.2	12.17	0.68	5.91	92.67	0.00	0.03	0.13	431	0.16	16	84	0.41	0.29	0.54	0.25	2.11
	II-77	525.2	14.72	0.07	4.17	94.76	0.47	0.36	0.14	328*	0.32	113	44	0.69	0.07	4.32	0.37	3.12
	II-76	523.2	13.74	0.26	4.64	92.98	0.03	0.01		433				2.23	0.06			
	II-75	521.5	24.01	0.60	9.73	168.44	0.01	0.85	0.21	433	0.88	96	24	1.28	1.21	0.73	0.40	3.31
	84	521.2	13.60	0.75	5.24	100.03	0.01	0.01	0.20	437	0.21	5	93	0.80	0.03	6.77	0.59	4.91
	II-74	519.5	18.78	0.40	7.77	131.21	0.00	0.04	0.25	424	0.23	16	109	0.27	0.60	0.37	0.05	0.40
83	518.7	14.40	0.38	6.43	102.78	0.01	0.005*	0.34	447*	0.19	3	181	0.90	0.02	8.26	0.72	5.97	
	II-73	513.7	24.29	0.27	11.73	170.67	0.16	11.23	0.31	421	3.19	352	10	3.31	4.97	0.64	0.12	0.96
	82	512.5	14.67	0.45	6.53	105.43	0.08	5.19	0.10	431	2.17	214	5	2.57	1.71	1.27	0.40	3.35
	II-72	512	24.23	0.32	10.97	169.08	0.01	0.54	0.30	427	0.63	86	47	0.76	3.53	0.18	0.14	1.15
	II-71	510.5	22.71	0.45	10.53	160.98	0.24	15.59	0.30	418	3.91	399	8	3.94	4.77	0.82	0.03	0.28
	81	510	14.11	0.46	7.66	105.22	0.10	6.71	0.42	427	2.67	251	16	2.77	4.24	0.63	0.10	0.83

sample	meters to base	U	K	Th	DR	S1	S2	S3	Tmax	TOC	HI	OI	TC	S	TOC/S	TIC	CaCO <sub>3</sub>	
		[ppm]	[%]	[ppm]	[nGy/h]	[mgHC/g rock]			[°C]	[%]	[mgHC/gTOC]	[mgCO <sub>2</sub> /gTOC]	[%]			[%]		
Upper Dysodilic Shale Mbr. (homog. part)	II-70	509.5	14.20	0.36	5.63	99.40	0.05	1.59	0.34	427	0.87	183	39	1.09	3.11	0.28	0.23	1.88
	80	509.3	15.87	0.51	8.31	117.52	0.05	4.59	0.60	425	2.32	198	26	3.68	4.05	0.57	1.36	11.34
	79	494.5	17.30	0.45	6.93	121.39	0.26	12.98	0.41	418	3.58	363	11	3.29	4.00	0.88	0.00	0.00
	78	494	20.30	0.42	8.13	140.99	0.18	16.49	0.31	420	4.11	402	7	3.83	2.78	1.47	0.00	0.00
	II-69	492.4	20.45	0.77	7.91	145.80	0.27	10.61	0.27	424	2.65	401	10	2.76	4.08	0.65	0.12	0.99
	II-68	490.12	14.40	0.00	3.56	90.60	0.28	10.89	0.23	424	2.62	415	9	2.78	3.85	0.68	0.16	1.37
	II-67	488.5	15.07	0.00	5.75	99.83	0.16	7.16	0.15	427	2.16	332	7	2.17	4.00	0.54	0.02	0.16
	77	487.5	18.49	0.40	11.51	141.10	0.70	33.83	0.47	416	7.36	460	6	7.64	7.18	1.02	0.28	2.33
	II-66	487.62	15.13	0.13	6.07	102.76	0.28	10.77	0.25	425	2.56	421	10	2.69	3.61	0.71	0.13	1.10
	II-65	479	15.56	0.22	6.98	108.56	0.27	13.65	0.26	423	3.26	419	8	3.33	3.49	0.93	0.07	0.58
	76	475.1	10.78	0.35	3.65	74.88	0.06	1.62	0.25	426	1.01	160	24	1.09	1.65	0.61	0.08	0.63
	II-64	473	14.56	0.07	5.09	96.29	0.11	4.70	0.26	429	1.76	268	15	1.75	3.61	0.49	0.00	0.00
	II-63	471.5	15.30	0.01	6.36	102.79	0.55	22.01	0.37	420	4.98	442	7	4.95	5.31	0.94	0.00	0.00
	75	470.7	15.62	0.54	5.92	110.46	0.29	13.29	0.37	421	3.22	413	11	3.20	3.31	0.97	0.00	0.00
	II-62	470.1	16.44	0.21	6.46	112.12	0.23	10.39	0.19	427	2.75	378	7	2.69	4.16	0.66	0.00	0.00
	74	461.5	13.73	0.58	6.31	101.31	0.17	7.11	0.36	427	2.18	327	17	2.12	2.98	0.73	0.00	0.00
	II-61	460	13.51	0.29	6.48	96.55	0.21	10.75	0.30	424	3.00	359	10	2.98	3.85	0.78	0.00	0.00
	73	457.5	12.79	0.41	5.87	92.60	0.15	6.04	0.41	428	1.85	326	22	2.11	3.53	0.52	0.26	2.16
	II-60	455	15.95	0.43	7.76	115.45	0.31	12.47	0.12	426	2.80	445	4	2.94	3.34	0.84	0.14	1.20
	II-59	453.5	18.83	0.20	7.64	128.61	0.18	8.28	0.25	428	2.32	357	11	2.29	3.36	0.69	0.00	0.00
	72	452.5	12.91	0.48	5.94	94.32	0.18	8.73	0.33	427	2.40	364	14	2.54	2.88	0.83	0.15	1.22
	II-58	450	16.00	0.06	6.72	108.34	0.23	7.09	0.19	427	2.00	354	10	2.09	3.74	0.53	0.09	0.73
	II-57	448.5	18.30	0.20	7.19	124.42	0.19	8.27	0.30	428	2.29	361	13	2.39	3.10	0.74	0.10	0.85
71	447.5	12.40	0.31	5.64	88.44	1.98	53.70	0.46	412	13.39	401	3	13.04	3.98	3.37	0.00	0.00	
II-56	444.4	15.72	0.20	7.11	109.62	0.33	11.99	0.20	426	2.76	435	7	2.90	3.19	0.86	0.15	1.23	
II-55	442.5	16.00	0.29	7.60	113.71	0.29	8.60	0.27	421	2.40	359	11	4.17	4.56	0.53	1.78	14.82	
II-54	442.22	17.28	0.27	5.53	115.35	0.16	7.53	0.26	427	2.27	332	11	2.28	2.89	0.78	0.01	0.10	
70	434	12.97	0.49	7.42	92.55	0.19	9.73	0.37	426	3.34	292	11	3.02	3.38	0.99	0.00	0.00	
II-53	433.3	8.98	0.00	3.66	60.99	0.17	5.09	0.12	431	1.39	366	9	1.41	1.50	0.93	0.02	0.17	
69	431.3	12.21	0.74	6.36	94.78	0.22	11.00	0.25	426	2.95	373	8	3.01	2.93	1.01	0.06	0.49	
II-52	428.45	3.76	0.00	1.64	25.43													
II-51	425.3	7.25	0.26	2.93	51.84	0.20	5.46		426				1.31	1.08				

sample		meters to base	U [ppm]	K [%]	Th [ppm]	DR [nGy/h]	S1 [mgHC/g rock]	S2 [mgHC/g rock]	S3 [mgHC/g rock]	Tmax [°C]	TOC [%]	HI [mgHC/gTOC]	OI [mgCO <sub>2</sub> /gTOC]	TC [%]	S [%]	TOC/S	TIC	CaCO <sub>3</sub> [%]	
Upper Dysodilic Shale Mbr. (heterog. part)	68	423	14.74	0.84	7.48	103.37	0.11	8.80	0.19	427	2.36	373	8	2.24	1.69	1.40	0.00	0.00	
	II-50	420.2	7.50	0.00	2.16	47.96	0.08	3.16	0.09	428	0.94	336	9	0.98	0.73	1.29	0.04	0.29	
	II-49	417.1	8.26	0.22	2.68	56.49	0.11	5.00	0.11	429	1.24	403	8	1.35	0.96	1.29	0.11	0.94	
	67	416	12.80	0.85	5.50	97.50	0.20	8.84	0.25	427	2.33	379	11	2.38	2.29	1.02	0.05	0.39	
	II-48	414.6	10.55	0.10	4.02	71.25	0.06	3.48	0.08	427	0.96	364	8	0.98	0.66	1.44	0.02	0.20	
	II-47	412.1	9.16	0.12	3.68	62.79	0.03	1.30	0.12	427	0.52	252	23	0.53	0.43	1.19	0.01	0.09	
	66	411	12.81	0.83	5.51	97.32	0.27	12.02	0.33	426	3.87	311	9	3.45	3.30	1.17	0.00	0.00	
	II-46	409.6	8.25	0.28	4.22	60.99	0.09	3.86	0.12	428	1.00	387	12	1.07	0.75	1.32	0.07	0.60	
	II-45	407.1	6.94	0.00	2.79	46.32	0.10	1.91	0.08	429	0.51	378	15	0.52	0.35	1.45	0.01	0.11	
	II-44	404.6	6.21	0.04	2.42	41.83													
	II-43	399.6	1.40	0.00	0.31	8.71													
	II-42	394.6	6.91	0.00	2.65	45.85													
II-41	391.6	2.83	0.00	0.57	17.50														
II-40	386.6	3.13	0.02	1.58	22.05														
Kiiwa Sandstone	56	334.8	3.20	0.08	1.53	23.04													
	55	329.3	8.20	0.67	4.69	67.06	0.22	2.82	0.07	425	0.73	386	10	0.69	0.42	1.75	0.00	0.00	
	54	323	2.06	0.00	1.01	14.24	0.00	0.00	0.00	0.00	0.00	0.00	0.00	0.00	0.00	0.00	0.00	0.00	
	53	318.8	2.19	0.05	1.24	16.26													
	52	313.8	3.30	0.08	1.09	22.58													
	51	308.8	1.57	0.00	0.87	11.06													
	50	303.8	1.34	0.00	0.60	9.07													
	49	298.8	2.03	0.00	1.56	15.40													
Lower Dysodilic Shale Mbr.	48a	270.8	2.20	0.00	2.20	17.95	0.00	0.03	0.10	430	0.06	50	158	0.14	0.14	0.44	0.08	0.65	
	47	270.1	8.20	0.18	3.09	56.58	0.01	0.10	0.15	435	0.08	125	188	1.34	0.13	0.63	1.26	10.46	
	46a	268.1	9.04	0.19	4.24	64.33	0.02	0.21	0.45	428	0.26	81	173	1.09	0.23	1.11	0.83	6.95	
	45a	266.1	7.71	0.13	3.44	54.03	0.01	0.14	0.13	430	0.15	97	86	0.40	0.14	1.04	0.26	2.16	
	44	264.1	11.43	0.28	3.86	78.23	0.19	11.44	0.25	426	3.26	351	8	3.69	1.78	1.84	0.43	3.57	
	43	263.4	10.80	0.36	3.14	73.87	0.12	7.33	0.24	429	2.36	311	10	2.47	1.46	1.61	0.11	0.95	
	42b	258	10.07	0.22	4.35	70.91	0.13	9.20	0.27	429	2.87	320	9	2.68	1.99	1.44	0.00	0.00	
	42a	257.5	9.38	0.21	4.30	66.72	0.02	1.44	0.12	430	0.65	222	18	0.74	0.52	1.23	0.10	0.79	
	41b	255.5	9.85	0.19	3.84	67.90	0.01	0.22	0.16	430	0.17	129	94	0.56	0.12	1.42	0.39	3.26	
	41a	255	12.50	0.30	4.24	85.44	0.10	7.30	0.24	427	2.39	306	10	2.44	1.62	1.47	0.06	0.48	

sample	meters to base	U	K	Th	DR	S1	S2	S3	Tmax	TOC	HI	OI	TC	S	TOC/S	TIC	CaCO <sub>3</sub>	
		[ppm]	[%]	[ppm]	[nGy/h]	[mgHC/g rock]			[°C]	[%]	[mgHC/gTOC]	[mgCO <sub>2</sub> /gTOC]	[%]		[%]			
Lower Dysodilic Shale Mbr.	40	247.5	2.05	0.00	1.13	14.45												
	39	245.5	15.14	0.30	5.85	104.44	0.17	14.65	0.16	425	3.33	440	5	3.45	2.16	1.54	0.12	1.01
	38b	241.4	1.83	0.07	1.31	14.59												
	38a	240.7	13.47	0.54	6.48	99.64	0.77	46.70	0.40	416	11.62	402	3	11.10	2.75	4.22	0.00	0.00
	37	239	14.95	0.44	7.70	109.81	1.33	54.73	0.50	418	13.22	414	4	12.43	2.67	4.95	0.00	0.00
	36	237	13.12	0.40	15.70	93.97	0.12	17.67	0.33	430	3.99	443	8	3.92	2.46	1.62	0.00	0.00
	35	235.2	11.67	1.20	6.74	98.73	0.15	12.77	0.23	429	2.85	448	8	2.81	2.36	1.21	0.00	0.00
	34	233.3	12.60	0.44	5.27	90.31	0.24	17.42	0.28	425	3.54	492	8	3.59	2.08	1.70	0.05	0.43
	33	231	7.66	0.89	5.33	68.43	0.12	9.89	0.12	432	1.87	530	6	1.96	1.55	1.20	0.09	0.75
	32	224.5	7.34	0.28	4.26	62.99	0.13	12.16	0.15	430	2.22	548	7	2.37	1.49	1.49	0.15	1.24
	31	219	5.80	0.60	5.68	55.10												
	30	217	7.75	0.40	3.54	51.07	0.14	8.06	0.12	430	1.68	481	7	1.76	1.32	1.27	0.09	0.73
	29	215	5.88	0.91	4.06	55.35	0.12	7.24	0.14	428	1.54	472	9	1.64	1.04	1.48	0.11	0.88
	28	212.6	2.82	0.04	1.30	19.73												
	27	211	12.61	0.64	5.93	94.79	0.39	25.22	0.26	424	5.59	451	5	5.44	1.98	2.83	0.00	0.00
	26	208.6	6.17	0.66	3.11	51.35	0.10	0.81	0.08	429	0.21	393	37	0.30	0.17	1.23	0.09	0.76
	25	207	6.06	0.59	3.18	50.04	0.07	1.02	0.09	428	0.44	234	21	0.39	0.39	1.11	0.00	0.00
	24	204.6	4.86	0.26	2.05	36.06												
	23	202.6	6.57	0.70	3.42	55.00	0.05	1.20	0.10	431	0.34	357	30	0.34	0.28	1.21	0.00	0.00
	22	200.6	6.37	0.58	3.29	51.92	0.12	13.86	0.13	435	2.32	599	5	2.40	1.55	1.50	0.09	0.72
	21	197	9.46	0.41	4.20	69.62	0.53	17.82	0.23	416	4.38	407	5	4.33	1.29	3.40	0.00	0.00
20	192	8.82	1.01	4.57	74.58	0.13	20.24	0.29	434	3.36	603	9	3.27	2.15	1.56	0.00	0.00	
19	188	8.86	0.69	4.41	70.31	0.17	22.65	0.19	435	3.26	695	6	3.34	2.39	1.37	0.08	0.70	
18	187.8	5.41	0.16	2.50	39.11													
17	185	2.78	0.00	1.54	19.61													
16	182	7.25	0.38	3.55	55.01	0.11	12.50	0.14	434	2.21	566	6	2.15	1.95	1.14	0.00	0.00	
15b	180	5.10	0.01	1.97	33.95													
15a	179.35	7.96	0.16	2.89	54.43	0.16	9.46	0.16	432	1.77	534	9	1.74	1.90	0.93	0.00	0.00	
14	177.2	3.57	0.00	1.73	24.58													
13	175	9.67	0.17	4.01	67.09	0.48	26.21	0.22	424	5.26	498	4	4.69	2.69	1.95	0.00	0.00	
12	172.8	10.28	0.31	3.91		0.17	13.43	0.17	432	2.29	586	7	2.29	2.53	0.91	0.00	0.00	
11	170.4	8.78	0.55	4.15	67.42	1.74	4.03	0.14	423	0.78	517	17	0.70	0.54	1.43	0.00	0.00	

	10a	168.9	8.61	0.63	3.64	66.20	0.03	0.32	0.26	420	0.33	98	80	0.61	1.51	0.21	0.28	2.33
	9	167	13.78	0.52	5.42	99.10	0.14	16.20	0.24	431	3.21	505	7	3.30	2.05	1.56	0.09	0.75
	II-3b	164	3.97	0.03	1.81	27.40	0.07	1.47	0.17	430	0.38	386	45	0.62	0.10	6.22	0.24	2.00
<b>Bituminous Marl Mbr.</b>	II-3a	162	1.69	0.00	1.41	13.10	0.43	8.72	0.31	424	1.49	587	21	9.10	0.33	4.49	7.61	63.40
	8	161	2.85	0.03	0.97	19.03	0.52	14.41	0.32	430	2.25	642	14	5.79	0.61	3.71	3.54	29.50
	7	156.4	3.42	0.08	1.40	23.95	0.27	6.47	0.31	427	1.21	534	25	3.96	0.27	4.49	2.75	22.89
	6	152.4	2.92	0.17	1.48	22.56	0.15	5.88	0.29	428	1.12	525	25	4.84	0.29	3.84	3.72	30.96
	5	147.4	2.67	0.23	2.14	24.23	0.43	12.81	0.28	429	1.97	652	14	5.74	0.58	3.37	3.77	31.42
	4	142.4	3.76	0.12	2.27	28.50	0.42	11.31	0.30	428	1.84	615	16	5.64	0.40	4.64	3.80	31.65
	3	137.4	3.63	0.52	2.51	31.06	0.30	7.93	0.28	427	2.10	378	13	5.43	1.18	1.78	3.34	27.79
	2	132	3.62	0.00	1.81	25.08	0.31	9.10	0.34	429	2.07	439	16	5.93	0.41	5.09	3.86	32.17
	1	127	3.84	0.01	1.32	25.20	0.25	9.73	0.31	430	2.02	483	15	6.04	0.39	5.18	4.02	33.50
	II-4	95	1.95	0	1.24	14.14	0.35	5.20	0.475	420	1.16	448	41	11.28	0.40	2.91	10.12	84.34
<b>Biseri-cani Fm.</b>	II-2	68	10.37	0.00	3.87	68.51	0.04	1.25	0.25	431	0.74	170	33	1.48	0.83	1.78	0.75	6.24
	II-1	0	7.53	0.00	2.53	49.01	0.06	1.55	0.21	429	0.62	251	33	1.84	1.01	1.82	1.22	10.18
<b>sample</b>	<b>meters to base</b>	<b>U</b> [ppm]	<b>K</b> [%]	<b>Th</b> [ppm]	<b>DR</b> [nGy/h]	<b>S1</b> [mgHC/g rock]	<b>S2</b>	<b>S3</b>	<b>Tmax</b> [°C]	<b>TOC</b> [%]	<b>HI</b> [mgHC/gTOC]	<b>OI</b> [mgCO <sub>2</sub> /gTOC]	<b>TC</b> [%]	<b>S</b> [%]	<b>TOC/S</b>	<b>TIC</b>	<b>CaCO<sub>3</sub></b> [%]	

\*) not reliable



## Pyrolysis GC Data

Aliphatic components in pyrolysis products

sample	Upper Dysodilic Shale Mbr				LDSM		BMM	
	77	II-63	II-49	66	35	20	II-3A	1
meters to base [m]	487.5	471.5	417.1	410.9	235.2	192	162	127
HI [mgHC/gTOC]	460	442	403	311	448	603	587	483
TOC [%]	7.36	4.98	1.24	3.87	2.85	3.36	1.49	2.02
<b>Aliphatic [µg/gTOC]</b>								
Prist-1-en	31.5	20.5	1.5	4.4	0.0	0.0	6.0	4.9
Prist-2-en	12.5	14.4	2.5	6.5	0.0	0.0	5.0	6.4
Phenantrene	0.0	0.0	0.0	2.7	0.0	0.0	0.0	0.0
2MC3	27.6	18.4	4.2	13.9	11.6	12.2	6.3	9.3
nC1_Total	905.9	648.9	152.6	393.6	386.3	354.2	207.7	285.0
nC2ene+nC2	822.8	650.6	177.9	414.9	387.8	477.5	226.9	269.4
nC3ene+nC3	714.0	583.5	178.4	408.9	382.6	500.4	212.7	266.9
nC4-1ene	275.0	248.2	86.8	190.5	171.6	265.9	89.5	108.4
nC4	180.6	135.6	34.3	84.3	92.1	133.1	47.4	63.1
2MC4	59.2	45.1	10.1	27.3	26.9	33.4	18.5	26.0
nC5-1ene	111.3	90.8	31.7	62.2	67.8	112.6	37.3	45.9
nC5	116.7	80.9	21.3	51.5	56.7	83.3	23.2	34.8
nC5-2ene	0.0	0.0	0.0	0.0	0.0	0.0	0.0	0.0
nC6-1ene	130.6	109.2	39.4	75.1	87.9	159.5	51.1	62.2
nC6	89.6	62.4	17.4	41.0	47.0	76.3	18.2	27.2
nC7-1ene	100.2	79.3	27.1	50.7	60.8	110.3	33.5	41.0
nC7	94.3	65.1	19.1	44.6	50.5	81.5	19.2	28.5
nC8-1ene	82.2	62.1	20.7	36.7	47.3	82.5	25.7	29.5
nC8	82.3	56.4	18.8	40.4	47.9	78.3	17.4	25.6
nC9-1ene	69.2	48.8	16.3	32.6	38.6	73.4	20.5	24.4
nC9	65.8	43.9	12.4	30.0	33.8	58.6	12.5	18.3
nC10-1ene	62.7	47.1	15.0	30.6	38.1	72.0	21.8	26.8
nC10	55.2	38.6	10.8	27.2	31.9	55.2	11.5	17.8
nC11-1ene	62.6	46.6	15.3	30.7	36.0	65.4	19.0	24.4
nC11	54.6	38.5	11.3	27.4	30.6	52.2	11.8	17.4
nC12-1en	59.9	44.0	13.7	30.3	35.2	63.7	17.6	23.9
nC12	58.0	42.0	11.4	29.2	33.7	54.1	12.4	19.8
nC13-1en	52.4	43.1	12.0	28.3	31.2	51.9	15.2	21.1
nC14	55.4	36.0	10.3	32.2	29.0	53.0	10.5	18.1
nC13	58.3	42.0	11.3	32.7	34.3	58.5	12.1	19.8
nC14-1ene	51.6	40.2	12.7	32.2	31.4	52.3	15.5	22.5
nC15-1ene	47.1	37.5	10.7	23.3	31.0	46.6	13.3	19.5
nC15	43.7	32.0	9.6	27.4	28.7	52.0	9.8	17.6
nC16-1ene	28.6	24.5	6.9	16.5	23.4	39.8	9.9	14.9
nC16	38.9	27.7	8.1	22.5	27.3	48.8	8.9	15.4
nC17-1ene	29.0	25.1	6.8	16.1	20.4	38.9	9.3	13.9
nC17	38.5	29.5	8.7	24.3	27.3	50.0	9.3	16.4
nC18-1ene	25.6	18.5	4.6	11.5	15.5	33.1	8.1	11.6
nC18	31.8	23.4	7.0	19.0	24.1	45.9	7.8	13.5
nC19-1ene	19.0	15.5	4.0	9.9	13.3	29.0	6.5	9.8
nC19	29.5	22.6	6.1	17.7	22.4	46.5	7.3	13.2
nC20-1ene	25.3	18.7	4.0	10.7	13.9	31.1	7.7	9.7
nC20	28.0	21.3	5.7	16.4	22.4	43.8	7.1	12.0
nC21-1ene	19.4	14.5	3.0	8.9	12.9	27.2	6.0	8.3
nC21	25.3	19.7	5.3	15.9	21.3	42.1	6.4	11.5
nC22-1ene	14.3	12.5	2.8	7.7	11.4	24.6	5.2	8.1
nC22	20.8	17.8	5.0	13.9	21.4	41.0	5.5	10.4

sample	Upper Dysodilic Shale Mbr				LDSM		BMM	
	77	II-63	II-49	66	35	20	II-3A	1
meters to base [m]	487.5	471.5	417.1	410.9	235.2	192	162	127
HI [mgHC/gTOC]	460	442	403	311	448	603	587	483
TOC [%]	7.36	4.98	1.24	3.87	2.85	3.36	1.49	2.02
nC23	19.6	16.5	4.6	12.6	20.6	40.6	5.4	10.4
nC24-1ene	11.1	10.0	2.1	5.6	9.2	21.1	3.7	6.0
nC24	17.6	15.4	4.1	11.8	18.7	39.3	4.5	8.6
nC25-1ene	9.5	9.3	2.0	4.8	8.0	19.4	3.1	5.1
nC25	14.7	13.4	3.9	10.2	16.5	35.3	4.1	7.6
nC26-1ene	6.9	6.9	1.4	3.4	5.8	15.4	2.6	4.1
nC26	11.3	11.9	3.1	8.6	13.6	31.1	3.6	6.8
nC27-1ene	5.8	5.7	1.2	2.7	4.8	12.1	2.0	3.4
nC27	11.0	10.2	2.8	7.4	12.4	27.9	3.3	6.7
nC28-1ene	5.1	4.9	0.9	2.0	3.9	10.8	2.1	3.5
nC28	8.1	8.7	2.2	5.9	9.6	22.3	2.7	5.4
nC29-1ene	4.0	3.9	0.8	1.9	2.5	9.5	1.0	4.2
nC29	6.8	6.6	1.8	4.4	6.6	16.7	1.7	3.9
nC30-1ene	3.2	2.8	0.4	1.1	1.8	5.9	1.0	1.5
nC30	5.6	5.5	1.2	3.0	5.5	13.4	2.2	3.1
nC31-1ene	3.3	2.3	0.4	0.9	1.5	3.7	1.6	2.5
nC31	8.6	5.9	1.1	2.9	4.0	9.9	2.9	4.2
nC32-1ene	0.0	1.9	0.4	0.0	1.5	3.6	0.8	0.0
nC32	3.7	3.2	0.8	2.6	2.8	7.7	2.5	3.2
nC33-1ene	0.0	0.0	0.0	0.0	0.0	1.6	0.0	0.0
nC33	2.6	2.3	0.4	1.2	1.7	4.6	0.8	1.0
nC34-1ene	0.0	0.0	0.0	0.0	0.0	0.0	0.0	0.0
nC34	0.0	1.0	0.2	0.8	1.0	3.1	0.8	0.0
nC35-1ene	0.0	0.0	0.0	0.0	0.0	0.0	0.0	0.0
nC35	0.0	0.0	0.2	0.5	1.0	2.2	0.0	0.0
nC36-1ene	0.0	0.0	0.0	0.0	0.0	0.0	0.0	0.0
nC36	0.0	0.0	0.1	0.0	0.5	1.6	0.0	0.0
nC37-1ene	0.0	0.0	0.0	0.0	0.0	0.0	0.0	0.0
nC37	0.0	0.0	0.0	0.0	0.5	1.5	0.0	0.0
nC38-1ene	0.0	0.0	0.0	0.0	0.0	0.0	0.0	0.0
nC38	0.0	0.0	0.0	0.0	0.0	1.2	0.0	0.0
nC39-1ene	0.0	0.0	0.0	0.0	0.0	0.0	0.0	0.0
nC39	0.0	0.0	0.0	0.0	0.0	0.6	0.0	0.0
nC40-1ene	0.0	0.0	0.0	0.0	0.0	0.0	0.0	0.0
nC40	0.0	0.0	0.0	0.0	0.0	0.4	0.0	0.0
C1-5single	3185.4	2483.5	693.2	1633.1	1571.8	1960.4	863.3	1099.5
nC6-14	1512.9	1117.0	348.0	765.3	869.7	1494.7	406.0	549.1
nC15+	638.1	521.1	137.3	362.9	502.3	1028.8	185.3	304.0
nC9:1+nC25:1	78.7	58.1	18.4	37.4	46.6	92.8	23.7	29.6
C1-5total	3487.9	2687.6	767.7	1806.6	1730.7	2138.1	948.6	1201.8

Aromatic components in pyrolysis products

Sample	Upper Dysodilic Shale Mbr				LDSM		BMM	
	77	II-63	II-49	66	35	20	II-3A	1
meters to base [m]	487.5	471.5	417.1	410.9	235.2	192	162	127
HI [mgHC/gTOC]	460	442	403	311	448	603	587	483
TOC [%]	7.36	4.98	1.24	3.87	2.85	3.36	1.49	2.02
<b>Aromatic [µg/gTOC]</b>								
Benz	61.9	44.2	22.6	60.4	27.2	58.8	15.6	21.5
Ebenz	38.2	21.8	7.9	20.3	18.9	26.8	7.5	11.6
1M2EBenz	20.9	15.4	5.2	13.9	13.3	17.4	4.7	6.3
1M3EBenz	21.0	15.5	6.7	17.3	16.2	22.1	5.6	7.8
1M4EBenz	11.6	7.5	3.2	7.9	8.5	9.4	3.0	3.9
1,2,3TMBenz	26.2	19.0	6.9	17.1	14.0	13.9	6.4	7.3
1,2,4TMBenz	40.1	36.1	13.3	32.6	29.2	32.8	11.5	14.3
1,2,3,4TeMBenz	32.7	27.8	7.0	21.5	15.9	16.2	7.8	8.5
1,3,5TMBenz	12.5	8.0	1.7	8.1	8.5	8.5	3.5	4.0
Propylbenzene	15.9	0.0	3.7	7.3	9.4	12.2	0.0	0.0
Naphthalene	16.1	11.6	7.0	17.5	9.1	14.1	3.8	5.8
1,2DMNaphthalene	3.1	8.5	2.6	9.3	4.8	0.0	1.9	3.6
1,3+1.7DMNaphthalene	9.2	12.0	4.4	15.8	8.6	0.0	3.0	4.6
1,4+2,3DMNaphthalene	3.7	4.7	1.5	7.7	3.6	0.0	1.2	2.8
1,5DMNaphthalene	8.9	8.6	2.8	7.5	4.0	0.0	2.2	3.7
1,6 DMNaphthalene	17.3	11.5	2.9	11.7	7.1	0.0	2.8	4.0
1,8DMNaphthalene	0.0	0.0	0.0	0.0	0.0	0.0	0.0	0.0
2,6DMNaphthalene	0.0	0.0	0.0	0.0	0.0	0.0	0.0	0.0
2,7DMNaphthalene	10.3	6.4	1.9	6.1	0.0	0.0	0.0	0.0
1ENaphthalene	14.6	9.4	3.5	6.9	4.3	0.0	3.3	5.0
2ENaphthalene	0.0	4.7	1.1	7.5	3.6	0.0	1.1	0.0
1MNaphthalene	16.7	17.8	6.9	22.3	15.1	17.8	4.3	7.1
2MNaphthalene	20.9	21.8	6.7	22.4	18.5	20.6	8.9	9.7
1,2,5TMNaphthalene	0.0	2.6	0.8	3.0	3.3	0.0	0.8	0.0
1,3,6TMNaphthalene	0.0	5.8	1.5	4.8	3.3	0.0	1.6	2.9
1,3,7TMNaphthalene	0.0	6.7	2.0	5.9	5.1	0.0	2.4	4.1
1,3,5+1.4.6TMNaphthalene	0.0	7.8	2.3	6.5	5.5	0.0	2.0	3.4
1,6,7TMNaphthalene	0.0	6.2	2.2	7.8	6.6	0.0	1.8	4.6
2,3,6TMNaphthalene	0.0	4.7	1.4	4.8	3.4	0.0	1.0	2.5
Tol	119.6	78.8	31.4	63.1	58.9	75.2	25.1	31.9
oXylene	57.5	39.1	14.6	31.8	30.1	42.4	12.6	15.4
m+pXylene	114.5	72.4	26.8	59.1	52.7	58.7	28.1	35.4
Phenol	25.7	30.6	7.9	17.9	19.6	11.9	4.8	5.2
2MPhenol	18.8	21.7	5.4	15.1	15.6	8.8	3.6	4.4
3+4MPhenol	34.0	47.1	9.2	28.3	22.9	10.5	5.0	5.8
Styrene	30.6	19.1	7.6	13.4	14.0	20.3	7.1	8.9
<b>Sulfur components</b>								
Thio	18.1	10.3	4.5	9.6	10.2	11.9	3.3	3.1
2MThio	64.2	41.1	13.1	33.2	34.1	33.8	11.2	12.7
3MThio	15.8	9.8	4.8	10.3	9.9	8.1	2.3	3.3
2,3DMThio	20.8	12.2	4.7	10.6	10.2	10.6	4.0	3.8
2,4DMThio	28.4	15.3	5.4	12.8	12.4	8.8	4.9	5.4
2,5DMThio	43.7	18.9	5.1	12.1	12.7	14.9	4.9	6.8
2ETHio	32.5	19.8	7.4	14.5	14.7	13.2	8.3	7.9
2,3,5TMThio	0.0	0.0	0.0	0.0	0.0	0.0	0.0	0.0
2E5MThio	0.0	0.0	0.0	0.0	0.0	0.0	0.0	0.0
2E4MThio	0.0	0.0	0.0	0.0	0.0	0.0	0.0	0.0